Electronic Supplementary Material (ESI) for Chemical Science.

Supplementary Materials and Methods for

$Au^{I}Cl$-bound N-heterocyclic carbene ligands form $M^{II}_{4}(LAuCl)_{6}$ integrally gilded cages

William J. Ramsay, Jonathan A. Foster, Katharine L. Moore, Tanya K. Ronson, Raphaël J. Mirgalet, David A. Jefferson, and Jonathan R. Nitschke

Contents

1. Experimental

1.1 General

Commercial solvents and reagents were used without further purification unless specified otherwise. HPLC grade acetonitrile was purchased from Fisher Scientific with a 0.008% water content (max. 0.01%). Anhydrous acetonitrile (99.8%) was purchased from Sigma Aldrich with a < 0.001% water content; it was used as received and stored and manipulated in a glovebox. Chloro(tetrahydrothiophene)gold(I) (Au(tht)Cl, tht = tetrahydrothiophene),[1] cadmium(II) di[bis(trifluoromethylsulfonyl)imide] ($Cd(NTf_2)_2$, NTf_2 = triflimide),[2] and bis(2,4,6-trimethoxybenzonitrile)gold(I) hexafluoroantimonate ($Au(tmbn)_2SbF_6$, tmbn = 2,4,6-trimethoxybenzonitrile)[3] were prepared as previously described. NMR spectra were recorded on Bruker Avance DRX 400 MHz, DCH 500 MHz dual cryoprobe, DPX 500 MHz BB ATM and 500 MHz TCI cryoprobe NMR spectrometers. Chemical shifts for ^{1}H, ^{13}C, and ^{19}F are reported in ppm on the δ scale; ^{1}H and ^{13}C were referenced to the residual solvent peak, and ^{19}F was referenced to C_6F_6 in CD_3CN at −164.9 ppm. Coupling constants (*J*) are reported in hertz (Hz). The following abbreviations are used to describe signal multiplicity for ^{1}H and ^{13}C NMR spectra: s: singlet, d: doublet, t: triplet, m: multiplet, br: broad. DOSY experiments were performed on a Bruker Avance DPX 500 MHz BB ATM spectrometer. Maximum gradient strength was 6.57 G/cmA. The standard Bruker pulse program, ledbpgp2s, employing a stimulated echo and longitudinal eddy-current delay (LED) using bipolar gradient pulses for diffusion using 2 spoil gradients was utilized. Rectangular gradients were used with a total duration of 1.5 ms. Gradient recovery delays were 500-950 μs. Diffusion times were 100 ms. Individual rows of the quasi-2D diffusion databases were phased and baseline corrected. Elemental analyses were obtained on an Exeter Analytical CE-440 Elemental Analyzer. Electronic absorbance spectra were measured in acetonitrile with a Perkin Elmer Lambda 750 UV/Vis/NIR spectrometer. Infrared

absorbance spectra were measured on a Perkin Elmer Spectrum One Frontier IR spectrometer equipped with a ZnSe/diamond ATR accessory; the following abbreviations were used to describe the wavenumber peaks: s: strong, m: medium, w: weak, sh: sharp, and br: broad. High resolution electrospray ionization mass spectrometry (HRMS-ESI) was performed on a Waters LCT Premier Mass Spectrometer featuring a Z spray source with electrospray ionization and modular LockSpray interface. Low resolution electrospray ionization mass spectrometry (ESI-MS) was obtained on a Micromass Quattro LC, infused from a Harvard Syringe Pump at a rate of 10 μL per minute. High Resolution Transmission Electron Microscopy (HRTEM) analysis was carried out on a JEOL JEM-3011 electron microscope operated at 300 kV. This machine was fitted with a high-resolution pole piece (Cs = 0.6 mm, Cc = 1.2 mm) giving an interpretable point resolution of ca. 1.6 Å. Samples were prepared for analysis by pipetting several drops of an acetonitrile solution onto a carbon coated copper grid (Agar Scientific, 300 mesh) and left to dry before inserting the grid into the microscope. Elemental analysis was carried out in the microscope using Energy Dispersive X-ray Analysis (EDS) with electron beam probe diameters in the range 500 –100 Å. A PGT thin-window Si/Li detector with a resolution of 138 eV was employed and the program PGT eXcalibur was used to gather and analyze the EDS data. Significant peaks were seen for Cu Kα and Cu Kβ radiation, which were generated from scattered electrons impinging on the copper grid bars as well as from the specimen holder. The morphology of the samples was also investigated by atomic force microscopy (AFM) with a Veeco Dimension 3100 microscope operating in tapping-mode using RTESP tips, with a nominally 8 nm end radius. Samples were prepared analogously to TEM studies, in which 1 drop of an acetonitrile solution was dropped onto a quartz plate and allowed to dry in air overnight before analysis.

General procedure of Au NP synthesis. A 2.0 mL solution ($2.8 – 3.0 \times 10^{-4}$ M) of **A** or **D** (with and without equimolar quantities of either $Zn(NTf_2)_2$ or $Cd(NTf_2)_2$) was prepared in dry acetonitrile, to which 100 μL (1.0 equiv) of $Au(tmbn)_2SbF_6$ was added from a solution prepared in dry acetonitrile. Similarly, a 2.0 mL solution ($4.7 – 5.0 \times 10^{-5}$ M) of **1** or **2** was prepared in acetonitrile, to which 100 μL (6.0 equiv) of $Au(tmbn)_2SbF_6$ was added; the concentration of $Au(tmbn)_2SbF_6$ was kept constant across all experiments. UV-Vis spectra were recorded at specific intervals over a 90 minute period, with agitation of the solution for 30 seconds between spectra acquisition.

1.2 Synthesis and Characterization of Subcomponents A – D

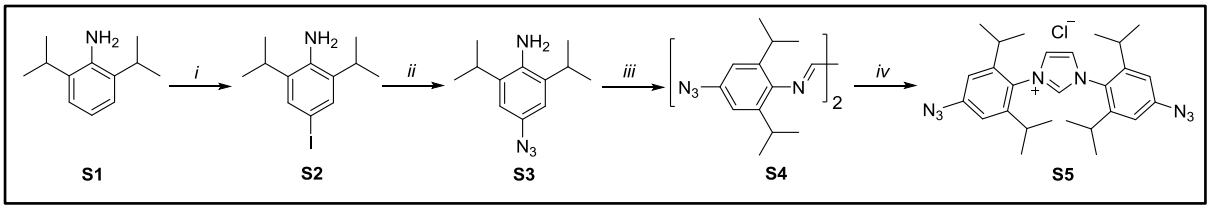

Scheme S1. Synthesis of subcomponents **S2** – **S5**, reagents and conditions: (i) I_2, aq. $NaHCO_3$, Et_2O, 25 °C, 2 h, 97 %; (ii) NaN_3, N,N′-Me_2en cat., CuI cat., sodium ascorbate cat., DMSO/H_2O, 50 °C, 16 h, 95 %; (iii) glyoxal, MeOH, 50 °C – 25 °C, 4 h, 80 %; (iv) $(CH_2O)_n$, TMSCl, AcOEt, 70 °C, 16 h, 68 %.

4-iodo-2,6-diisopropylaniline (S2)[4]

Iodine (59.2 g, 233 mmol, 1.1 equiv) and a saturated sodium bicarbonate solution (600 mL) were added successively to a rapidly stirred solution of 2,6-diisopropylaniline (40.0 mL, 212 mmol, 1.0 equiv) in 200 mL of Et_2O. Gas evolution was observed. After 2 h, excess iodine was destroyed by addition of sodium thiosulfate (6.64 g, 42.0 mmol) and S2 was

recovered by separation of the ethereal phase and further extraction (2 × 100 mL Et_2O) of the aqueous phase. The combined organic phases were washed with 200 mL of water and evaporated to dryness under vacuum to yield 62.4 g (206 mmol, 97 %) of S2 as a brown oil. ^{1}H NMR (400 MHz, 298 K, $CDCl_3$): δ 7.28 (2H, s, H^{Ar}), 3.73 (2H, s (br), -N$\underline{H}_2$), 2.84 (2H, sept, *J* = 6.8 Hz, -C($\underline{H}$)$(CH_3)_2$), 1.25 (12H, d, *J* = 6.8 Hz, -C(H)(C$\underline{H}_3)_2$. ^{13}C NMR (100 MHz, 298 K, $CDCl_3$): δ 140.2, 135.1, 131.8, 81.2, 27.9, 22.3. HRMS (ESI^+): *m/z* calcd for $C_{12}H_{19}NI$ $[M + H]^+$: 304.0562, found: 304.0568. Analyses match previously reported data.[4]

4-azido-2,6-diisopropylaniline (S3)[4]

S2 (30.0 g, 98.9 mmol, 1.0 equiv), NaN_3 (12.9 g, 198 mmol, 2.0 equiv) and N,N′-dimethylethylenediamine (1.60 mL, 14.9 mmol, 15 mol %) were dissolved in DMSO/water (180 mL/45 mL). Ascorbic acid (1.70 g, 9.65 mmol, 10 mol%) and NaOH (400 mg, 10.0 mmol, 10 mol %) were added and the reaction mixture was degassed by bubbling nitrogen for 30 min at 50 °C. CuI (1.90 g, 9.98 mmol, 10 mol%) was added and the resulting mixture was stirred at 50 °C overnight. Brine (200 mL) was added and the aqueous layer was extracted with 3 × 100 mL of Et_2O, dried over $MgSO_4$ and evaporated to dryness under vacuum to yield 20.5 g of a brown oil (94.0 mmol, 95%). ^{1}H NMR (400 MHz, 298 K, $CDCl_3$): δ 6.71 (2H, s, H^{Ar}), 3.68 (2H, s (br), -N$\underline{H}_2$), 2.92 (2H, sept, *J* = 6.8 Hz, -C($\underline{H}$)$(CH_3)_2$), 1.26 (12H, d, *J* = 6.8 Hz, -C(H)(C$\underline{H}_3)_2$. ^{13}C NMR (100 MHz, 298 K, $CDCl_3$): δ 137.7, 134.2, 129.8, 113.7, 28.1, 22.2. HRMS (ESI^+): *m/z* calcd for $C_{12}H_{19}N_4$ $[M + H]^+$: 219.1610, found: 219.1603. Analyses match previously reported data.[4]

N,N′-Bis(4-azido-2,6-diisopropylphenyl)1,4-diazabuta-1,3-diene (S4)[4]

S3 (10.0 g, 45.8 mmol, 1.0 equiv) was dissolved in 25 mL of methanol at 50 °C. Glyoxal (40 % w/w in water, 2.5 mL, 21.9 mmol, 0.48 equiv) and acetic acid (0.25 mL, 4.38 mmol,

0.10 equiv) were added and the resulting mixture was stirred at room temperature for 4 h. The solid which separated was filtered and washed with cold methanol (20 mL) to afford, after drying under vacuum, 8.42 g of a yellow powder (18.4 mmol, 80 %). ^{1}H NMR (400 MHz, 298 K, DMSO-d_6): δ 8.16 (2H, s, H^{imine}), 6.90 (4H, s, H^{Ar}), 2.86 (4H, sept, J = 6.8 Hz, -C(H)$(CH_3)_2$), 1.14 (24H, d, J = 6.8 Hz, -C(H)$(CH_3)_2$. ^{13}C NMR (100 MHz, 298 K, DMSO-d_6): δ 163.0, 144.6, 138.4, 136.3, 114.0, 27.8, 22.8. HRMS (ESI^+): *m/z* calcd for $C_{26}H_{35}N_8$ $[M + H]^+$: 459.2985, found: 459.2976. Analyses match previously reported data.[4]

N,N′-Bis(4-azido-2,6-diisopropylphenyl)imidazolium chloride (S5)[4]

To 200 mL of ethyl acetate (70 °C) were added under stirring S4 (5.00 g, 10.9 mmol, 1.0 equiv) and paraformaldehyde (0.49 g, 16.4 mmol, 1.50 equiv). TMSCl (1.4 mL, 10.9 mmol, 1.0 equiv) diluted in 20 mL of ethyl acetate was added dropwise and the reaction mixture was stirred overnight. After cooling to room temperature, the solvent was evaporated under vacuum and the resulting oil was triturated with *tert*-butylmethylether until a solid separated. A brown powder was recovered by filtration (3.78 g, 7.46 mmol, 68%). ^{1}H NMR (400 MHz, 298 K, DMSO-d_6): δ 10.18 (1H, t, J = 1.5 Hz, NCHN), 8.54 (2H, d, J = 1.5 Hz, NCHCHN), 7.21 (4H, s, H^{Ar}), 2.32 (4H, sept, J = 6.8 Hz, -C(H)$(CH_3)_2$, [1.25 (12H, d, J = 6.8 Hz, -C(H)$(CH_3)_2$, 1.15 (12H, d, J = 6.8 Hz, -C(H)$(CH_3)_2$]. ^{13}C NMR (100 MHz, 298 K, DMSO-d_6): δ 147.1, 143.1, 139.8, 126.6, 126.3, 115.3, 28.9, 23.8, 22.8. HRMS (ESI^+): *m/z* calcd for $C_{27}H_{35}N_8$ $[M]^+$: 471.2985, found: 471.2979. Analyses match previously reported data.[4]

N,N′-Bis(4-amino-2,6-diisopropylphenyl)imidazolium chloride (A)

S5 (0.50 g, 0.99 mmol) was dissolved in 250 mL of MeOH, to which 50.0 mg of palladium on activated charcoal (10% Pd, 10 wt %) was added. The reaction was stirred under an atmosphere of H_2 for 24 h, after which the solution was filtered and evaporated to dryness

under vacuum to yield a tan powder (0.45 g, 98 %). ^{1}H NMR (400 MHz, 298 K, DMSO-d_6): δ 9.87 (1H, t, J = 1.5 Hz, NC<u>H</u>N), 8.27 (2H, d, J = 1.5 Hz, NC<u>H</u>C<u>H</u>N), 6.57 (4H, s, H^{Ar}), 5.67 (4H, s (br), -N<u>H</u>$_2$), 2.22 (4H, sept, J = 6.8 Hz, -C(<u>H</u>)(CH$_3$)$_2$, [1.17 (12H, d, J = 6.8 Hz, -C(H)(C<u>H</u>$_3$)$_2$, 1.09 (12H, d, J = 6.8 Hz, -C(H)(C<u>H</u>$_3$)$_2$]. ^{13}C NMR (100 MHz, 298 K, DMSO-d_6): δ 151.1, 145.2, 140.5, 126.5, 118.6, 108.6, 28.3, 24.2, 23.2. IR (cm^{-1}): 3289 (w, br), 3162 (w, br), (w, br), 2961 (m, sh), 2926 (m, sh), 2871 (w, sh), 1631 (m, sh), 1602 (s, sh), 1533 (m, sh), 1469 (m, sh), 1387 (w, sh), 1358 (m, sh), 1225 (m, sh), 1053 (m, sh), 850 (m, sh), 753 (m, sh), 692 (m, sh). UV/Vis (CH$_3$CN, λ_{max}, nm): 249 (ε 2.66 × 10^4 M^{-1}cm^{-1}), 290 (ε 4.43 × 10^3 M^{-1}cm^{-1}). HRMS (ESI$^+$): *m/z* calcd for $C_{27}H_{39}N_4$ [M]$^+$: 419.3175, found: 419.3183. Elemental analysis (%): Calcd for $C_{27}H_{39}N_4Cl$·0.25 CH_2Cl_2: C, 68.71; H, 8.36; N, 11.76. Found: C, 68.62; H, 8.41; N, 11.45.

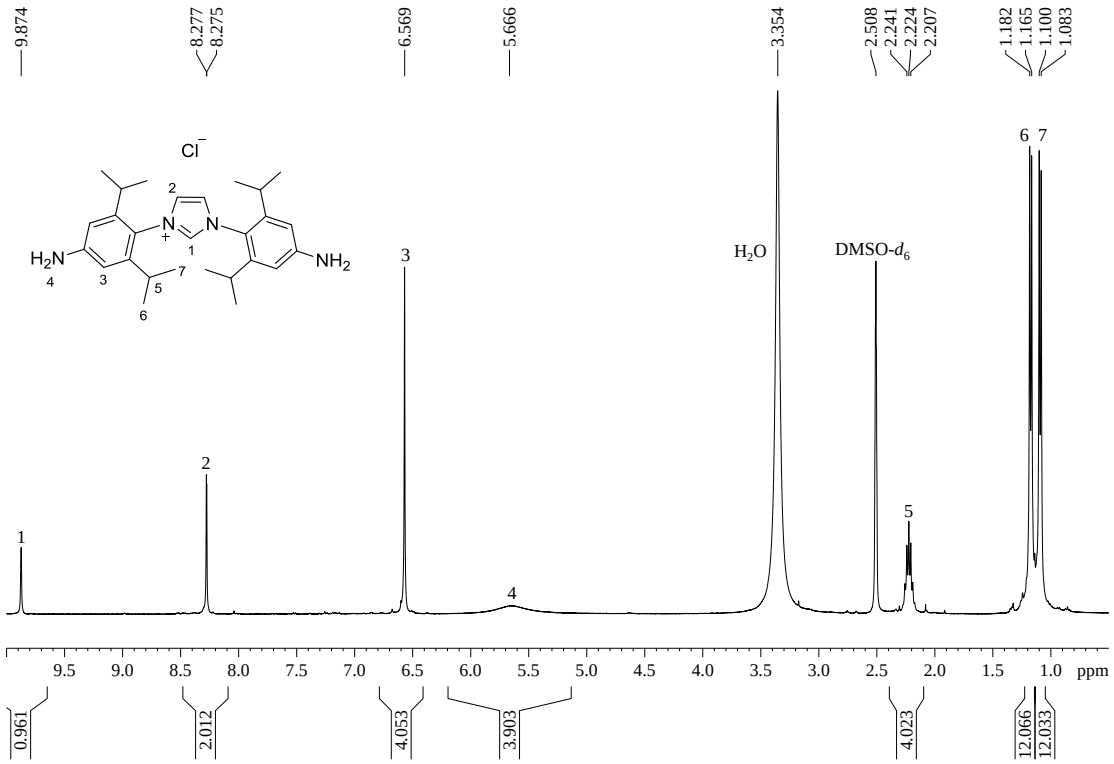

Figure S1. ^{1}H NMR of **A** in DMSO-d_6 at 25 °C with assignments.

[N,N′-Bis(4-amino-2,6-diisopropylphenyl)-imidazol-2-ylidene]-chlorocopper(I) (B)

According to an adapted literature procedure[5], a vial was charged with **A** (14.78 mg, 0.032 mmol, 1.0 equiv), CuCl (3.20 mg, 0.032 mmol, 1.0 equiv), and Na_2CO_3 (6.90 mg, 0.065 mmol, 2 equiv). The resulting mixture was suspended in 5.0 mL of acetone, and stirred at 60 °C for 16 h. After this time the mixture was filtered through silica, and the silica rinsed with DCM (3 × 1 mL). The solvent was evaporated to dryness under vacuum and the tan powder dried over P_2O_5 overnight (12.25 mg, 90 %). ^{1}H NMR (400 MHz, 298 K, CD_3CN): δ 7.26 (2H, s, NC<u>H</u>C<u>H</u>N), 6.58 (4H, s, H^{Ar}), 4.31 (4H, s (br), -N<u>H</u>$_2$), 2.44 (4H, sept, J = 6.9 Hz, -C(<u>H</u>)$(CH_3)_2$, [1.19 (12H, d, J = 6.9 Hz, -C(H)(C<u>H</u>$_3)_2$, 1.15 (12H, d, J = 6.9 Hz, -C(H)(C<u>H</u>$_3)_2$]. ^{13}C NMR (125 MHz, 298 K, CD_3CN): δ 181.7, 150.3, 147.5, 125.7, 125.0, 110.4, 29.3, 24.9, 23.8. IR (cm^{-1}): 3444 (w, br), 3315 (w, br), 2960 (s, sh), 2923 (m, sh), 2868 (w, sh), 1619 (m, sh), 1603 (s, sh), 1472 (s, sh), 1385 (w, sh), 1347 (m, sh), 1231

(m, sh), 1075 (w, sh), 943 (w, sh), 850 (m, sh), 759 (m, sh), 705 (m, sh). UV/Vis (CH_3CN, λ_{max}, nm): 211 (ε 6.83 × 10^4 $M^{-1}cm^{-1}$), 248 (ε 3.29 × 10^4 $M^{-1}cm^{-1}$), 296 (ε 4.83 × 10^3 $M^{-1}cm^{-1}$). Elemental analysis (%): Calcd for $C_{27}H_{38}N_4CuCl{\cdot}0.5\ CH_2Cl_2{\cdot}0.5\ C_3H_6O$: C, 59.12; H, 7.19; N, 9.51. Found: C, 59.42; H, 7.07; N, 9.41.

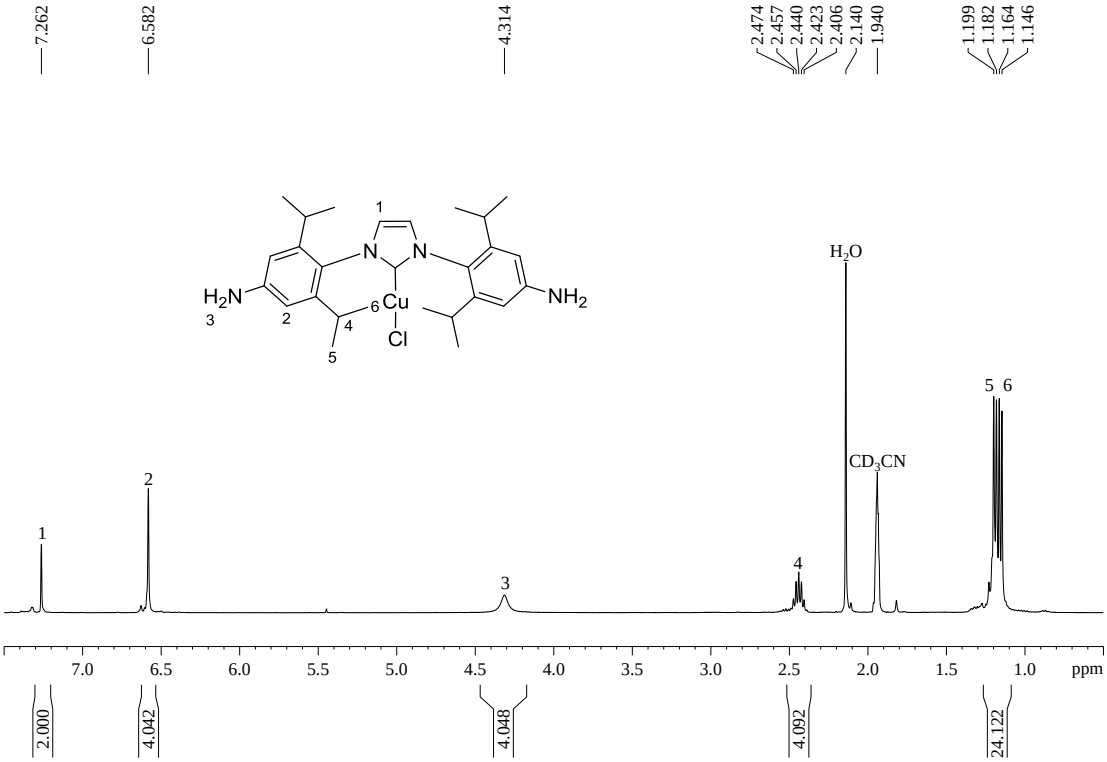

Figure S2. ^{1}H NMR of **B** in CD_3CN at 25 °C with assignments.

[N,N′-Bis(4-amino-2,6-diisopropylphenyl)-imidazol-2-ylidene]-chlorosilver(I) (C)

According to an adapted literature procedure[4], **A** (12.80 mg, 0.028 mmol, 1.0 equiv) and Ag_2O (4.25 mg, 0.018 mmol, 0.65 equiv) were added to 10 mL of dichloromethane, and the mixture was stirred in the dark for 2 h at room temperature. The solution was then filtered over celite, and the solvent removed under vacuum. The resulting off yellow powder was dissolved in 1 mL of acetonitrile, and filtered over a plug of silica. The silica was rinsed with acetonitrile (3 × 1 mL), and the solvent evaporated to dryness under vacuum to yield a tan powder, which was dried overnight over P_2O_5 (14.21 mg, 90 %). ^{1}H NMR (500 MHz, 298 K,

CD_3CN): δ 7.36 (2H, d, $^4J_{H,Ag}$ = 1.8 Hz, NC<u>H</u>C<u>H</u>N), 6.59 (4H, s, H^{Ar}), 4.34 (4H, s (br), -N<u>H</u>$_2$), 2.43 (4H, sept, *J* = 6.9 Hz, -C(<u>H</u>)$(CH_3)_2$, [1.17 (12H, d, *J* = 7.0 Hz, -C(H)(C<u>H</u>$_3)_2$), 1.16 (12H, d, *J* = 7.0 Hz, -C(H)(C<u>H</u>$_3)_2$)]. ^{13}C NMR (125 MHz, 298 K, CD_3CN): δ 185.2 (2 × d, $^1J_{C,Ag}$ = 271/235 Hz), 150.5, 147.6, 125.8, 125.4 (d, $^3J_{CAg}$ = 7.3 Hz), 110.5, 29.2, 24.8, 23.9. IR (cm^{-1}): 3345 (w, br), 3215 (w, br), 2961 (s, sh), 2923 (m, sh), 2870 (w, sh), 1621 (s, sh), 1604 (s, sh), 1471 (s, sh), 1385 (m, sh), 1347 (s, sh), 1230 (m, sh), 1074 (w, sh), 943 (w, sh), 854 (m, sh), 749 (m, sh), 711 (m, sh). UV/Vis (CH_3CN, λ_{max}, nm): 212 (ε 7.90 × 10^4 $M^{-1}cm^{-1}$), 248 (ε 2.84 × 10^4 $M^{-1}cm^{-1}$), 296 (ε 2.59 × 10^3 $M^{-1}cm^{-1}$). Elemental analysis (%): Calcd for $C_{27}H_{38}N_4AgCl$·0.15 CH_2Cl_2: C, 56.74; H, 6.72; N, 9.75. Found: C, 57.03; H, 6.65; N, 9.38.

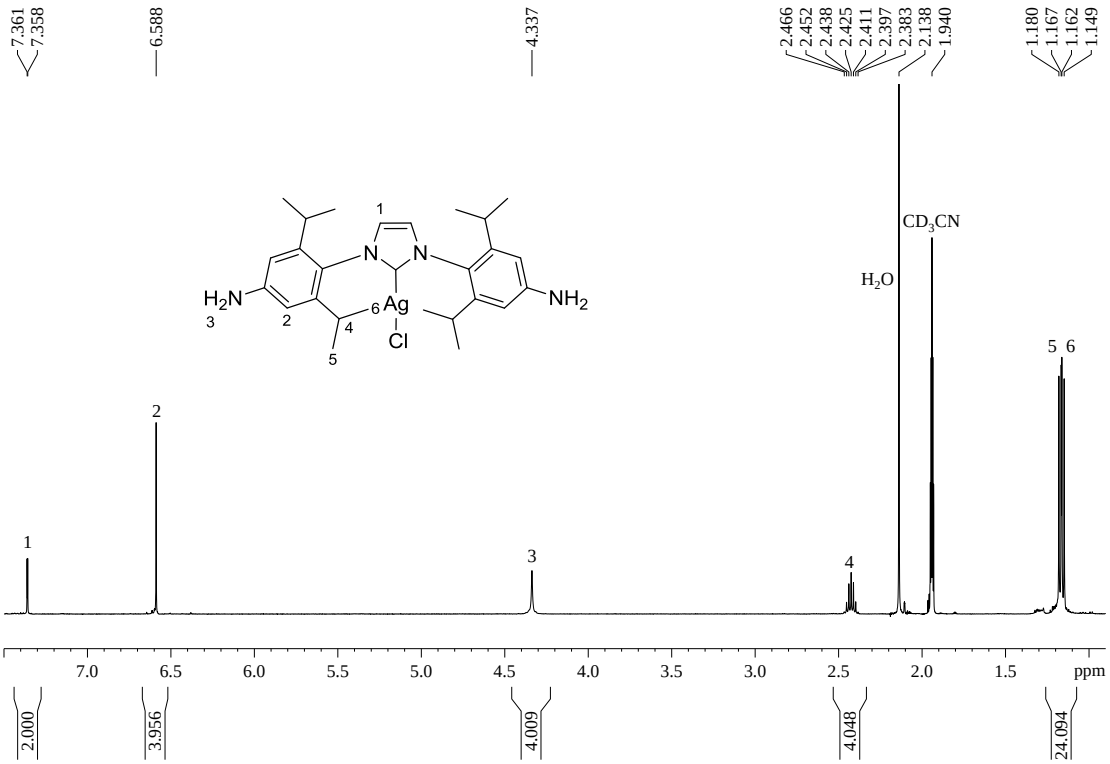

Figure S3. ^{1}H NMR of **C** in CD_3CN at 25 °C with assignments.

Synthesis of [N,N′-Bis(4-amino-2,6-diisopropylphenyl)-imidazol-2-ylidene]-chlorogold(I) (D)

According to an adapted literature procedure[6], **A** (104.53 mg, 0.23 mmol, 1.0 equiv) and Au(tht)Cl (73.63 mg, 0.23 mmol, 1.0 equiv) were dissolved in 20 mL of dichloromethane. A 10 mL aqueous solution of Na_2CO_3 (0.37 g, 3.5 mmol, 15 equiv) was added, and the biphasic mixture stirred rapidly for 30 minutes. The organic phase was separated, filtered, and evaporated to dryness under vacuum to yield a light brown powder, which was dried overnight over P_2O_5 (138.45 mg, 92 %). Crystals suitable for X-ray diffraction were grown from vapor diffusion of *n*-pentane into a concentrated DCM solution of **D**. ^{1}H NMR (400 MHz, 298 K, CD_3CN): δ 7.33 (2H, s, NC<u>H</u>C<u>H</u>N), 6.58 (4H, s, H^{Ar}), 4.34 (4H, s (br), -N<u>H</u>$_2$), 2.43 (4H, sept, *J* = 6.9 Hz, -C(<u>H</u>)$(CH_3)_2$, [1.23 (12H, d, *J* = 6.9 Hz, -C(H)(C<u>H</u>$_3)_2$), 1.15 (12H, d, *J* = 6.9 Hz, -C(H)(C<u>H</u>$_3)_2$). ^{13}C NMR (125 MHz, 298 K, CD_3CN): δ 176.3, 150.7, 147.7, 125.3, 125.2, 110.5, 29.4, 24.6, 24.0. IR (cm^{-1}): 3341 (w, br), 3214 (w, br), 2960 (s, sh), 2923 (m, sh), 2868 (w, sh), 1620 (s, sh), 1603 (s, sh), 1473 (s, sh), 1385 (m, sh), 1347 (s, sh), 1230 (s, sh), 1081 (w, sh), 943 (m, sh), 853 (s, sh), 747 (s, sh), 710 (m, sh). UV/Vis (CH_3CN, λ_{max}, nm): 212 (ε 7.18 × 10^4 $M^{-1}cm^{-1}$), 247 (ε 3.27 × 10^4 $M^{-1}cm^{-1}$), 295 (ε 3.35 × 10^3 $M^{-1}cm^{-1}$). Elemental analysis (%): Calcd for $C_{27}H_{38}N_4AuCl$: C, 49.81; H, 5.88; N, 8.61. Found: C, 49.55; H, 5.97; N, 8.39.

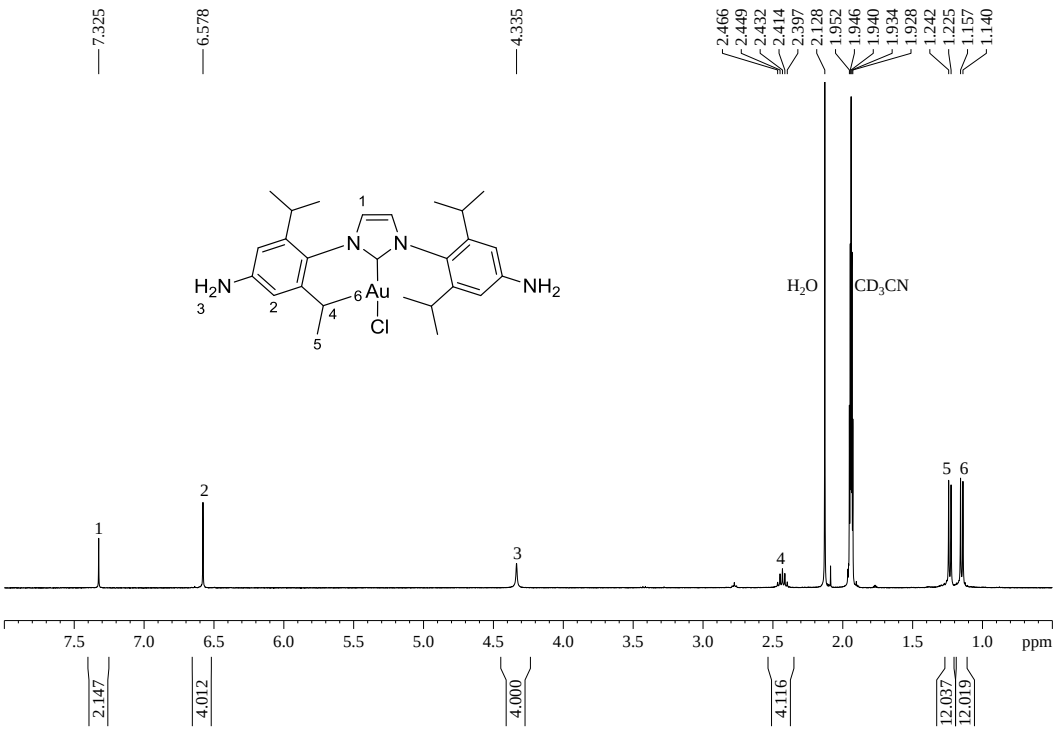

Figure S4. ^{1}H NMR of **D** in CD_3CN at 25 °C with assignments.

1.3 Synthesis and Characterization of 1

Zinc(II) triflimide (51.14 mg, 0.082 mmol, 4 equiv), 2-formylpyridine (23.3 μL, 0.24 mmol, 12 equiv) and **D** (79.57 mg, 0.12 mmol, 6 equiv) were added to 10 mL of acetonitrile under nitrogen which was stirred at 50 °C for 16 h to produce a dark yellow solution. The reaction volume was then reduced to 2 mL *via* vacuum and diethyl ether (5 mL) was added to precipitate a yellow powder from solution. The supernatant was decanted, the yellow powder rinsed twice with 5 mL portions of diethyl ether, and then dried under vacuum over P_2O_5. Yield: 0.12 g (79 %). ^{1}H NMR (500 MHz, CD_3CN, 298 K): δ 9.30 (1H, s, A5), 9.15 (1H, s, B5), 9.08 (1H, s, C5), 8.91 (1H, d, *J* = 5.0 Hz, A1), 8.66 (1H, d, *J* = 4.8 Hz, C1), 8.35 (2H, m, C3/A3), 8.26 (3H, m, A4/C4/B3), 8.10 (1H, d, *J* = 5.0 Hz, B1), 8.05 (1H, d, *J* = 7.8 Hz, B4), 7.90 (1H, t, *J* = 4.8 Hz, A2), 7.79 (1H, t, *J* = 5.0 Hz, C2), 7.69 (1H, t, *J* = 5.0 Hz, B2), 7.59 (1H, s, A8), 7.55 (1H, d, ^{TS}J = 1.9 Hz, C8), 7.51 (1H, d, *J* = 2.2 Hz, B6), 7.19 (1H, d, ^{TS}J = 1.9 Hz, B8), 7.16 (1H, d, *J* = 2.4 Hz, A6), 7.01 (2H, m, C7/B7), 6.82 (1H, d, *J* = 2.4 Hz, A7),

6.76 (1H, d, *J* = 2.3 Hz, C6), 2.62 (2H, sept, *J* = 6.9 Hz, C9), 2.44 (2H, sept, *J* = 6.9 Hz, B10), 2.34 (2H, sept, *J* = 6.7 Hz, A9), 2.28 (2H, sept, *J* = 6.7 Hz, A10), 2.07 (2H, sept, *J* = 6.9 Hz, B9), 1.90 (2H, sept, *J* = 6.9 Hz, C10), 1.20 (3H, d, *J* = 6.9 Hz, B11), 1.16 (3H, d, *J* = 6.7 Hz, A11), 1.12 (9H, m, C11/C12/B12), 0.97 (9H, m, B13/A12/C13), 0.74 (3H, d, *J* = 6.7 Hz, A13), 0.48 (3H, d, *J* = 6.9 Hz, C14), 0.38 (3H, d, *J* = 6.9 Hz, B14), 0.29 (3H, d, *J* = 6.7 Hz, A14). ^{13}C NMR (125 MHz, CD_3CN, 298 K): δ 176.6, 175.5, 175.4, 164.9, 164.4, 162.2, 151.8, 150.8, 150.1, 149.8, 149.5, 149.4, 148.9, 148.7, 148.0, 147.4, 147.2, 147.0, 146.9, 144.4, 144.0, 143.1, 143.0, 136.5, 135.7, 135.4, 135.2, 132.7, 132.5, 132.1, 131.5, 125.0, 124.7, 122.2, 121.7, 121.3, 120.9, 119.6, 117.8, 117.5, 117.1, 110.6, 30.5, 30.1, 29.9, 29.7, 29.5, 29.3, 25.2, 25.0, 24.6, 24.5, 24.4, 24.1, 23.9, 23.7, 23.6, 23.3, 23.2, 23.0. ^{19}F NMR (376 MHz, CD_3CN, 298 K): δ −80.5. IR (cm^{-1}): 2970 (w, sh), 2931 (w, sh), 2876 (w, sh), 1631 (w, sh), 1595 (w, sh), 1471 (w, sh), 1446 (w, sh), 1422 (w, sh), 1389 (w, sh), 1348 (m, sh), 1225 (m, sh), 1184 (s, sh), 1134 (s, sh), 1056 (s, sh), 1020 (w, sh), 975 (w, sh), 944 (w, sh), 904 (w, sh), 879 (w, sh), 778 (w, sh), 740 (w, sh), 709 (w, sh). UV/Vis (CH_3CN, λ_{max}, nm): 240 (ε 2.20 × 10^5 $M^{-1}cm^{-1}$), 290 (ε 1.37 × 10^5 $M^{-1}cm^{-1}$), 330 (ε 1.41 × 10^5 $M^{-1}cm^{-1}$), 460 (ε 3.23 × 10^3 $M^{-1}cm^{-1}$). HRMS (ESI^+): *m/z* calcd for $Zn_4Au_6Cl_6C_{240}H_{264}N_{39}F_{18}O_{12}S_6$ ([**2**]$^{+5}$): 1215.4514; found: 1215.4575. Elemental analysis (%): Calcd for $C_{250}H_{264}Au_6Zn_4Cl_6F_{48}N_{44}O_{32}S_{16}$: C, 40.15; H, 3.56; N, 8.24. Found: C, 40.40; H, 3.60; N, 7.81.

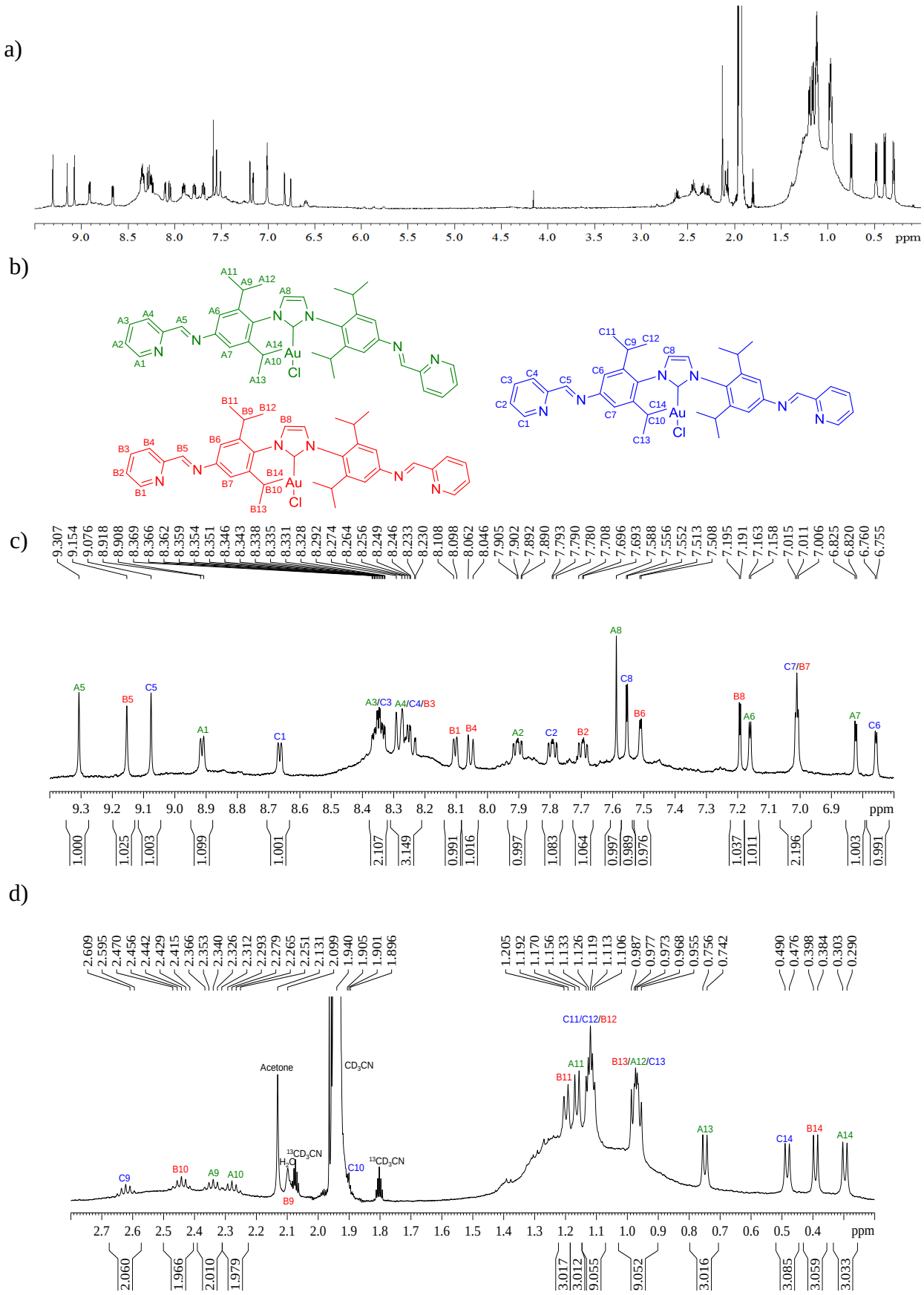

Figure S5. a) ^{1}H NMR spectrum of **1** in CD_3CN at 25 °C; the three ligand environments of **1** are defined (b), and assigned to the aromatic (c) and aliphatic (d) regions of the spectrum.

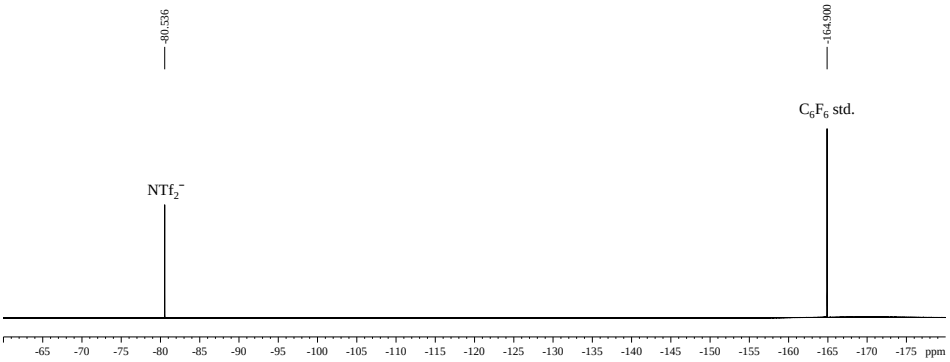

Figure S6. ^{19}F NMR spectrum of **1** in CD_3CN at 25 °C.

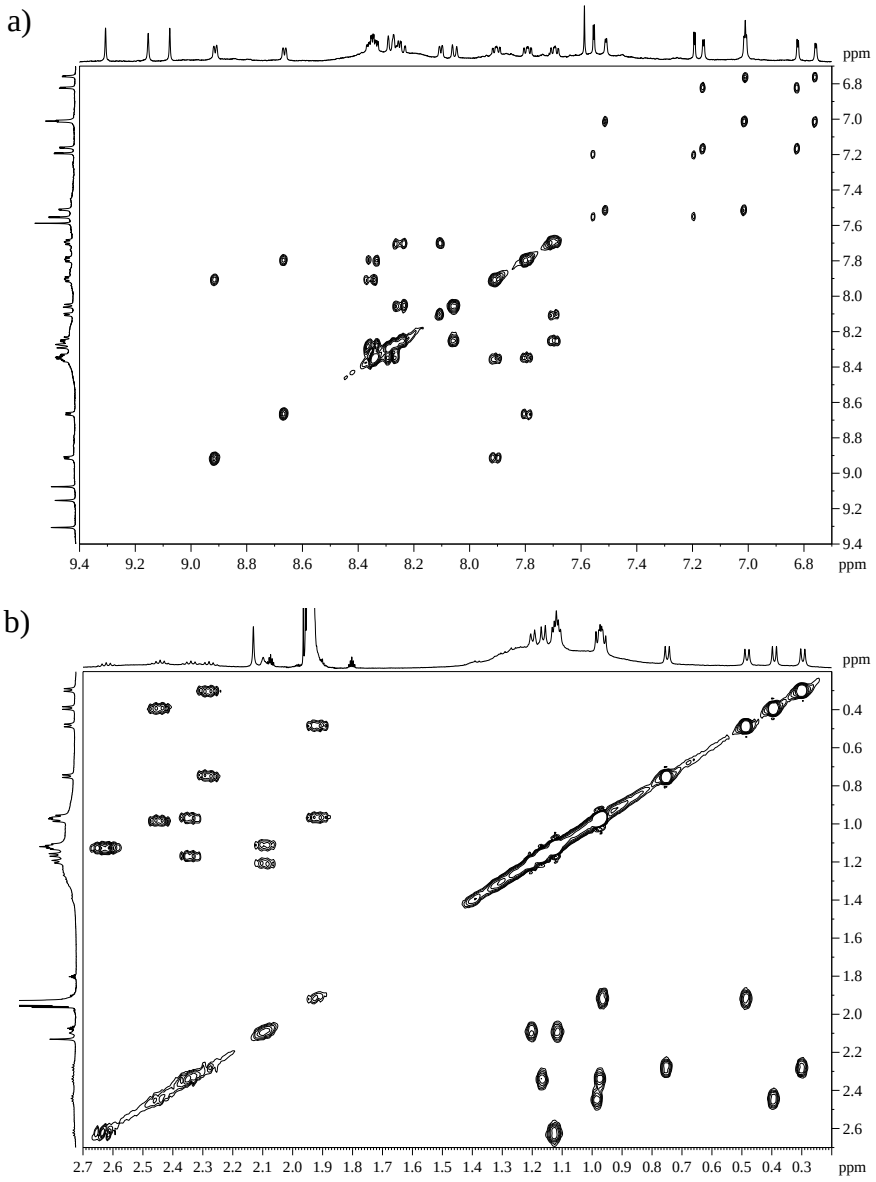

Figure S7. $^1H - ^1H$ COSY of (a) the aromatic and (b) the aliphatic regions of **1** in CD_3CN at 25 °C.

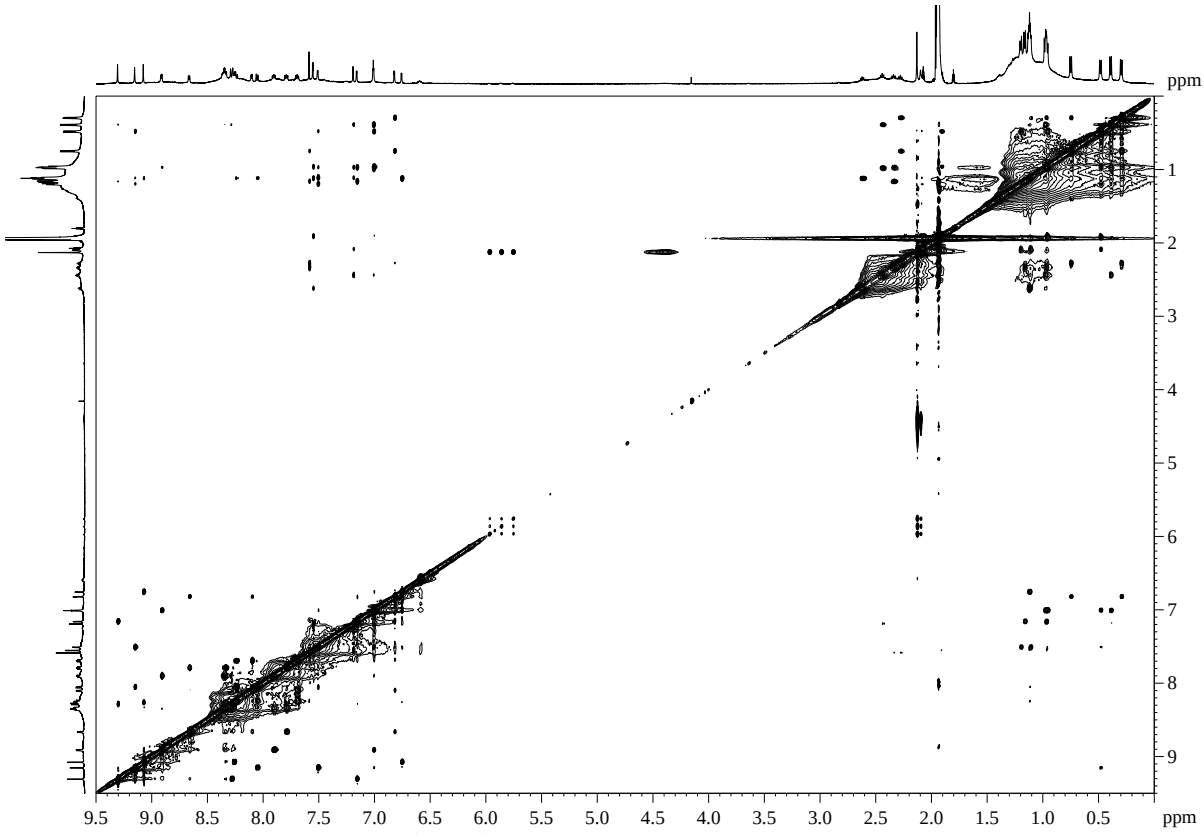

Figure S8. $^{1}H - {}^{1}H$ NOESY of **1** in CD_3CN at 25 °C.

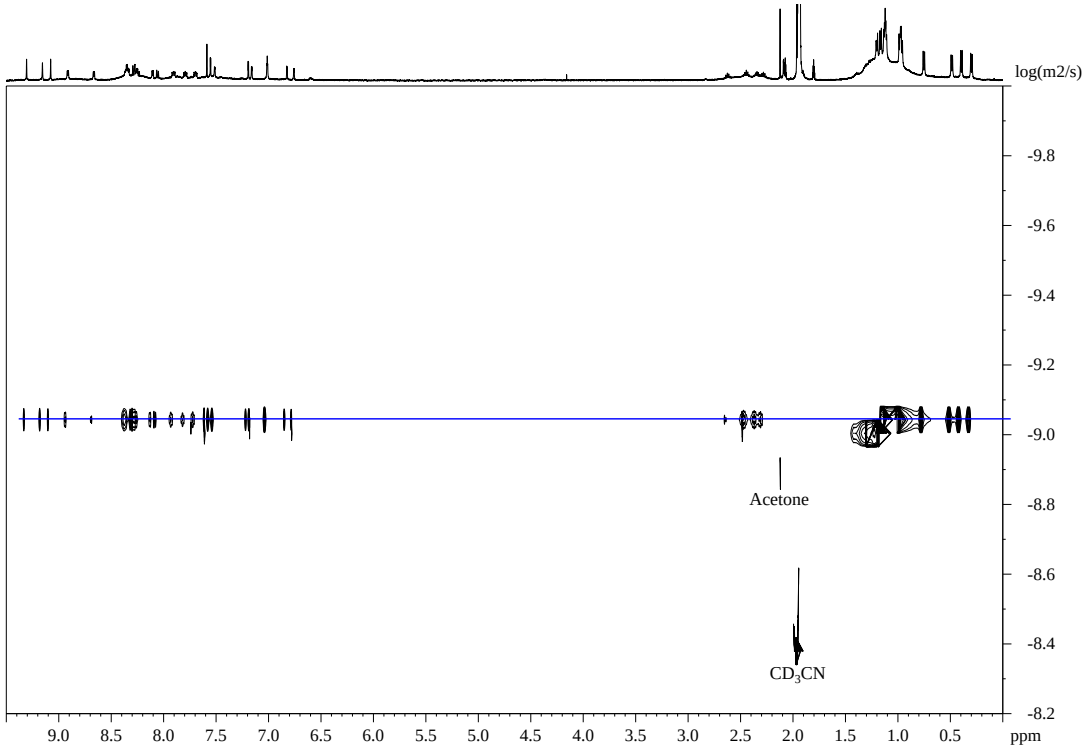

Figure S9. DOSY spectrum of **1** in CD_3CN at 25 °C. The cage is observed as a single band at $\log(D) = -9.06$ (8.69×10^{-10} m^2/s).

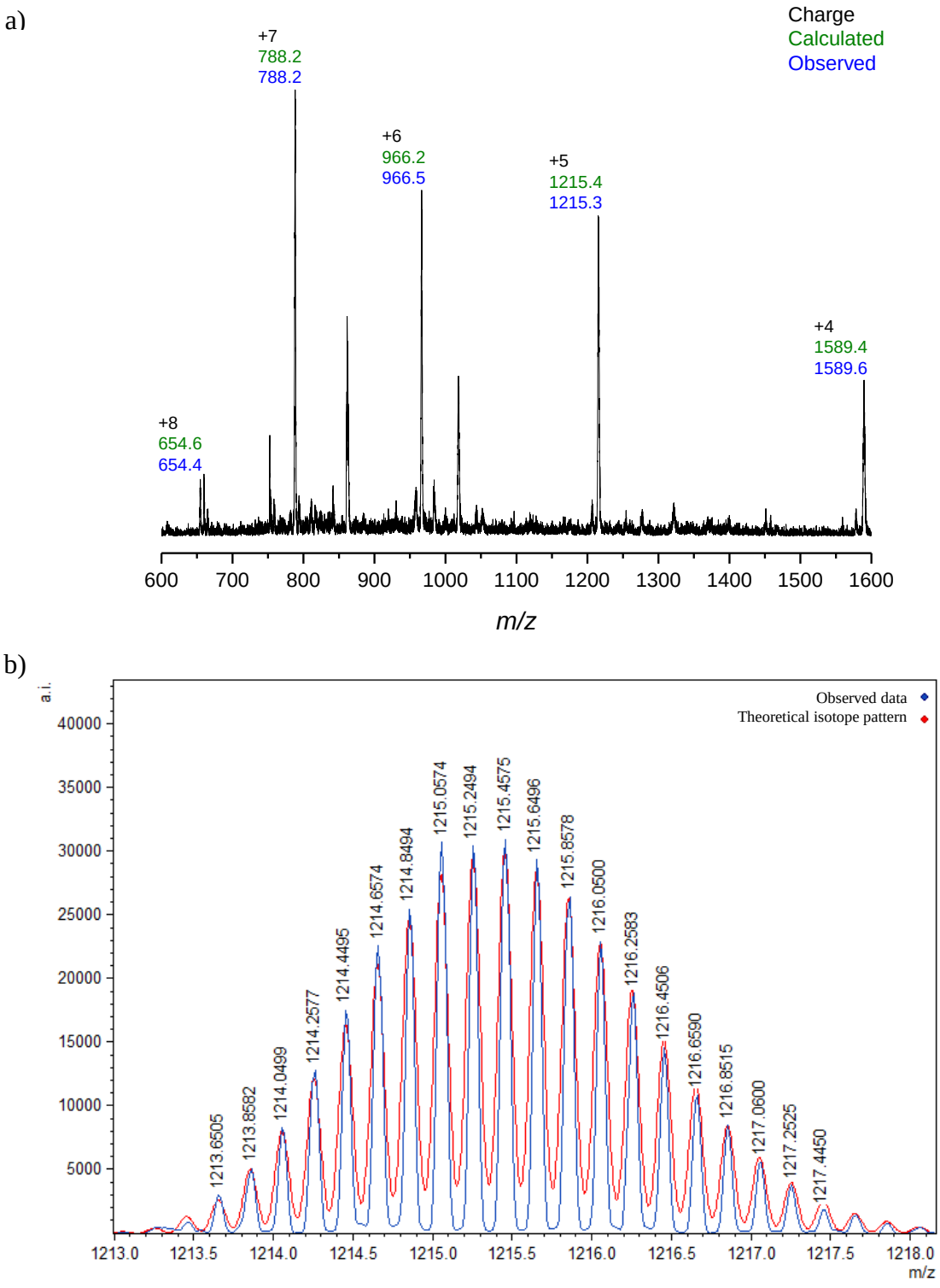

Figure S10. a) ESI-MS of **1** in CH_3CN; b) simulated (red trace) and recorded (blue trace) HRMS spectrum (*m/z*) of $[\mathbf{1}]^{+5}$ in CH_3CN: Calc. for $[\{Zn_4Au_6Cl_6C_{240}H_{264}N_{36}\}\{(CF_3SO_2)_2N\}_3]^{+5}$: 1215.4514; found: 1215.4575.

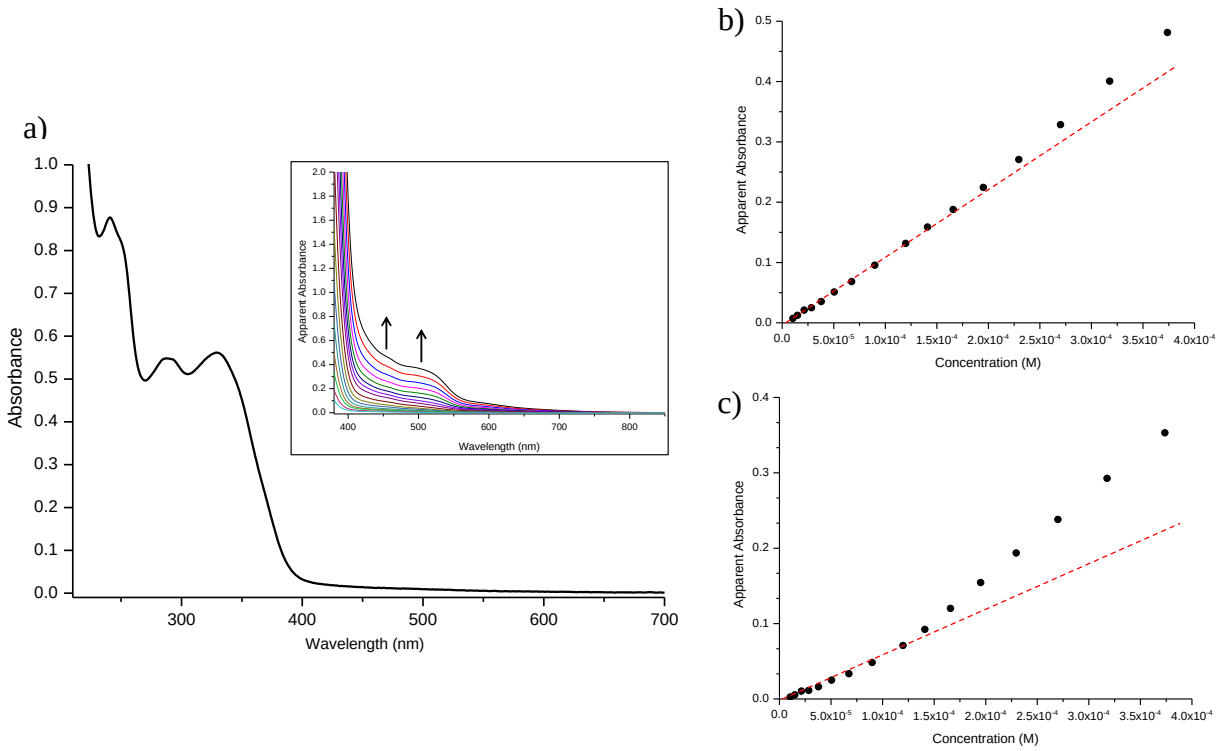

Figure S11. a) UV-Vis absorption spectrum of **1** in dry acetonitrile (3.99×10^{-6} M). Inset: UV-Vis absorption spectra changes of **1** in dry acetonitrile as the concentration increases from 1.05×10^{-5} to 3.74×10^{-4} M; a plot of absorbance at b) 460 nm and c) 510 nm as a function of concentration for **1**. Experimental (●) and theoretical (---) fit to Beer's Law.

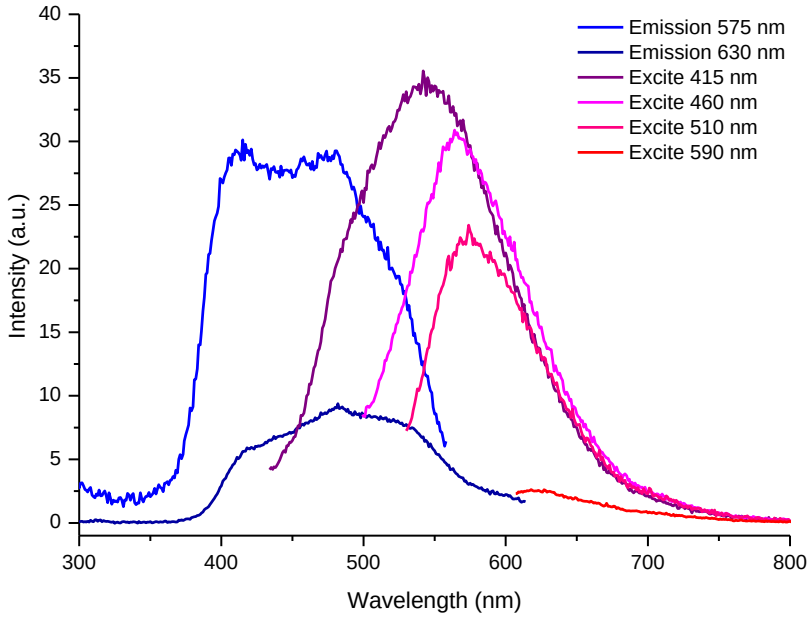

Figure S12. Excitation and emission spectra of **1** in dry acetonitrile.

Luminescent bands at 415, 460 and 510 nm were observed in the excitation spectrum of **1** (Figure S12). The band at 415 nm in the spectrum is assigned to an intramolecular transition occurring within the single cage (from adjacent ligands). The absorption bands above 450 nm are assigned as transitions associated with extended $Au^{I\cdots}Au^{I}$ interactions arising from intermolecular interactions of aggregated cages, as observed with related systems[7] (see Figure S22 for a model of cage aggregation). Upon increasing the concentration of **1** (Figure S11), a plot of absorbance at 460 nm and 510 nm against the concentration were not found to obey Beer's law but showed a nonlinear relationship, which supported our hypothesis for aggregation of the cages in solution. Upon photoexcitation, **1** emits strongly at 575 nm and weakly at 630 nm.

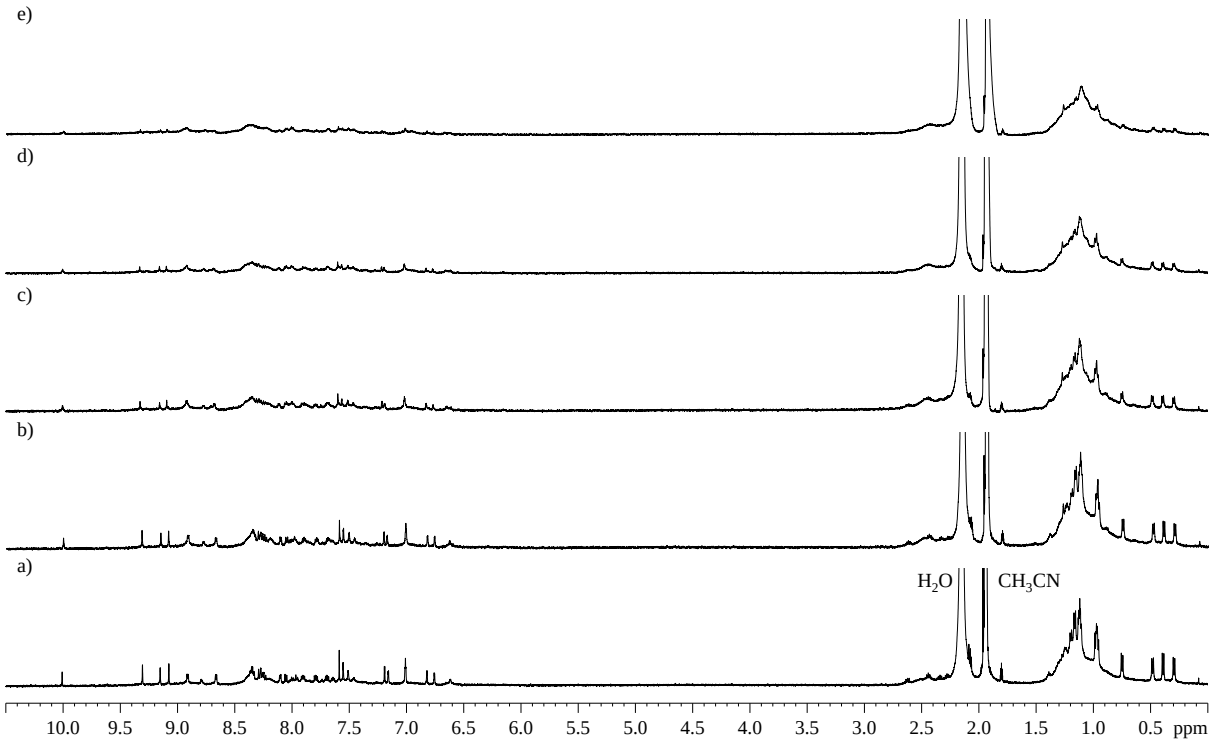

Figure S13. ^{1}H NMR titration of $AgBF_4$ into a solution of **1** in CD_3CN at 25 °C: a) 0.0 equiv., b) 1.0 equiv., c) 2.1 equiv., d) 3.1 equiv., and e) 6.3 equiv.; see Figure S5 for peak assignment.

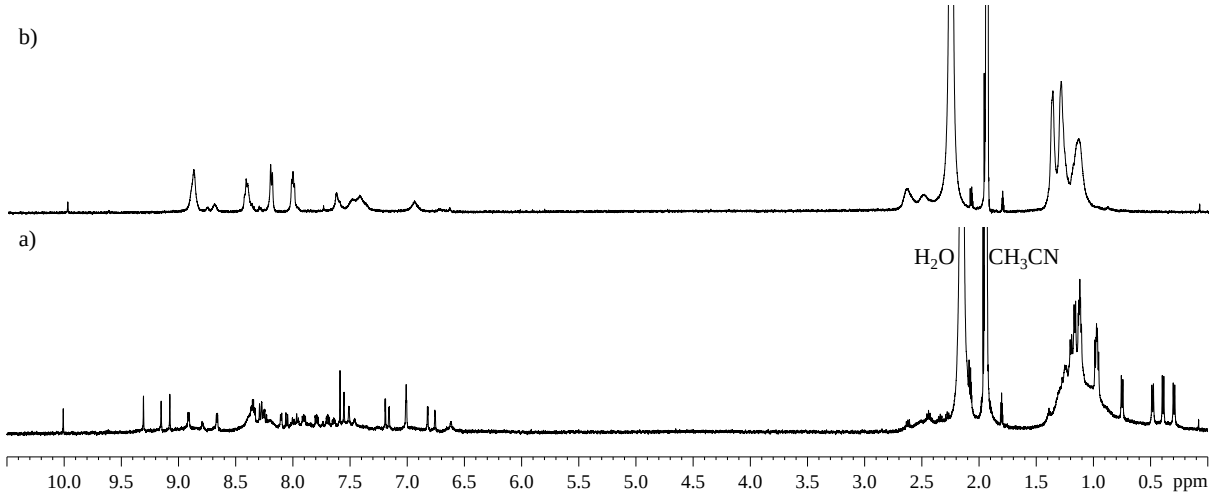

Figure S14. When 6.0 equiv. of $Zn(NTf_2)_2$ were added to **1** (a), dissociation of the cage framework was observed (b) in the ^{1}H NMR spectra in CD_3CN; see Figure S5 for peak assignment.

1.4 Synthesis and Characterization of 2

Cadmium(II) triflimide (34.55 mg, 0.051 mmol, 4 equiv), 2-formylpyridine (14.7 μL, 0.15 mmol, 12 equiv) and **D** (50.07 mg, 0.077 mmol, 6 equiv) were added to 10 mL of acetonitrile under nitrogen which was stirred at 50 °C for 16 h to produce a dark yellow solution. The reaction volume was then reduced to 2 mL *via* vacuum and diethyl ether (5 mL) to precipitate a yellow powder from solution. The supernatant was decanted, the yellow powder rinsed twice with 5 mL portions of diethyl ether, and then dried under vacuum over P_2O_5. Yield: 90.42 mg (92 %). ^{1}H NMR (500 MHz, CD_3CN, 298 K): δ 9.27 (1H, s, $J_{Cd,H}$ = 18.6 Hz, A5), 9.24 (1H, s, $J_{Cd,H}$ = 18.3 Hz, B5), 9.10 (1H, s, $J_{Cd,H}$ = 15.2 Hz, C5), 8.69 (1H, d, *J* = 4.8 Hz, A1), (1H, d, *J* = 4.6 Hz, C1), 8.35 (3H, m, A3/C3/B1), 8.26 (2H, m, A4/C4), 8.21 (1H, t, *J* = 7.3 Hz, B3), 8.07 (1H, d, *J* = 7.6 Hz, B4), 7.83 (1H, t, *J* = 6.5 Hz, A2), 7.77 (1H, t, *J* = 6.5 Hz, C2), 7.69 (1H, t, *J* = 6.5 Hz, B2), 7.61 (1H, d, *J* = 2.2 Hz, B6), 7.56 (1H, s, A8), 7.52 (1H, d, ^{TS}J = 1.9 Hz, C8), 7.19 (1H, d, ^{TS}J = 1.9 Hz, B8), 7.12 (1H, d, *J* = 2.1 Hz, A6), 7.09 (1H, d, *J* = 2.3 Hz, B7), 6.95 (1H, d, *J* = 2.3 Hz, A7), 6.91 (1H, d, *J* = 2.2 Hz, C7), 6.83 (1H, d, *J* = 2.2 Hz, C6), 2.60 (2H, sept, *J* = 6.8 Hz, C9), 2.47 (2H, sept, *J* = 6.9 Hz, B10), 2.34 (2H, sept, *J* = 6.9 Hz, A9), 2.23 (2H, sept, *J* = 6.9 Hz, A10), 2.07 (2H, sept, *J* = 6.9 Hz, B9), 1.90 (2H, sept, *J* = 6.8 Hz, C10), 1.22 (3H, d, *J* = 6.7 Hz, B11), 1.15 (3H, d, *J* = 6.9 Hz, A11), 1.13 (9H, m, C11/C12/B12), 1.00 (3H, d, *J* = 6.9 Hz, B13), 0.96 (3H, d, *J* = 6.8 Hz, A12), 0.93 (3H, d, *J* = 6.8 Hz, C13), 0.74 (3H, d, *J* = 6.8 Hz, A13), 0.50 (3H, d, *J* = 6.9 Hz, C14), 0.38 (3H, d, *J* = 6.9 Hz, B14), 0.32 (3H, d, *J* = 6.8 Hz, A14). ^{13}C NMR (125 MHz, CD_3CN, 298 K): δ 175.9, 175.4, 175.0, 163.9, 163.5, 161.8, 151.7, 151.4, 151.2, 150.8, 149.8, 149.4, 148.9, 148.6, 148.1, 147.6, 147.4, 147.0, 143.9, 143.5, 142.7, 140.1, 138.1, 136.5, 135.3, 135.2, 132.7, 132.4, 132.1, 131.5, 131.0, 125.1, 124.9, 124.7, 122.1, 121.5, 119.8, 119.6, 117.1, 116.8, 116.7, 110.5, 30.4, 30.0, 29.9, 29.6, 29.5, 29.4, 29.3, 25.4, 24.7, 24.6, 24.4, 24.1, 23.9, 23.8, 23.6, 23.4, 23.0, 22.5. ^{19}F NMR (376 MHz, CD_3CN, 298 K): δ

−80.6. IR (cm^{-1}): 2966 (w, sh), 2928 (w, sh), 2871 (w, sh), 1632 (w, sh), 1593 (w, sh), 1471 (w, sh), 1446 (w, sh), 1423 (w, sh), 1389 (w, sh), 1348 (m, sh), 1224 (m, sh), 1184 (s, sh), 1134 (s, sh), 1056 (s, sh), 1016 (w, sh), 974 (w, sh), 944 (w, sh), 903 (w, sh), 878 (w, sh), 778 (w, sh), 740 (w, sh), 709 (w, sh). UV/Vis (CH_3CN, λ_{max}, nm): 245 (ε $2.02 \times 10^5\ M^{-1}cm^{-1}$), 292 (ε $1.32 \times 10^5\ M^{-1}cm^{-1}$), 328 (ε $1.31 \times 10^5\ M^{-1}cm^{-1}$), 435 (ε $1.95 \times 10^3\ M^{-1}cm^{-1}$). HRMS ($ESI^+$): *m/z* calcd for $Cd_4Au_6Cl_6C_{240}H_{264}N_{39}F_{18}O_{12}S_6$ ($[\mathbf{1}]^{+5}$): 1253.0333; found: 1253.0340. Elemental analysis (%): Calcd for $C_{250}H_{264}Au_6Cd_4Cl_6F_{48}N_{44}O_{32}S_{16}$: C, 39.17; H, 3.47; N, 8.04. Found: C, 39.31; H, 3.53; N, 7.69.

Satellite signals associated with the imines are attributed to *J*-coupling with the two spin-1/2 isotopes of cadmium.[8]

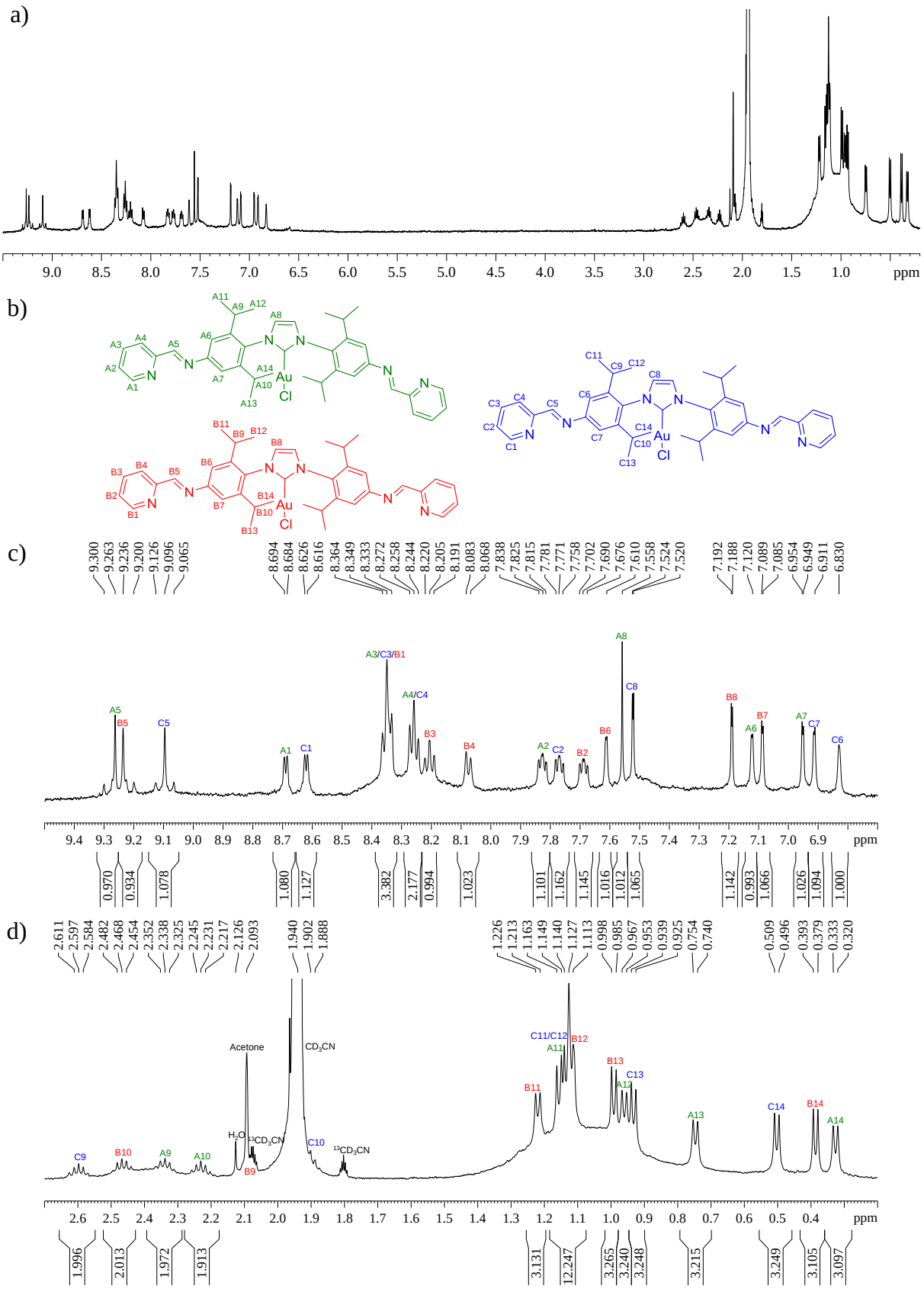

Figure S15. a) ^{1}H NMR spectrum of **2** in CD_3CN at 25 °C; the three ligand environments of **2** are defined (b), and assigned to the aromatic (c) and aliphatic (d) regions of the spectrum.

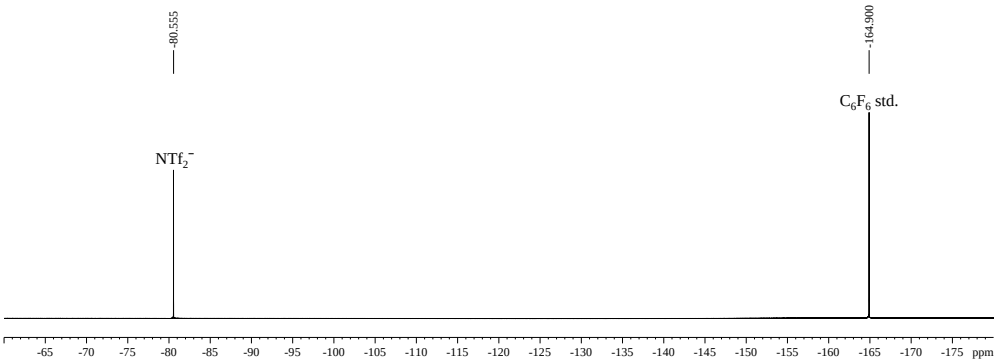

Figure S16. ^{19}F NMR spectrum of **2** in CD_3CN at 25 °C.

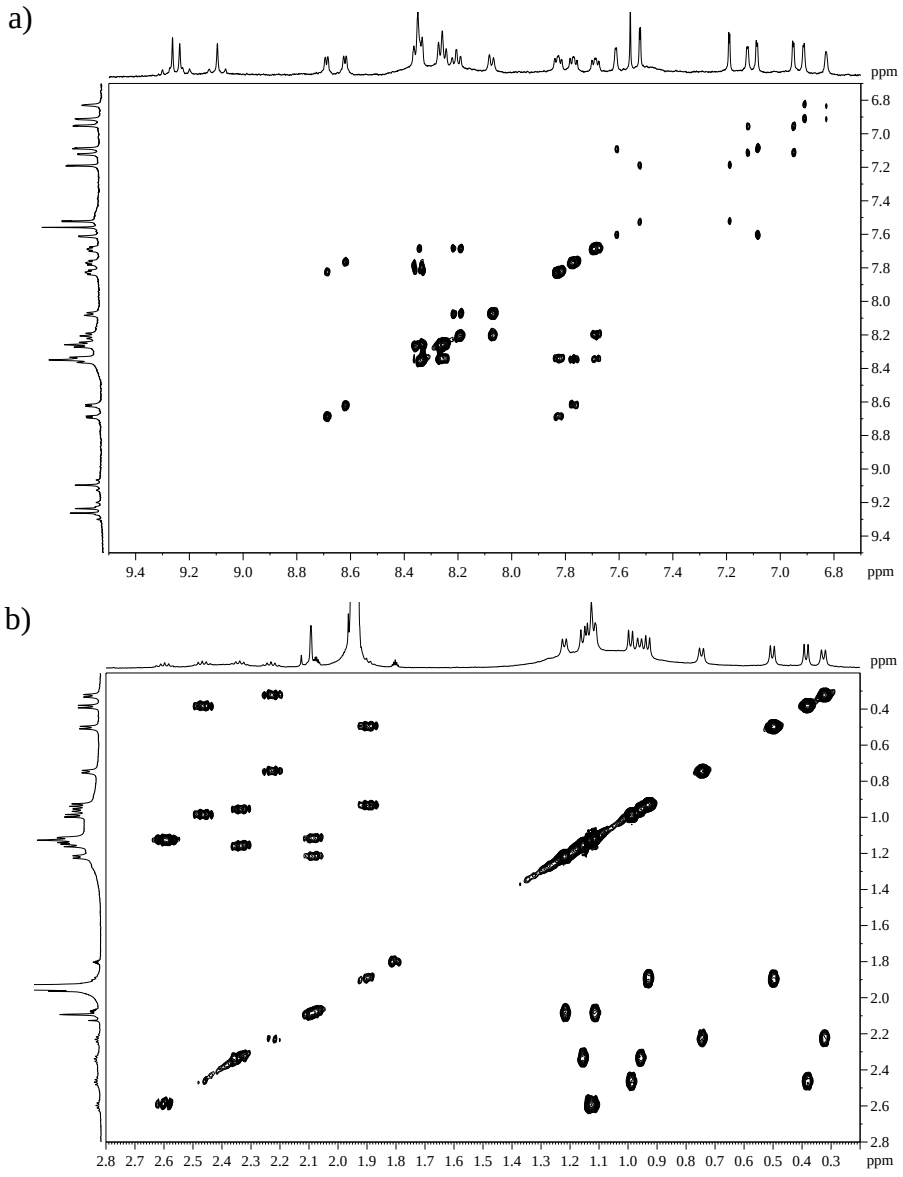

Figure S17. $^1H - ^1H$ COSY of (a) the aromatic and (b) the aliphatic regions of **2** in CD_3CN at 25 °C.

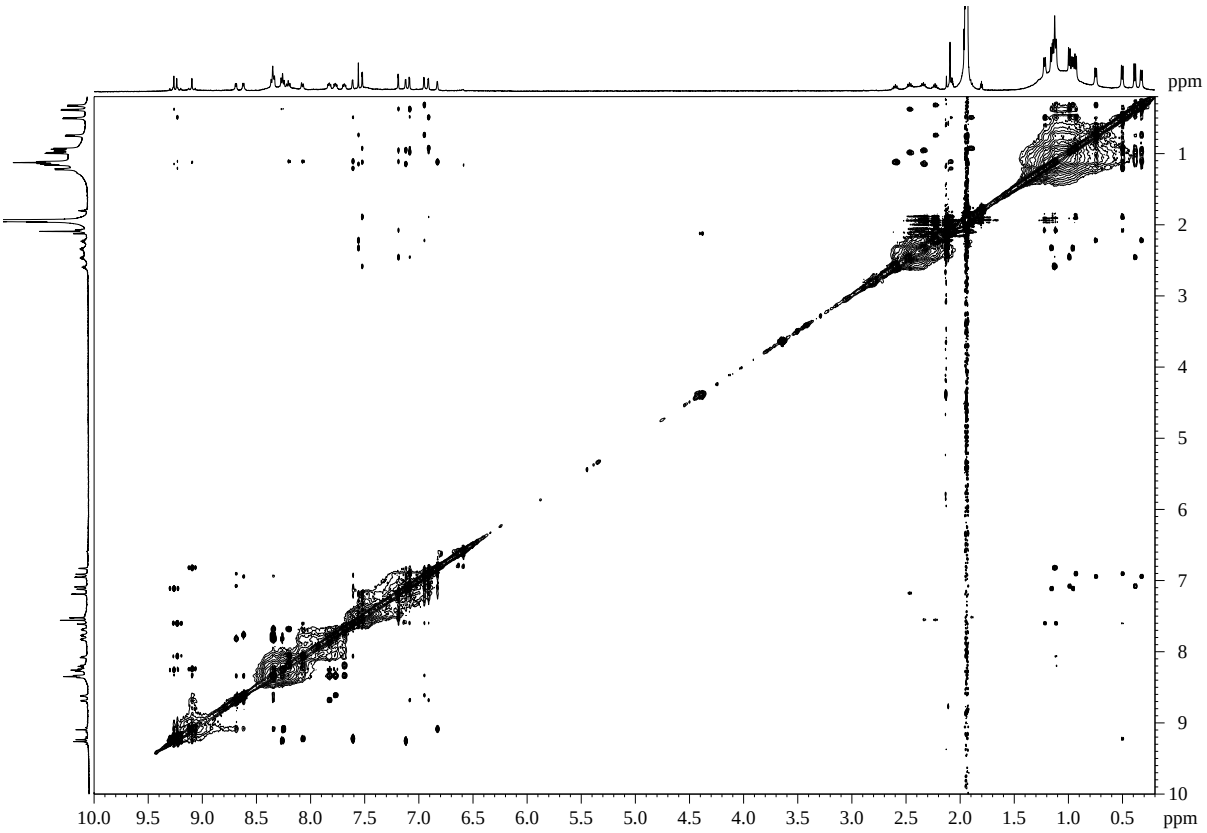

Figure S18. $^{1}H - {}^{1}H$ NOESY of **2** in CD_3CN at 25 °C.

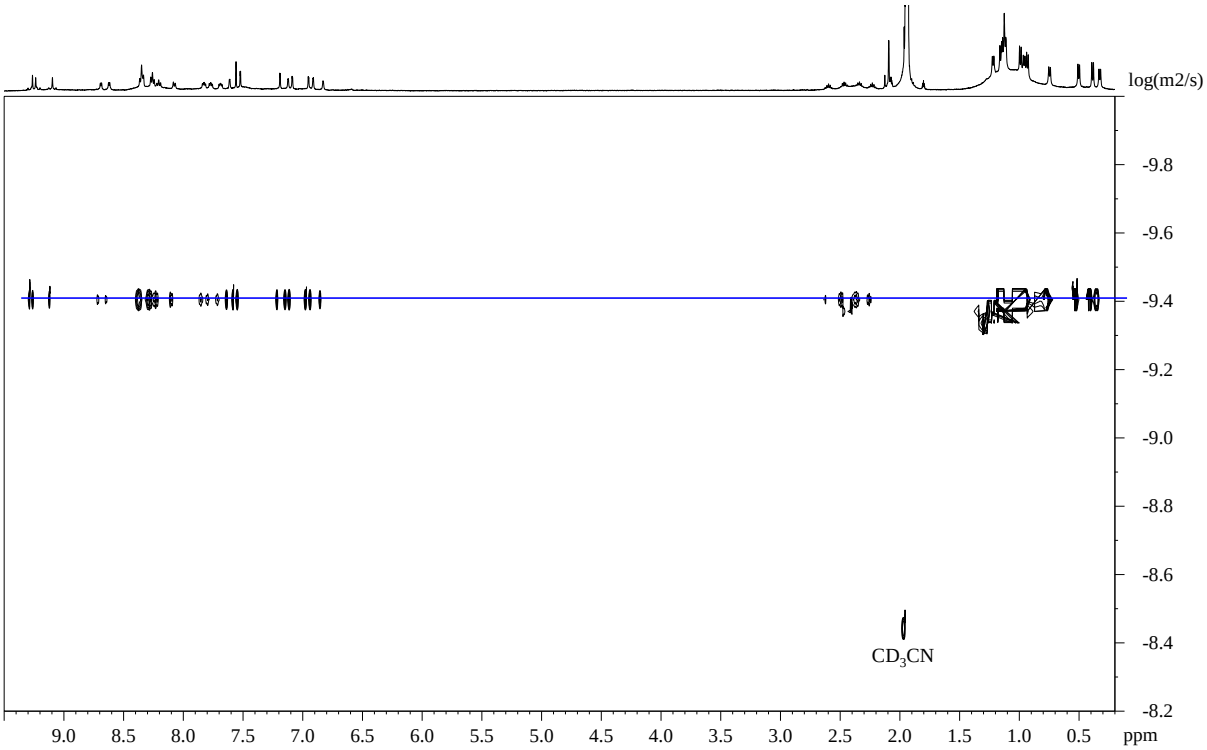

Figure S19. DOSY spectrum of **2** in CD_3CN at 25 °C. The cage is observed as a single band at log(D) = –9.42 (3.76×10^{-10} m^2/s).

a)

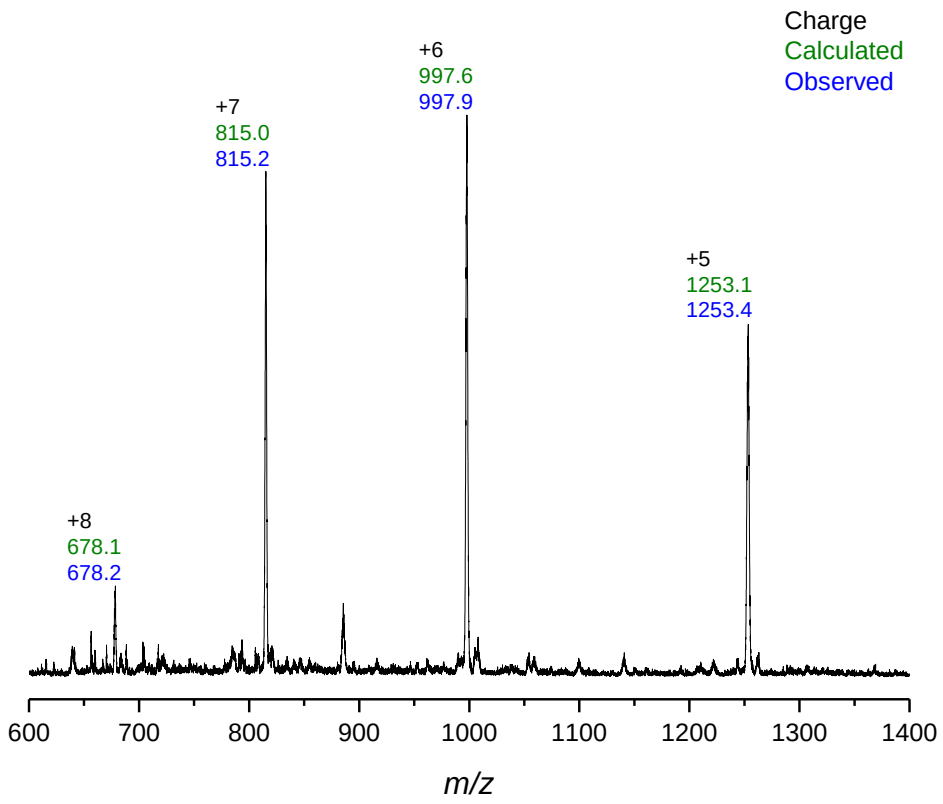

b)

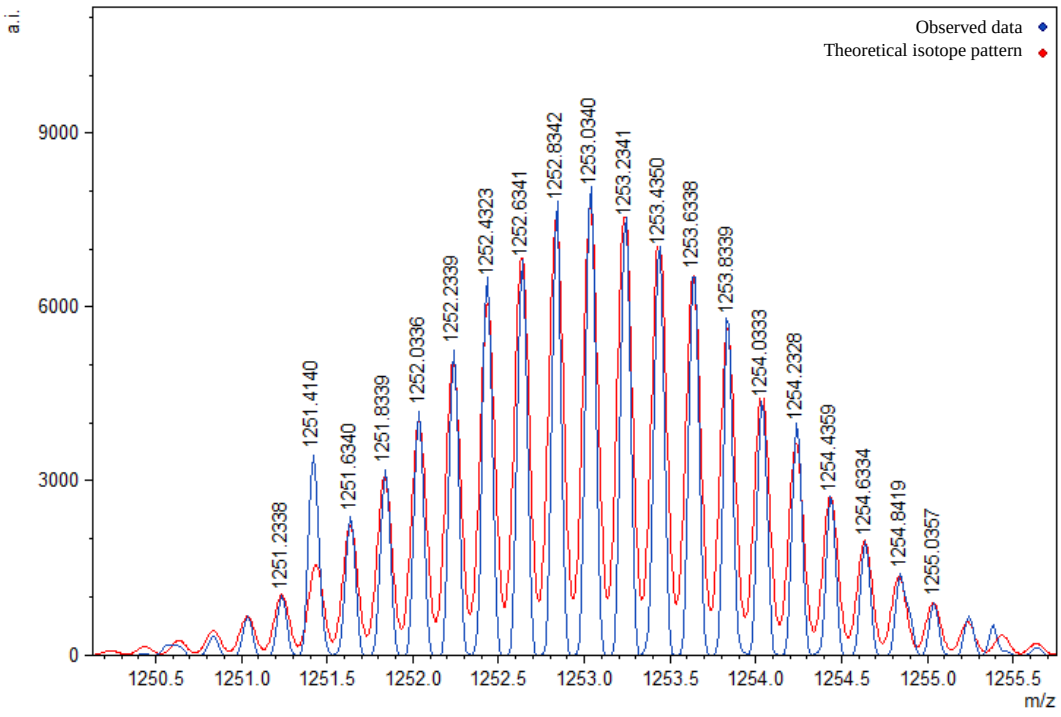

Figure S20. a) ESI-MS of **2** in CH_3CN; b) simulated (red trace) and recorded (blue trace) HRMS spectrum (*m/z*) of $[\mathbf{2}]^{+5}$ in CH_3CN: Calc. for $[\{Cd_4Au_6Cl_6C_{240}H_{264}N_{36}\}\{(CF_3SO_2)_2N\}_3]^{+5}$: 1253.0333; found: 1253.0340.

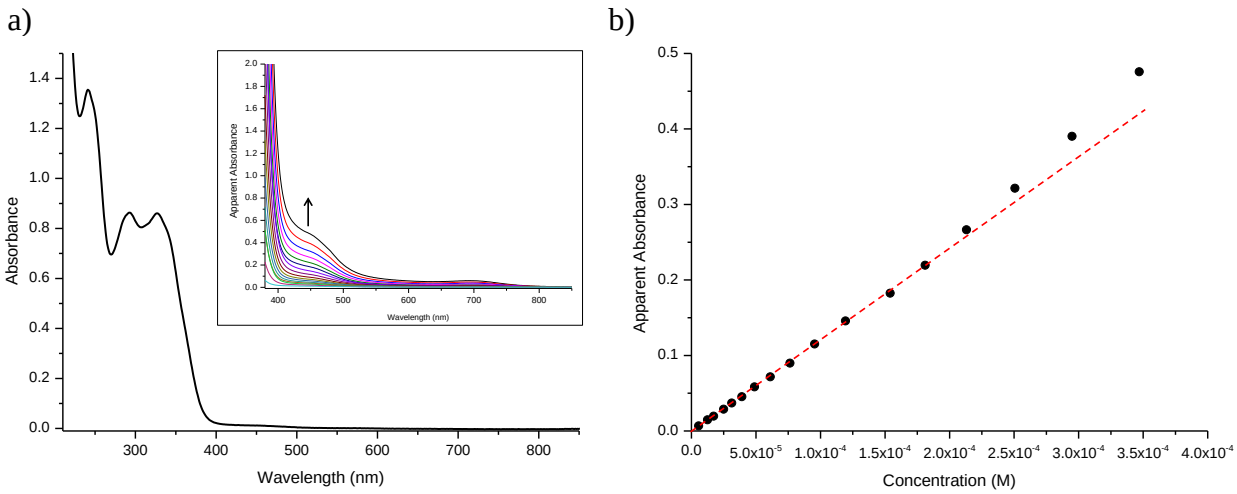

Figure S21. a) UV-Vis absorption spectrum of **2** in dry acetonitrile (6.55×10^{-6} M). Inset: UV-Vis absorption spectra changes of **2** in dry acetonitrile as the concentration increases from 5.61×10^{-6} to 3.47×10^{-4} M; b) a plot of absorbance at 450 nm as a function of concentration for **2**. Experimental (●) and theoretical (---) fit to Beer's Law.

Luminescent bands at 410 and 450 nm in the excitation spectrum of **2** were observed (Figure S22). The band at 410 nm is assigned to an intramolecular transition occurring within the single cage (from adjacent ligands). The absorption band at 450 nm is assigned to a transition associated with extended $Au^{I\cdots}Au^{I}$ interactions arising from intermolecular interactions of aggregated cages, as observed with related systems.[7] Upon increasing the concentration of **2** (Figure S21), a plot of absorbance at 450 nm against the concentration was not found to obey Beer's law but showed a nonlinear relationship, which supported our hypothesis for aggregation of the cages in solution. Upon photoexcitation, **2** emits strongly at 525 nm and weakly at 650 nm.

a)

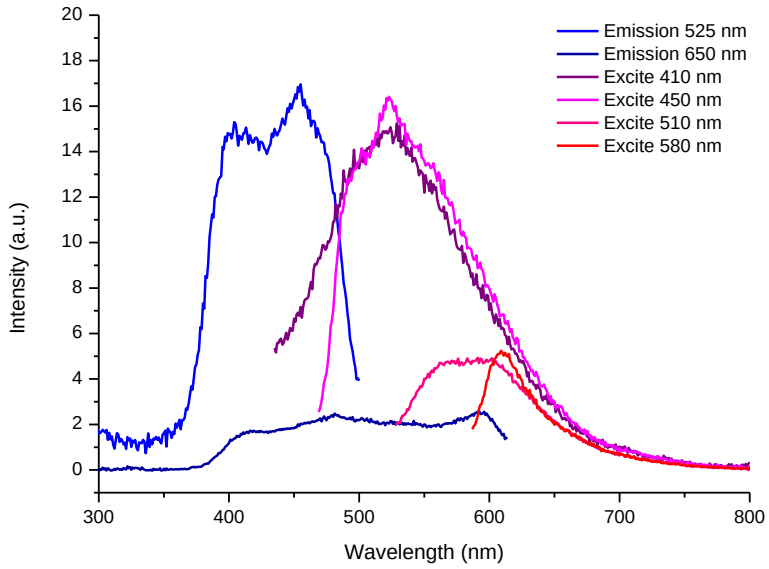

b)

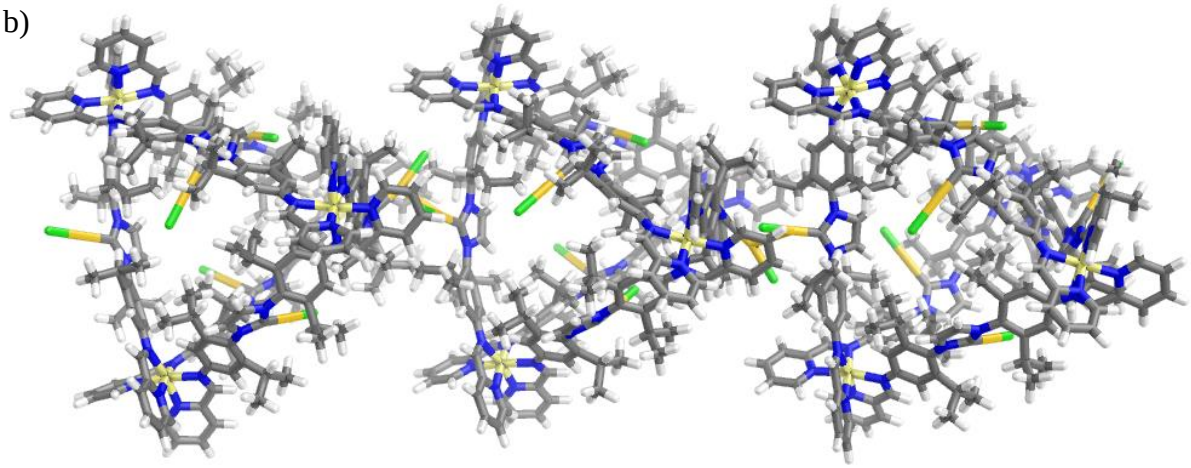

c)

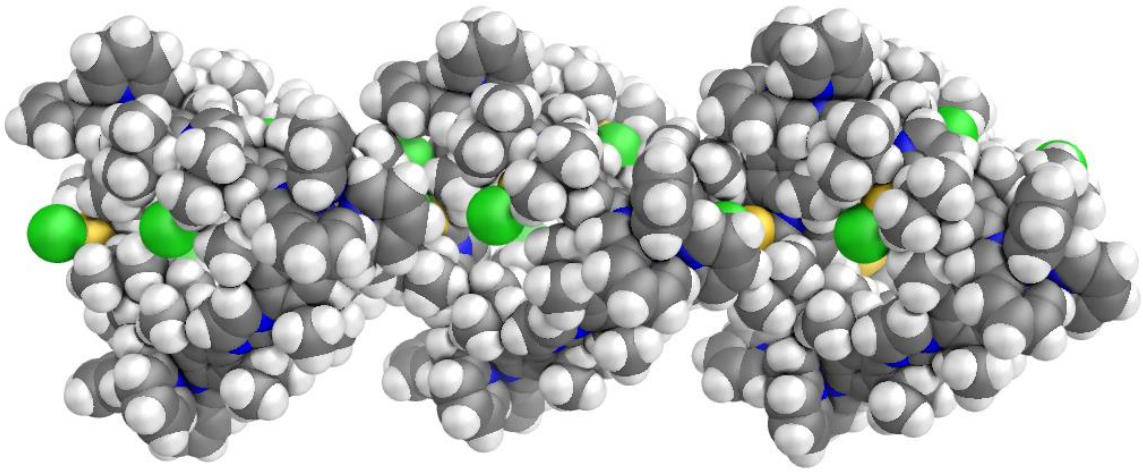

Figure S22. a) Excitation and emission spectra of **2** in dry acetonitrile. To model the potential intermolecular cage interactions, an energy minimized model[9] of three aggregated cages (**2**) is shown in wireframe (b) and space-filling (c).

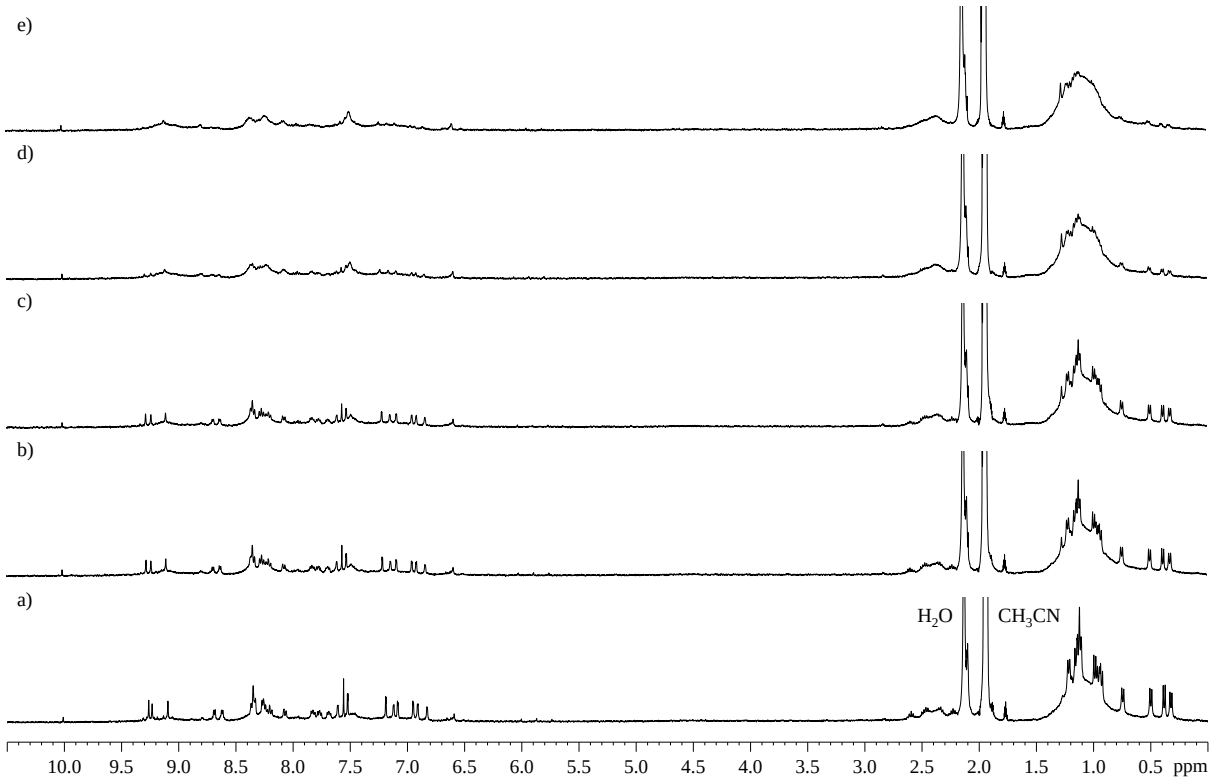

Figure S23. ^{1}H NMR titration of $AgBF_4$ into a solution of **2** in CD_3CN at 25 °C: a) 0.0 equiv., b) 1.0 equiv., c) 2.1 equiv., d) 3.1 equiv., and e) 6.3 equiv.; see Figure S13 for peak assignment.

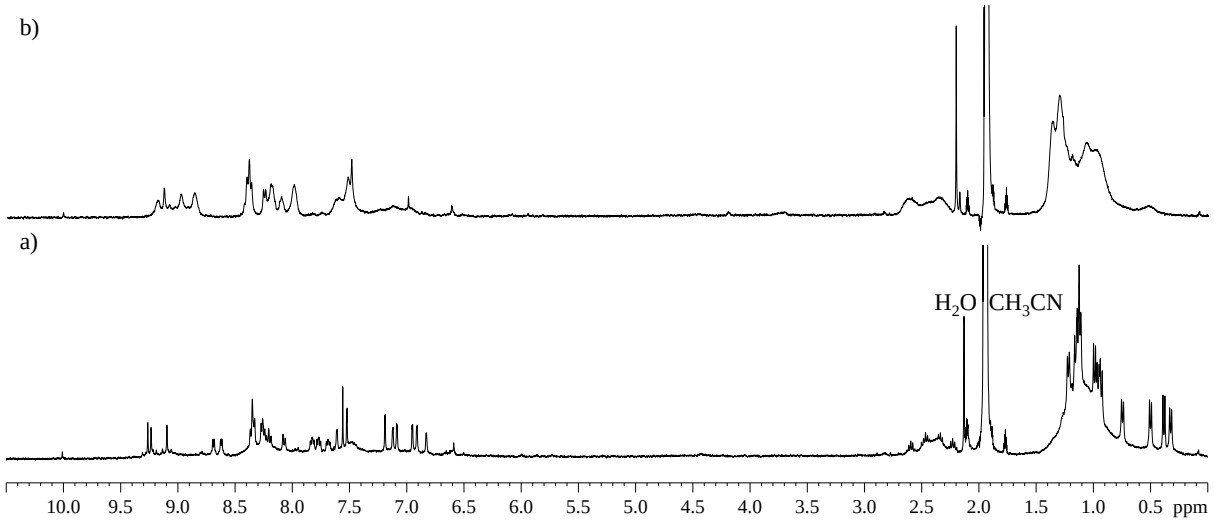

Figure S24. When 6.0 equiv. of $Cd(NTf_2)_2$ were added to **2** (a), dissociation of the cage framework was observed (b) in the ^{1}H NMR spectra in CD_3CN; see Figure S13 for peak assignment.

2. X-Ray Crystallography

Data for **D**·CH_2Cl_2·H_2O were collected using a Bruker D8 VENTURE equipped with high-brilliance IμS Cu-Kα radiation (1.54178 Å), with ω and ψ scans at 180(2) K. Data integration and reduction were undertaken with SAINT and XPREP.[10] Subsequent computations were carried out using the WinGX-32 graphical user interface.[11] A Multi-scan empirical absorption correction was applied to the data using SADABS.[10] The structure was solved by charge-flipping using SUPERFLIP[12] then refined and extended with SHELXL-2013.[13] In general non-hydrogen atoms with occupancies greater than 0.5 were refined anisotropically. Carbon-bound hydrogen atoms were included in idealised positions and refined using a riding model. Nitrogen-bound hydrogen atoms were first located in the difference Fourier map before refinement. The structure shows substantial disorder. This disorder was treated using standard crystallographic methods including bond length and thermal parameter restraints where necessary. One diisopropylaniline ring was modelled as disordered over two locations with occupancies of 0.71643/0.28357 and the AuCl unit was modelled as disordered over two locations with occupancies of 0.75751/0.24249. The CH_2Cl_2 solvent molecule was modelled as disordered over three locations and a remaining area of electron density was modelled as a disordered water molecule. The hydrogen atoms on the disordered water molecule could not be located in the electron density map and were not included in the model. Crystallographic data have been deposited with the CCDC (CCDC 1061936).

Formula $C_{28}H_{42}AuCl_3N_4O$, *M* 753.97, Tetragonal, space group I 41/a (#88), *a* 37.1846(13), *b* 37.1846(13), *c* 9.7430(3) Å, *V* 13471.6(10) $Å^3$, D_c 1.487 g cm^{-3}, *Z* 16, crystal size 0.37 by 0.10 by 0.09 mm, colour pale yellow, habit rod, temperature 180(2) Kelvin, λ(CuKα) 1.54178 Å, μ(CuKα) 10.589 mm^{-1}, $T(\text{SADABS})_{min,max}$ 0.2879, 0.7531, $2\theta_{max}$ 136.74, *hkl*

range -34 44, -44 37, -11 9, N 36192, N_{ind} 6152(R_{merge} 0.0553), N_{obs} 5350(I > 2σ(I)), N_{var} 502, residuals* $R1(F)$ 0.0472, $wR2(F^2)$ 0.1237, GoF(all) 1.044, $\Delta\rho_{min,max}$ -0.668, 0.687 e^- $Å^{-3}$.

*$R1 = \Sigma||F_o| - |F_c||/\Sigma|F_o|$ for $F_o > 2\sigma(F_o)$; $wR2 = (\Sigma w(F_o^2 - F_c^2)^2/\Sigma(wF_c^2)^2)^{1/2}$ all reflections, $w=1/[\sigma^2(F_o^2)+(0.0516P)^2+95.2095P]$ where $P=(F_o^2+2F_c^2)/3$

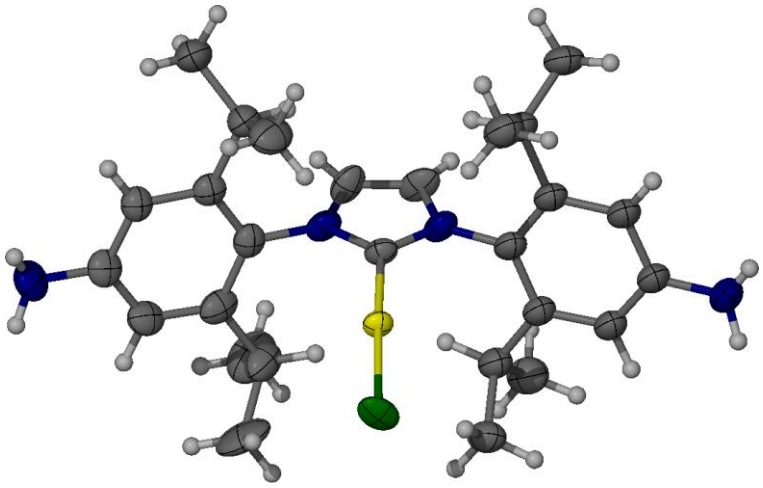

Figure S25. ORTEP representation of **D** showing thermal ellipsoids at 40% probability level. Solvent molecules and disorder are omitted for clarity.

3. Gold Nanoparticle (Au NP) Characterization

3.1 Production of AuNPs from 1

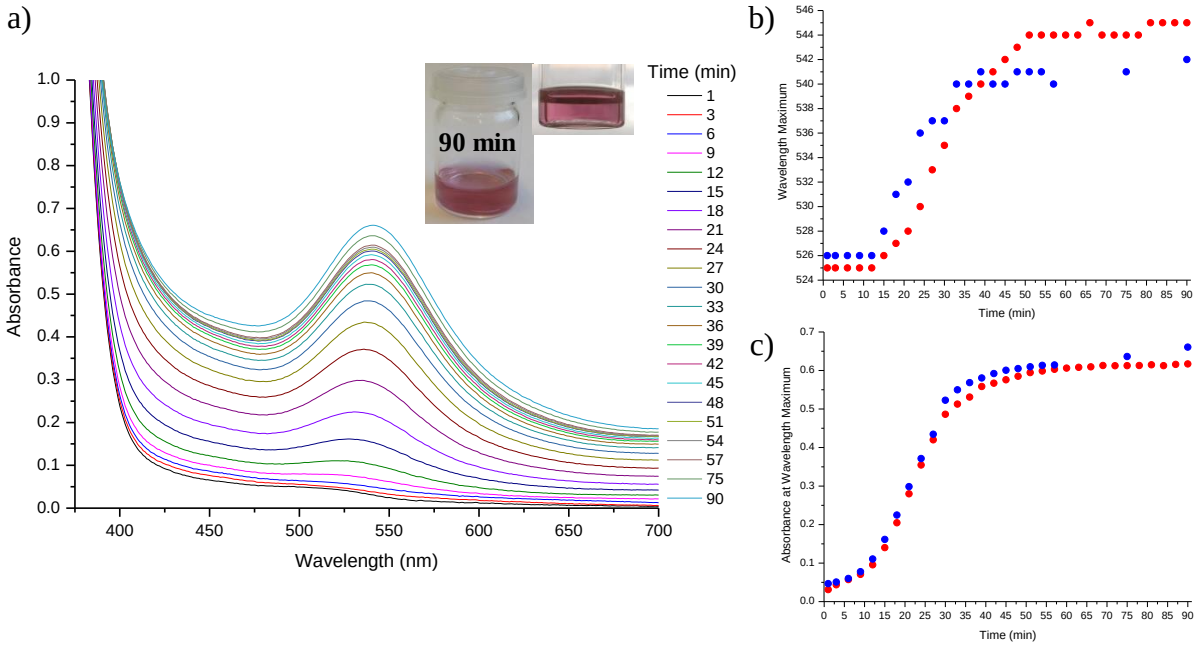

Figure S26. a) UV-Vis spectrum of a 4.7×10^{-5} M solution of **1** and 6.1 equiv. of $Au(tmbn)_2SbF_6$ followed over a 90 minute period (inset: Au NP solution obtained after 90 min); b) the λ_{max} vs. time and c) absorbance at λ_{max} vs. time is plotted in blue from the UV-Vis spectra presented in (a); the red trace is the data collected in a repeated experiment.

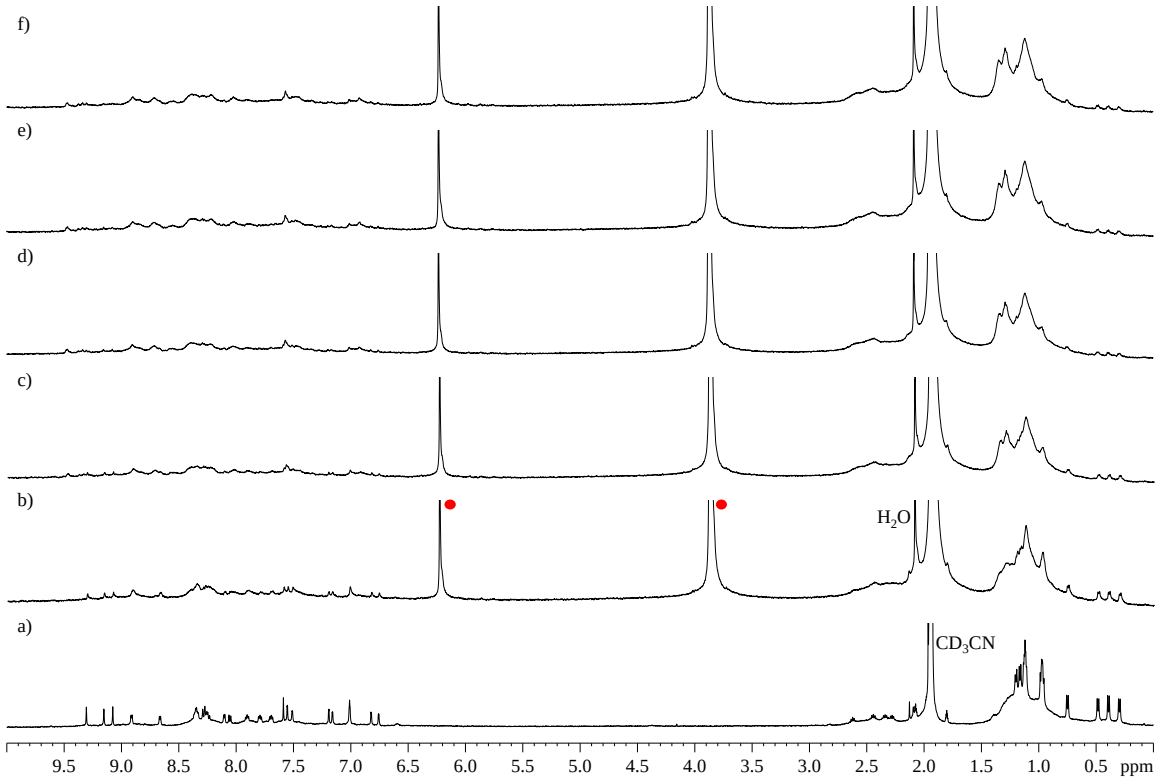

Figure S27. When 1.0 equiv. of $Au(tmbn)_2SbF_6$ was added to a solution of **1** (a) in dry CD_3CN at 25 °C, the ^1H NMR spectra were collected at: b) 2 min, c) 7 min, d) 14 min, e) 31 min and f) 59 min; peaks for tmbn are labelled with red dots.

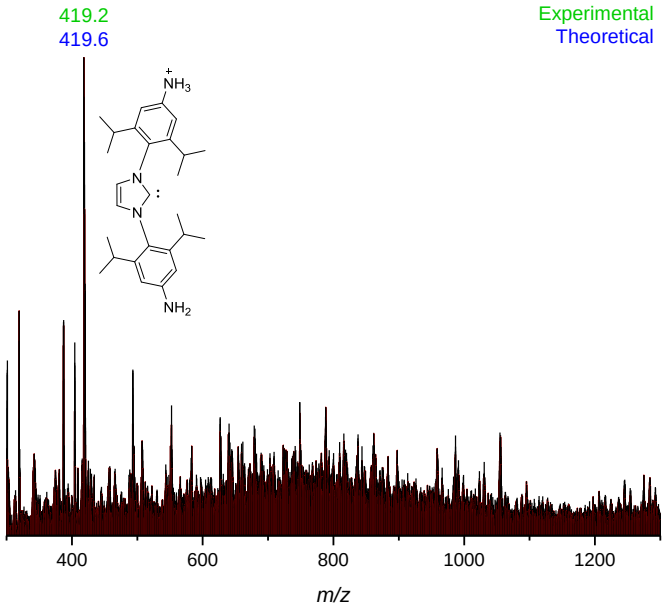

Figure S28. ESI-MS from a solution of Au NPs synthesized with **1** and 6.0 equiv. of $Au(tmbn)_2SbF_6$ (time of reaction: 90 min).

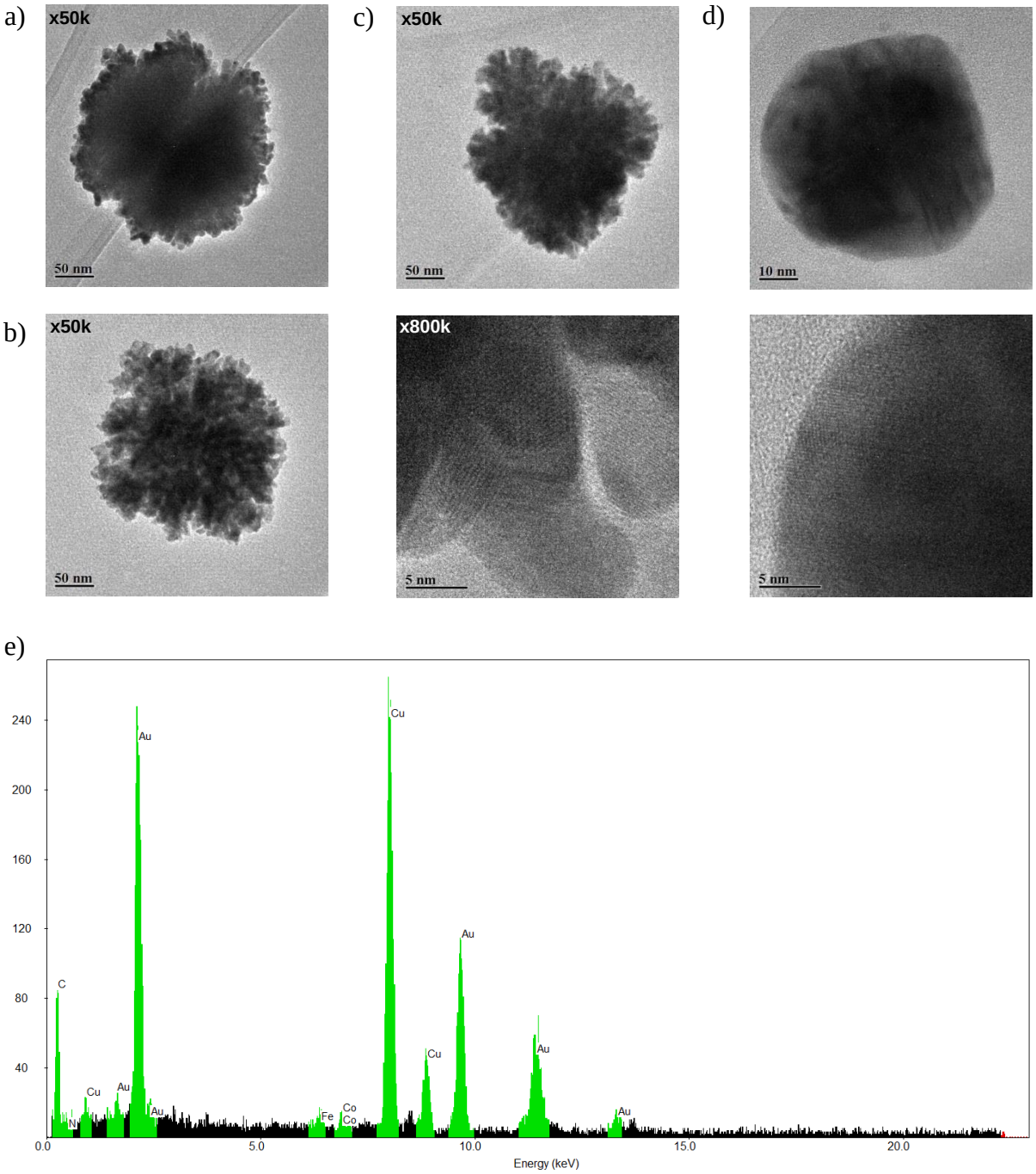

Figure S29. TEM images recorded after 90 min of reaction between **1** and 6.0 equiv. of $Au(tmbn)_2SbF_6$ displayed a), b) and c) clusters of approximately 5 nm nanoparticles (magnification of (c) is shown), and d) nanocrystalline species (with magnification); e) EDS spectrum obtained from (b).

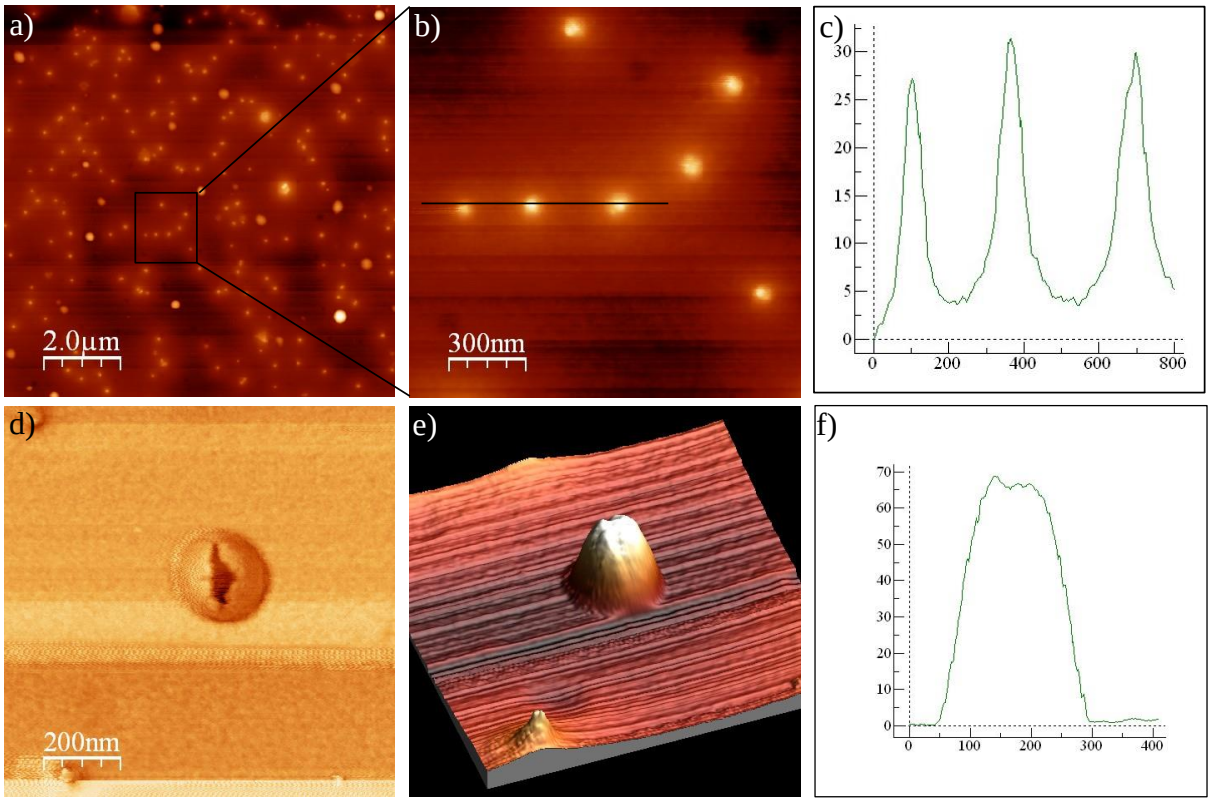

Figure S30. a) AFM image recorded after 90 min of reaction between **1** and 6.0 equiv. of $Au(tmbn)_2SbF_6$, with magnification (b). The height profile is shown for three Au NPs (c); a single Au NP is shown in a magnified view (d), and the 3D representation (e) and height profile (f) are displayed.

3.1.1 Production of Au NPs from D in the presence of $Zn(NTf_2)_2$

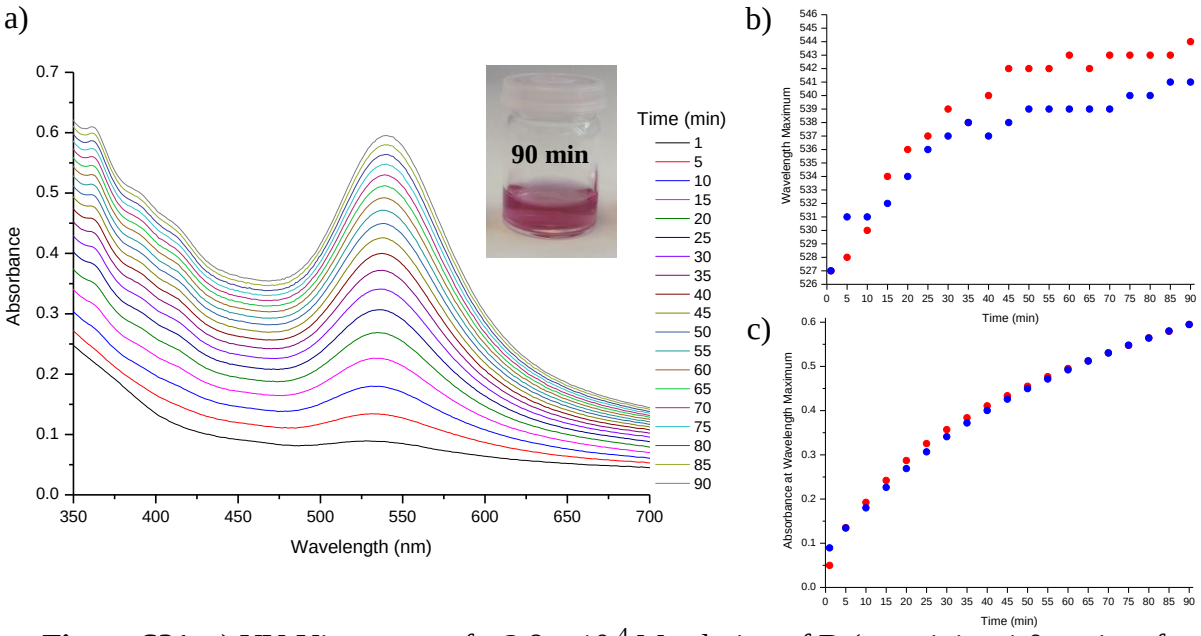

Figure S31. a) UV-Vis spectra of a 2.8×10^{-4} M solution of **D** (containing 1.0 equiv. of $Zn(NTf_2)_2$) and 1.0 equiv. of $Au(tmbn)_2SbF_6$) followed over a 90 minute period (inset: Au NP solution obtained after 90 min); b) the λ_{max} vs. time and c) absorbance at λ_{max} vs. time is plotted in blue from the UV-Vis spectra presented in (a); the red trace is the data collected in a repeated experiment.

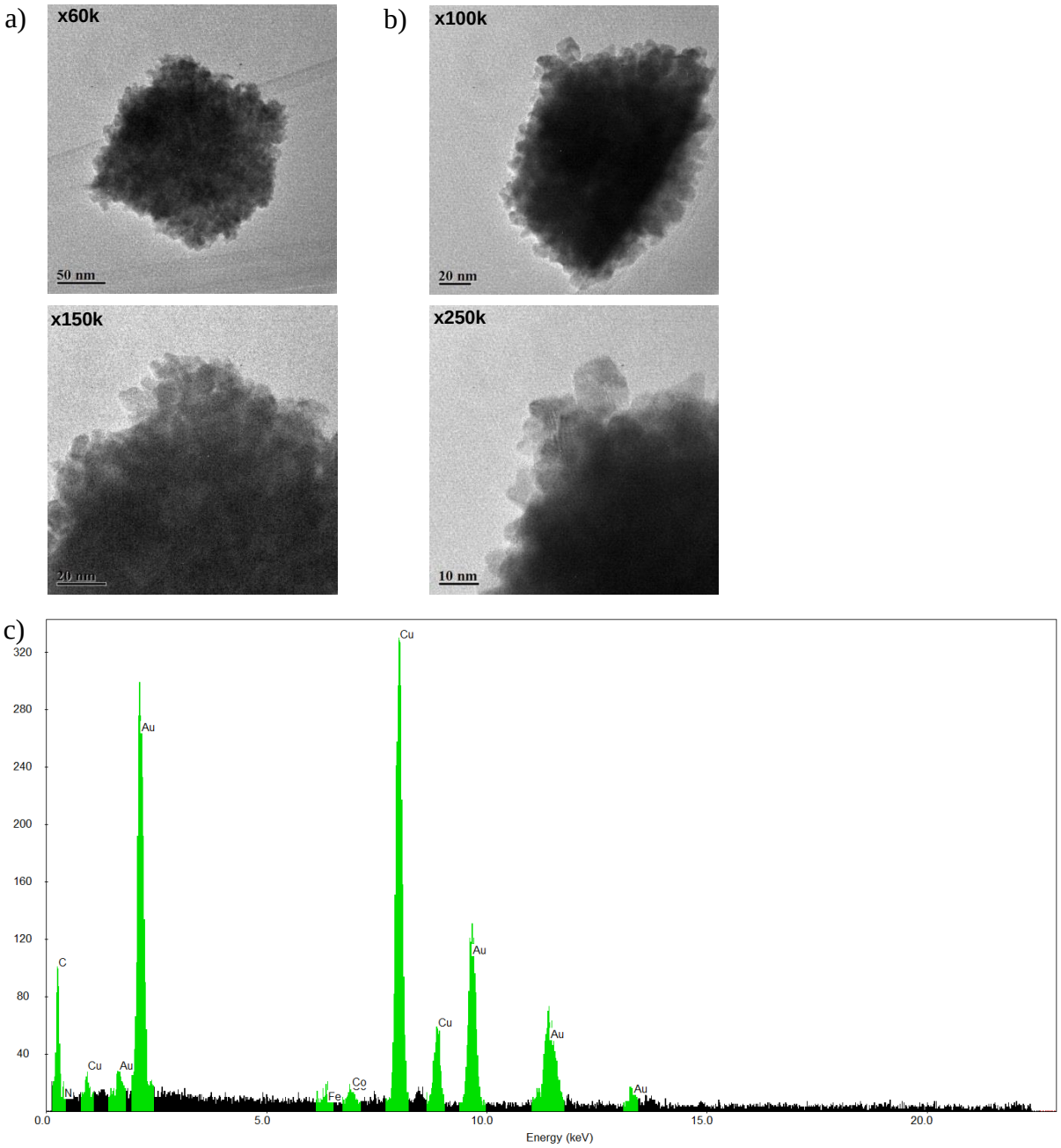

Figure S32. TEM images recorded after 90 min of reaction between equimolar amounts of **D,** $Au(tmbn)_2SbF_6$, and $Zn(NTf_2)_2$ displayed dense clusters of approximately 5 nm nanoparticles (with magnification) ((a) and (b)); c) EDS spectrum obtained from (b).

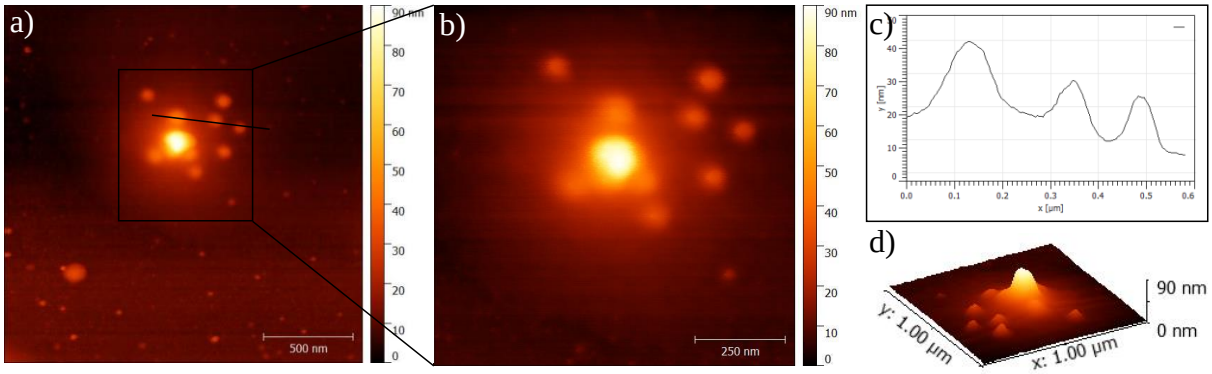

Figure S33. a) AFM image recorded after 90 min of reaction between equimolar amounts of **D**, $Au(tmbn)_2SbF_6$, and $Zn(NTf_2)_2$ with magnification (b), the height profile is shown for three Au NPs in (c) and (d).

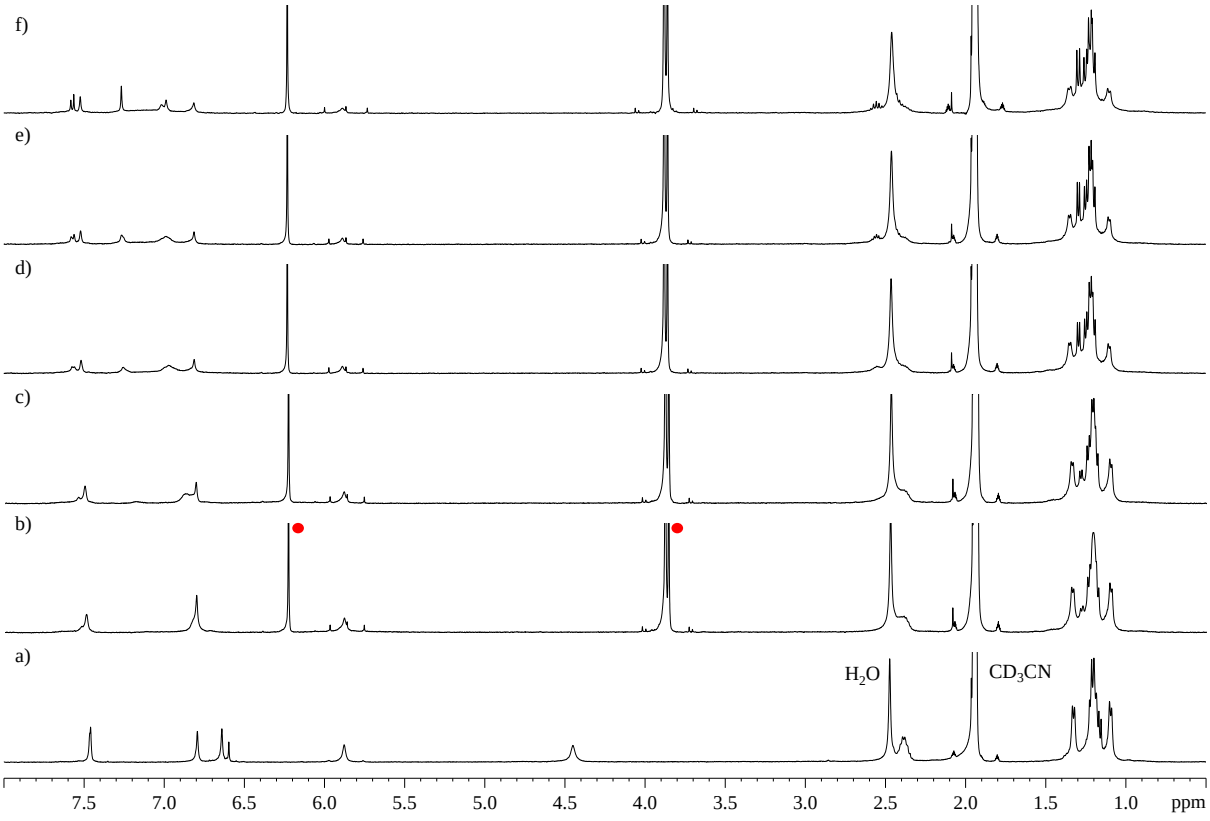

Figure S34. When 1.0 equiv. of $Au(tmbn)_2SbF_6$ was added to a solution of **D** with 1.0 equiv. of $Zn(NTf_2)_2$ (a) in CD_3CN at 25 °C, the ^1H NMR spectra were collected at: b) 2 min, c) 7 min, d) 16 min, e) 33 min and f) 56 min; peaks for tmbn are labelled with red dots.

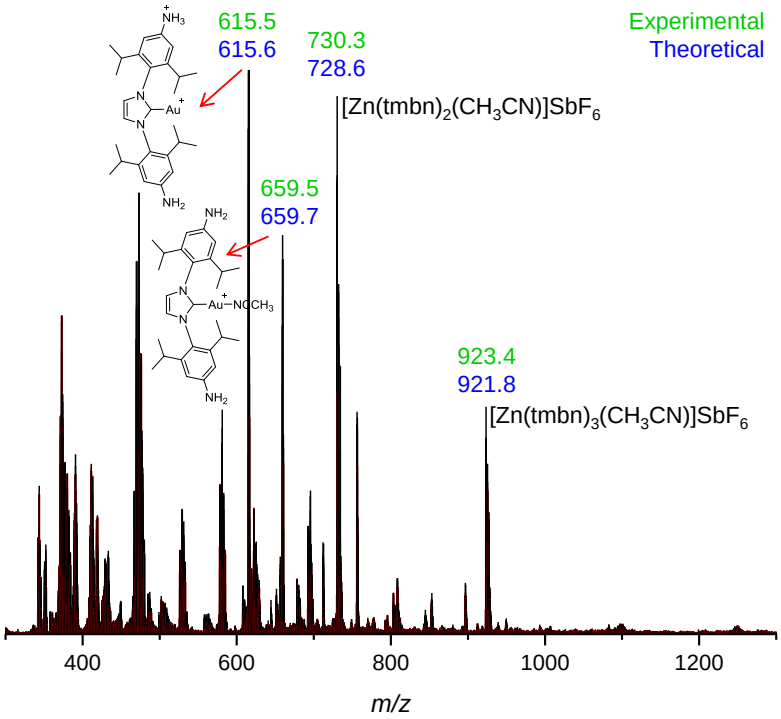

Figure S35. ESI-MS from a solution of Au NPs synthesized with **D** with 1.0 equiv of $Zn(NTf_2)_2$ and 1.0 equiv. of $Au(tmbn)_2SbF_6$ (time of reaction: 90 min).

3.2 Production of AuNPs from 2

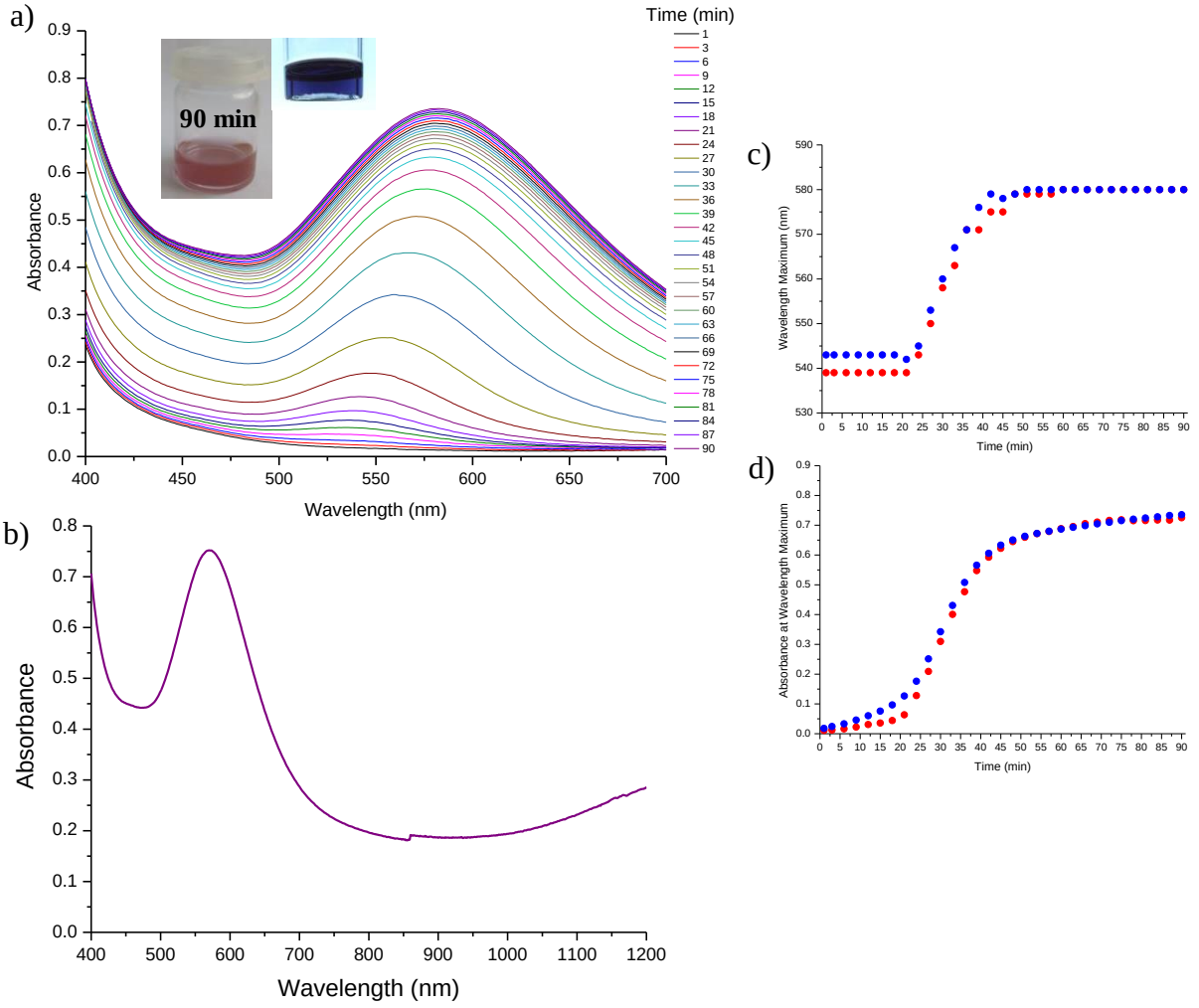

Figure S36. a) UV-Vis spectrum of a 5.0×10^{-5} M solution of **2** and 6.1 equiv. of $Au(tmbn)_2SbF_6$ followed over a 90 minute period (inset (left): turbid solution after 90 min, (right): when viewed transmitting sunlight); the observed transmission of blue light has been attributed to the presence of {111}-faceted triangular prisms (Figure S40).[14] b) Expanded UV-vis spectrum obtained after 90 min; c) the λ_{max} vs. time and d) absorbance at λ_{max} vs. time is plotted in blue from the UV-Vis spectra presented in (a); the red trace is the data collected in a repeated experiment.

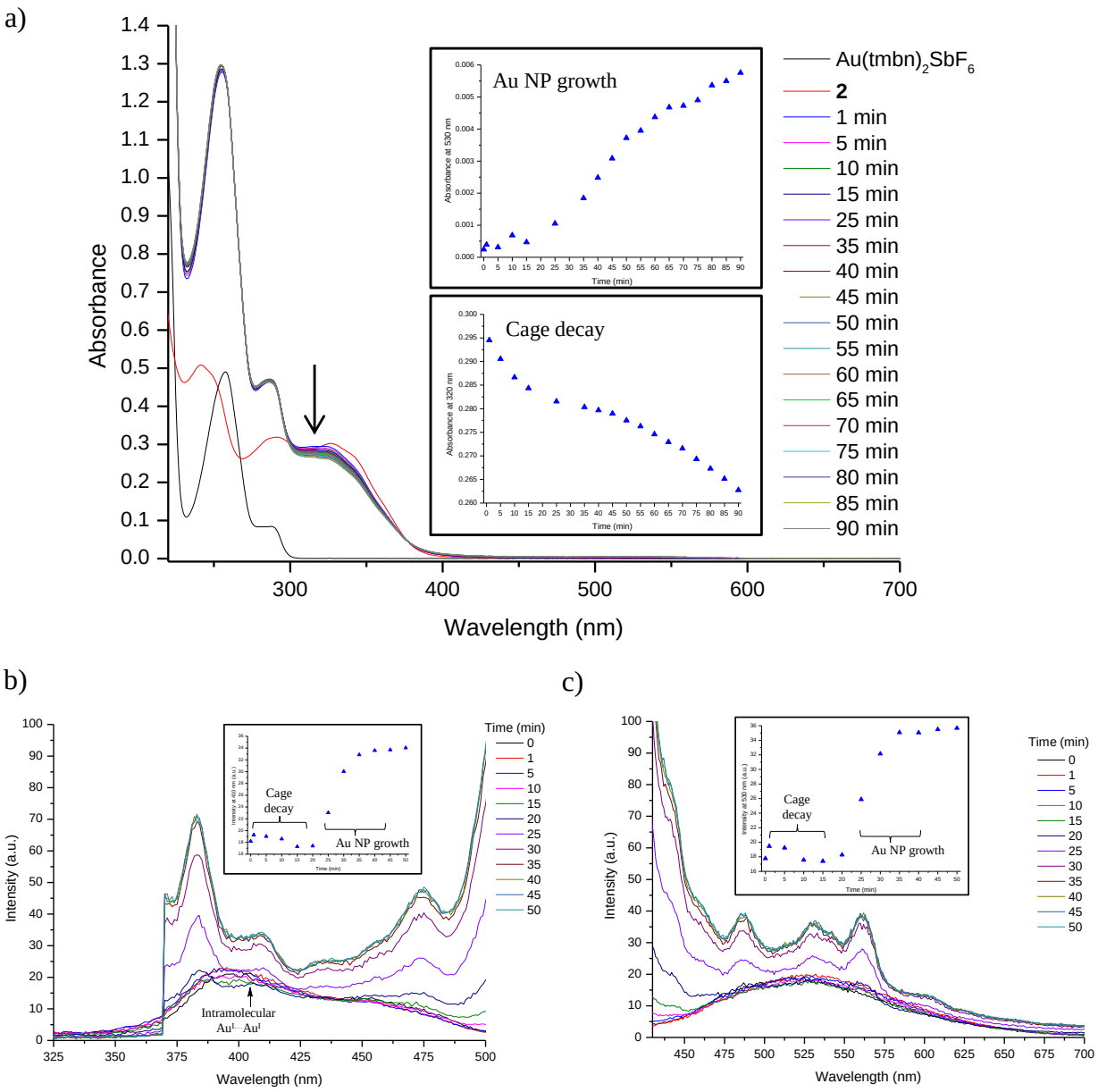

Figure S37. a) The decay of **2** (2.6×10^{-6} M) was followed at 320 nm over time upon addition of 6.1 equiv. of $Au(tmbn)_2SbF_6$ (inset, top: Au NP growth was followed over time as the increase in the SPR band at 530 nm; inset, bottom: cage decay was followed as a plot of absorbance at 320 nm vs. time). b) Excitation spectra of **2** (5.3×10^{-5} M) over time after addition of 6.1 equiv. of $Au(tmbn)_2SbF_6$. Inset: plot of intensity at 410 nm vs. time. c) Emission spectra of **2** (5.3×10^{-5} M) over time after addition of 6.1 equiv. of $Au(tmbn)_2SbF_6$. Inset: plot of intensity at 530 nm vs. time.

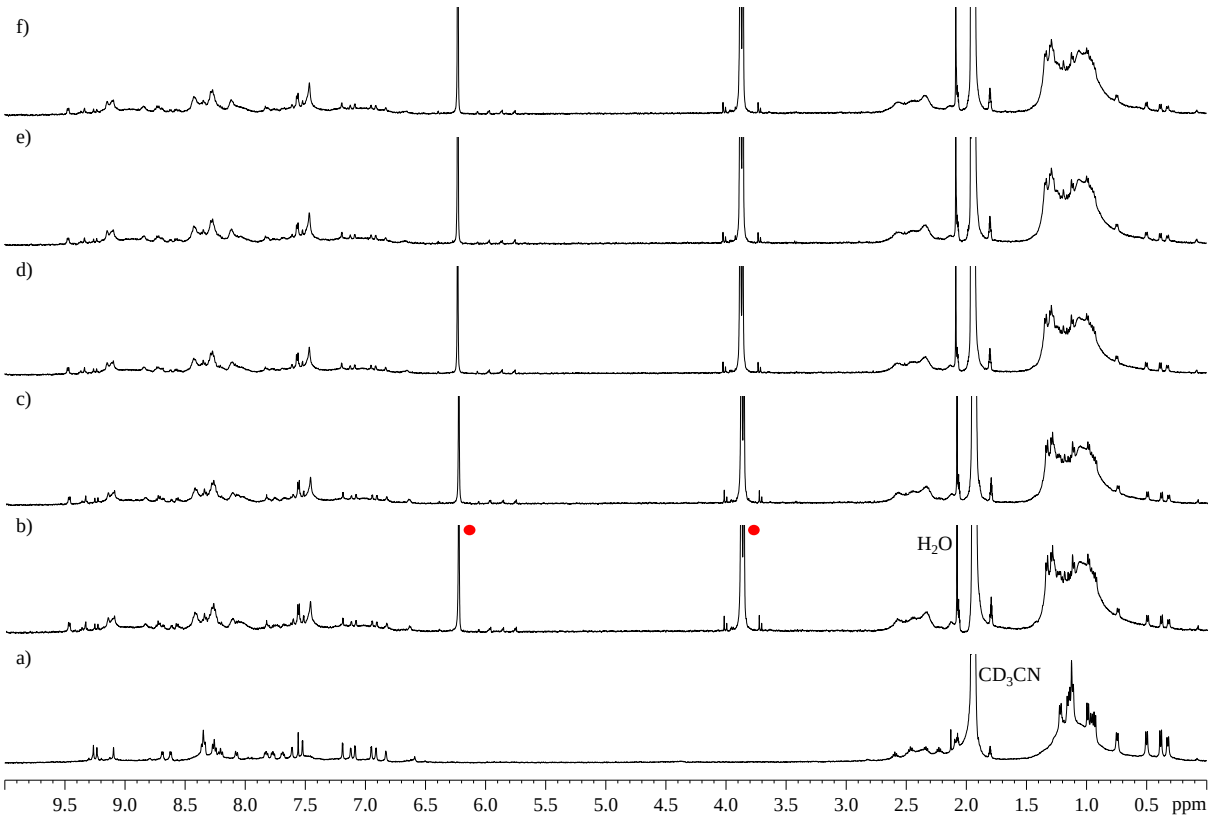

Figure S38. When 1.0 equiv. of $Au(tmbn)_2SbF_6$ was added to a solution of **2** (a) in CD_3CN at 25 °C, the ^1H NMR spectra were collected at: b) 2 min, c) 7 min, d) 13 min, e) 29 min and f) 60 min, indicating disassembly of **2** and broadening of the peaks, attributable to colloidal gold; peaks for tmbn are labelled with red dots.

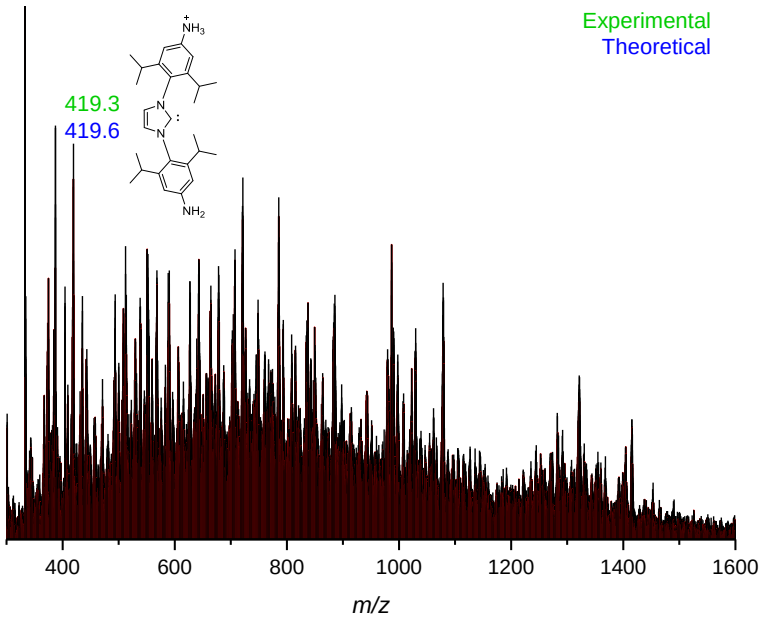

Figure S39. ESI-MS from a solution of Au NPs synthesized with **2** and 1.0 equiv. of $Au(tmbn)_2SbF_6$ (time of reaction: 90 min).

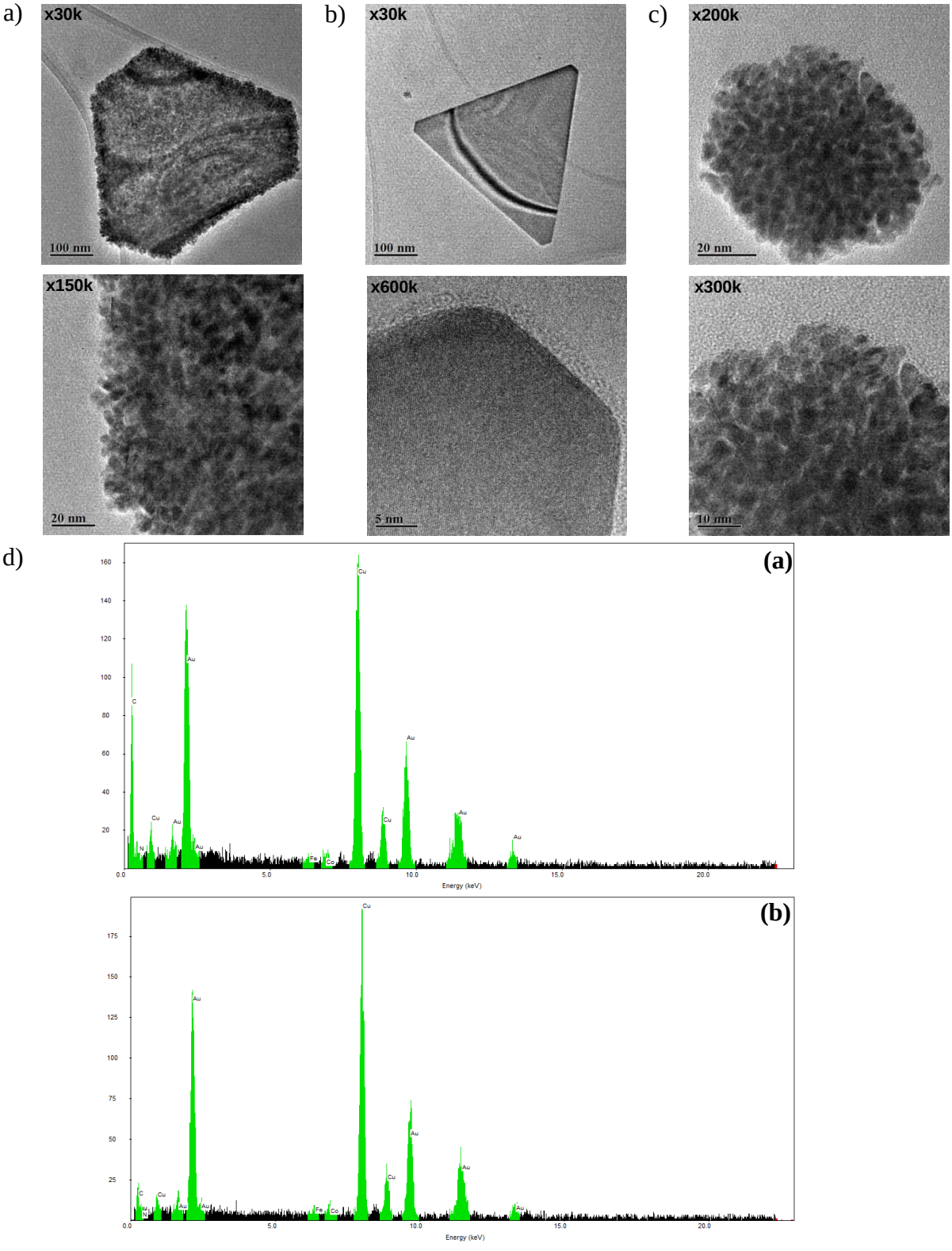

Figure S40. TEM images recorded after 90 min of reaction between **2** and 6.0 equiv. of $Au(tmbn)_2SbF_6$ displayed large, triangular clusters of approximately 5 nm nanoparticles (with magnification), b) {111} faceted triangular prisms (with magnification), and c) smaller spherical clusters of approximately 5 nm nanoparticles (with magnification); d) EDS spectrum obtained from (a) and (b).

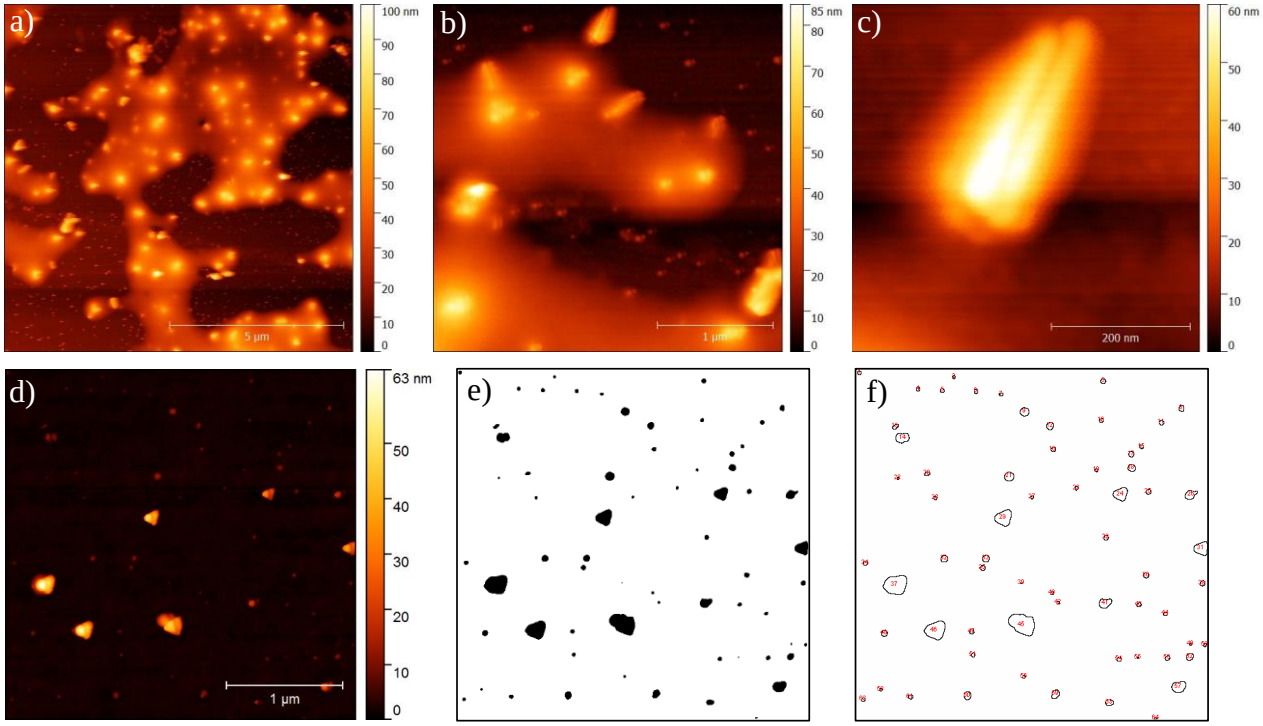

g)

Bin	Frequency	Cumulative	Cumulative %
0	0	0	0
250	4	4	6
500	5	9	14
750	8	17	27
1000	22	39	61
1250	0	39	61
1500	0	39	61
1750	0	39	61
2000	5	44	69
2250	0	44	69
2500	0	44	69
2750	0	44	69
3000	7	51	80
4000	2	53	83
5000	2	55	86
6000	0	55	86
7000	1	56	88
8000	1	57	89
9000	1	58	91
10000	2	60	94
20000	2	62	97
30000	2	64	100
More	0	64	100

h)

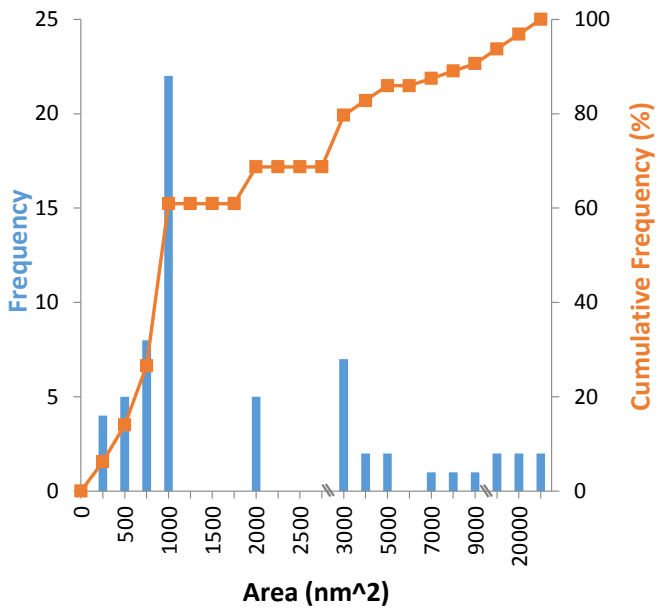

Figure S41. a) AFM image recorded after 90 min of reaction between **2** and 6.0 equiv. of $Au(tmbn)_2SbF_6$, with magnification (b) and (c). From the AFM images of the repeated experiment (d), Image J software[15] was used to isolate particles (e) and calculate areas (f and g) in order to create a histogram showing nanoparticle size distribution (h).

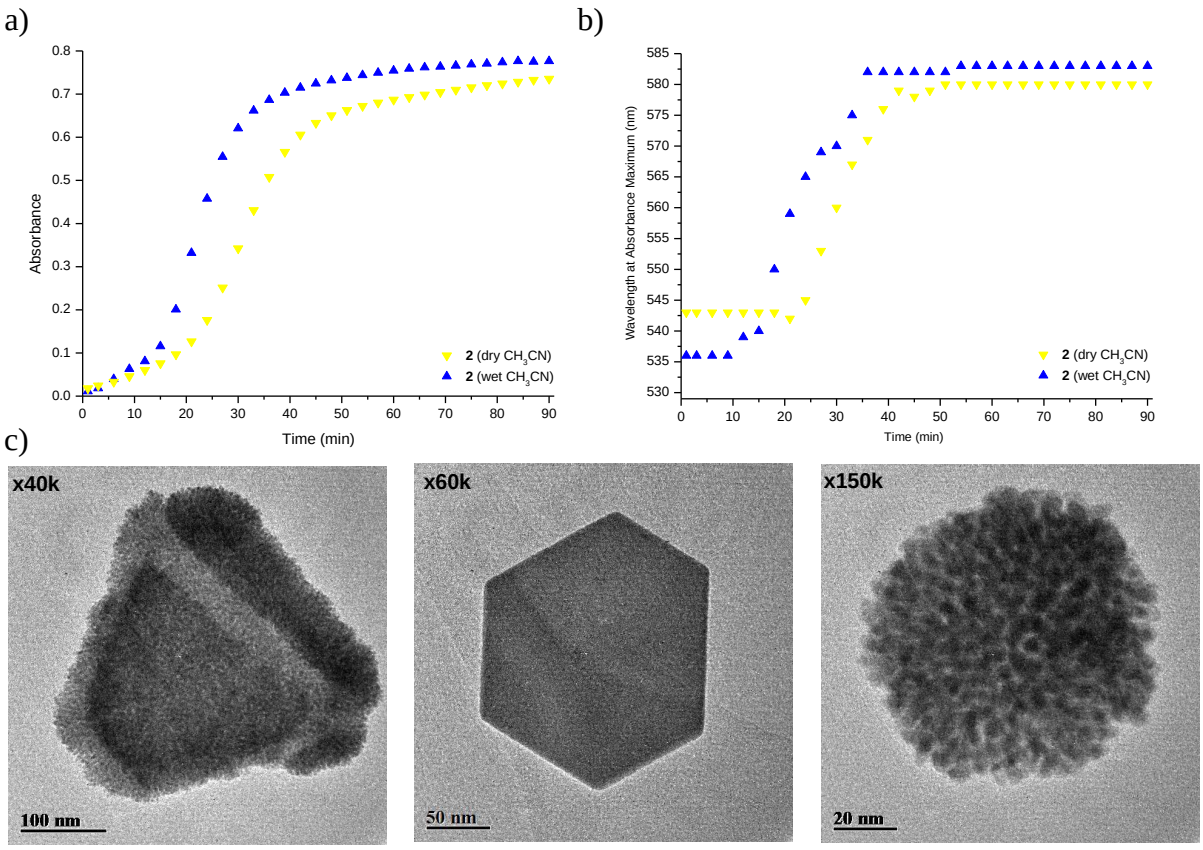

Figure S42. The results from the UV-Vis experiments following the synthesis of Au NPs with **2** over time prepared with wet acetonitrile is shown in blue: a) absorbance at λ_{max} vs. time and b) λ_{max} vs. time; the results of the experiments of Au NP production in dry acetonitrile (Figure S36) is shown in yellow for comparison. TEM images are shown in (c).

3.2.1 Production of Au NPs from D in the presence of $Cd(NTf_2)_2$

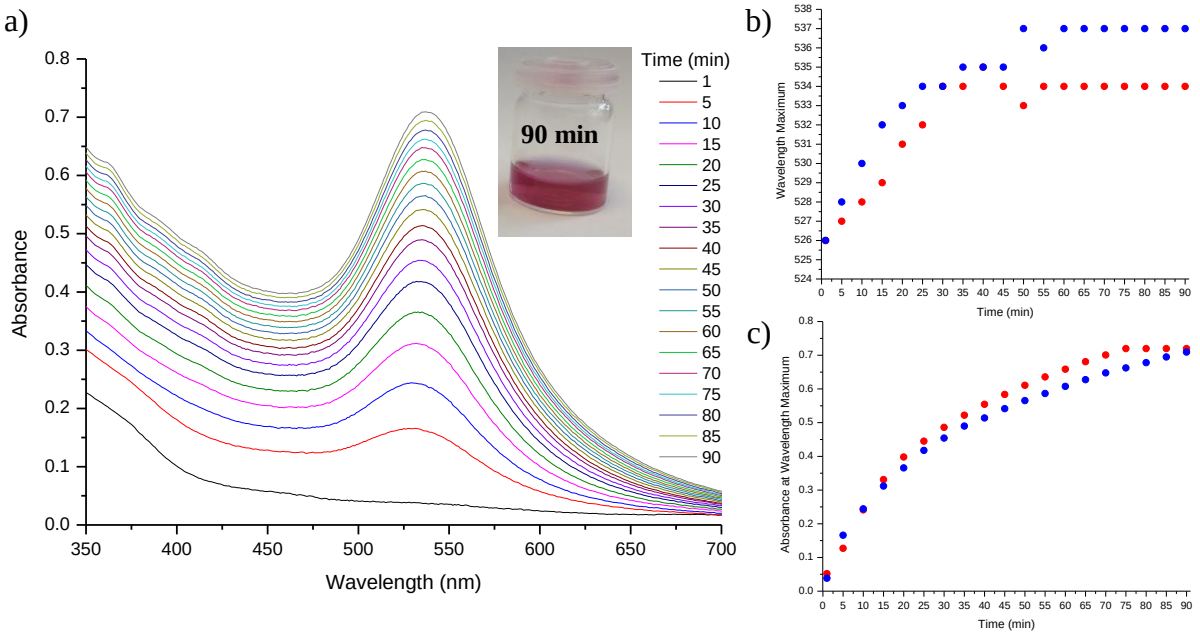

Figure S43. a) UV-Vis spectrum of a 2.9×10^{-4} M solution of **D** (containing 1.0 equiv. of $Cd(NTf_2)_2$) and 1.0 equiv. of $Au(tmbn)_2SbF_6$ followed over a 90 minute period (inset: Au NP solution obtained after 90 min); b) the λ_{max} vs. time and c) absorbance at λ_{max} vs. time is plotted in blue from the UV-Vis spectra presented in (a); the red trace is the data collected in a repeated experiment.

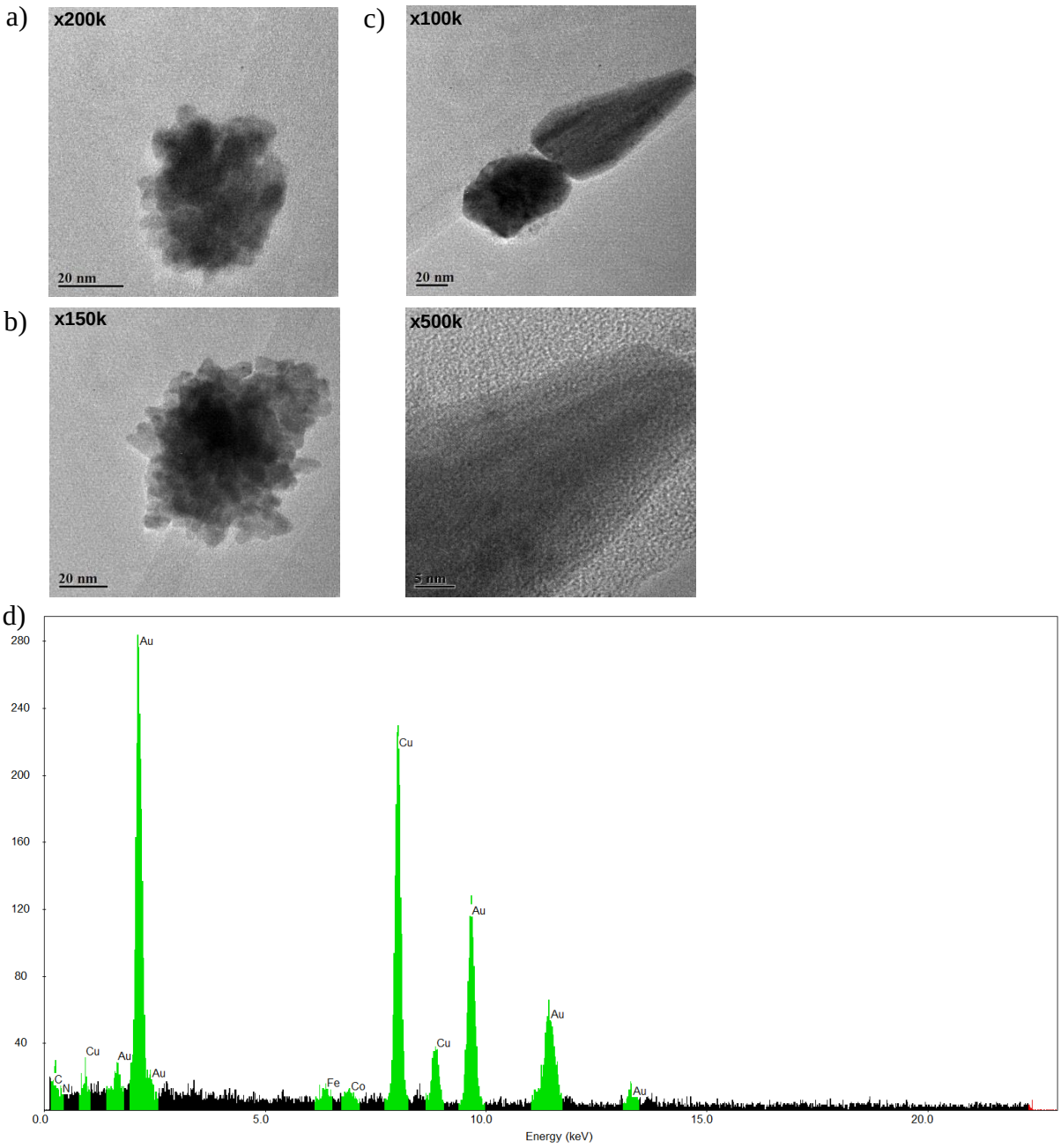

Figure S44. TEM images recorded after 90 min of reaction between equimolar amounts of **D**, $Au(tmbn)_2SbF_6$, and $Cd(NTf_2)_2$ displayed a) and b) clusters of approximately 5 nm nanoparticles, and c) nanocrystalline species (with magnification); d) EDS spectrum obtained from (c).

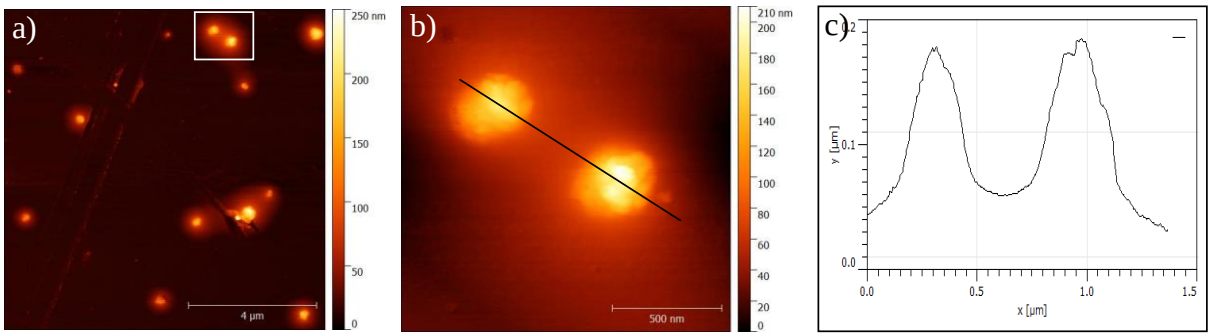

Figure S45. a) AFM image recorded after 90 min of reaction between equimolar amounts of **D**, $Au(tmbn)_2SbF_6$, and $Cd(NTf_2)_2$ with magnification (b), the height profile is shown for two Au NPs (c).

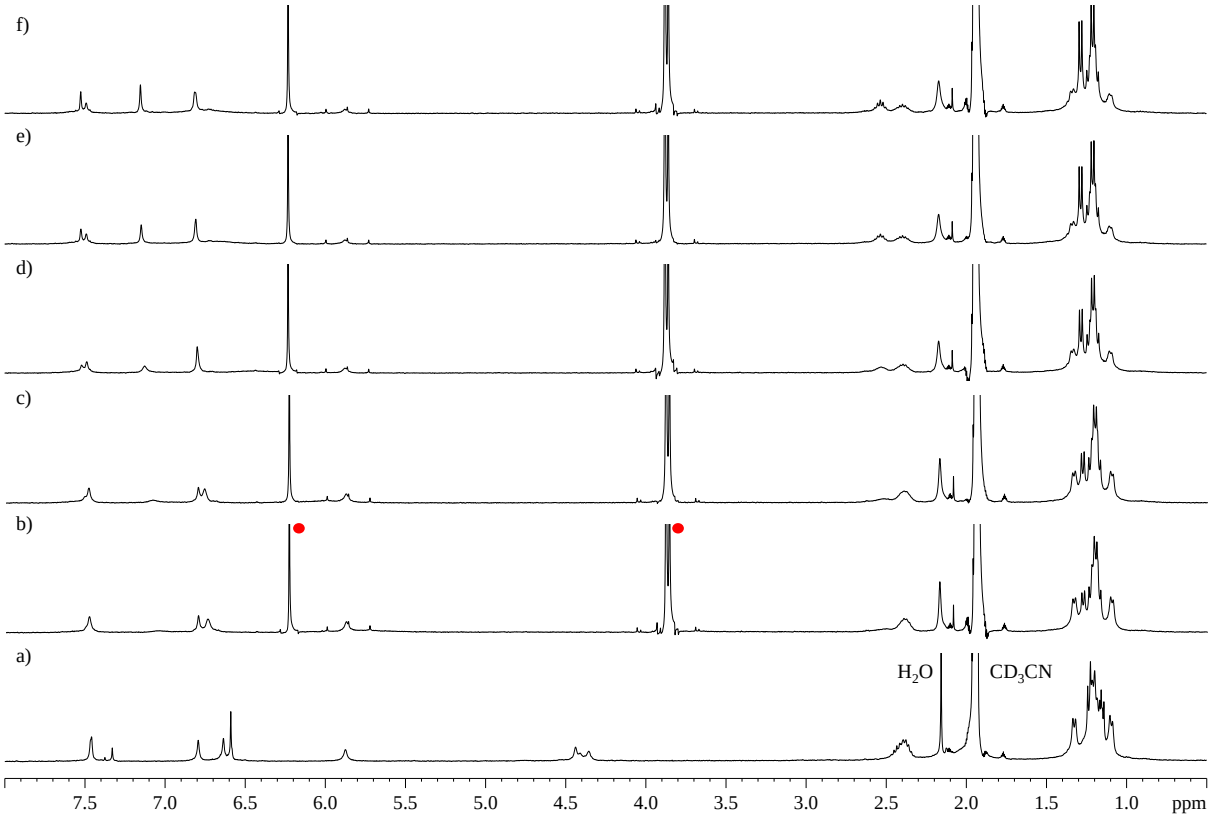

Figure S46. When 1.0 equiv. of $Au(tmbn)_2SbF_6$ was added to a solution of **D** with 1.0 equiv of $Cd(NTf_2)_2$ (a) in CD_3CN at 25 °C, the ^1H NMR spectra were collected at: b) 2 min, c) 7 min, d) 13 min, e) 30 min and f) 57 min; peaks for tmbn are labelled with red dots.

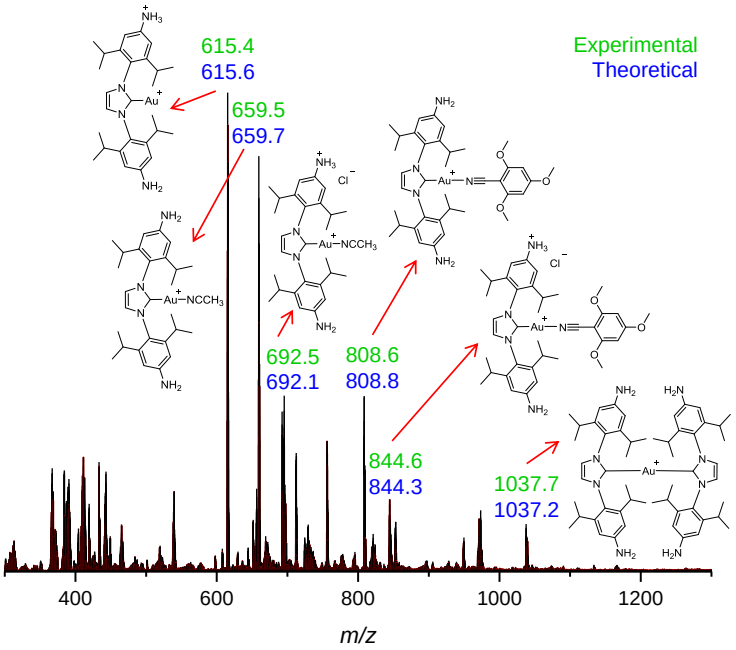

Figure S47. ESI-MS from a solution of Au NPs synthesized with **D** with 1.0 equiv of $Cd(NTf_2)_2$ and 1.0 equiv. of $Au(tmbn)_2SbF_6$ (time of reaction: 90 min).

3.3 Production of Au NPs from A

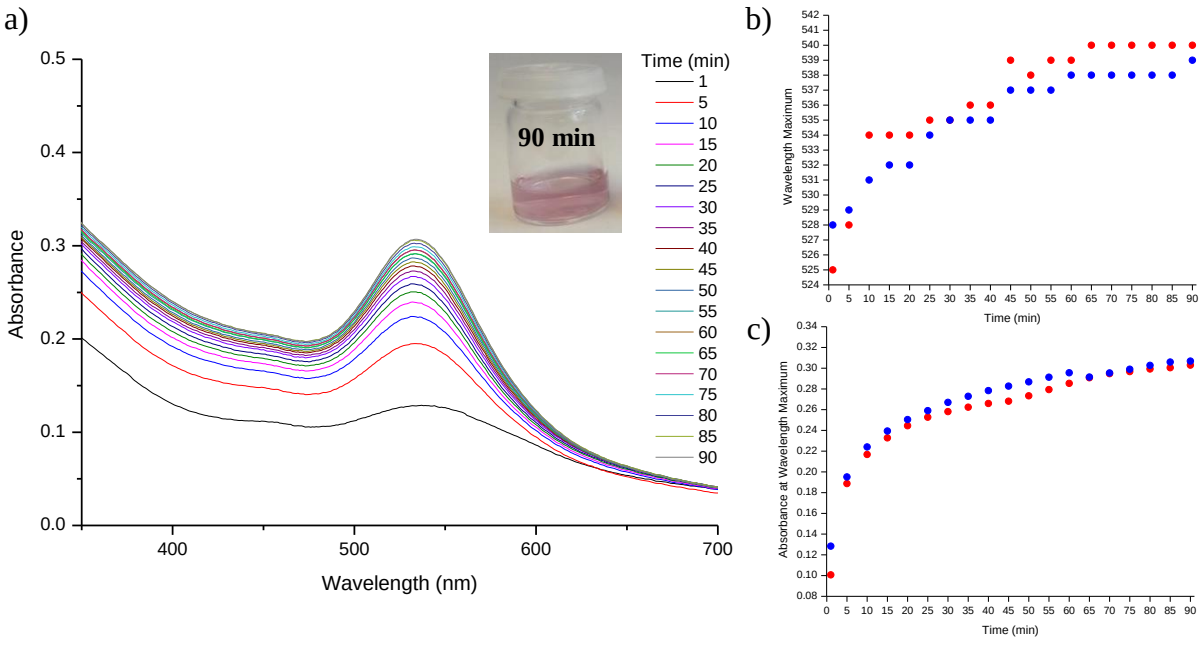

Figure S48. a) UV-Vis spectra of a 3.6×10^{-4} M solution of **A** and 0.9 equiv. of $Au(tmbn)_2SbF_6$ followed over a 90 minute period (inset: Au NP solution obtained after 90 min); b) the λ_{max} vs. time and c) absorbance at λ_{max} vs. time is plotted in blue from the UV-vis spectra presented in (a); the red points are the data collected in a repeated experiment.

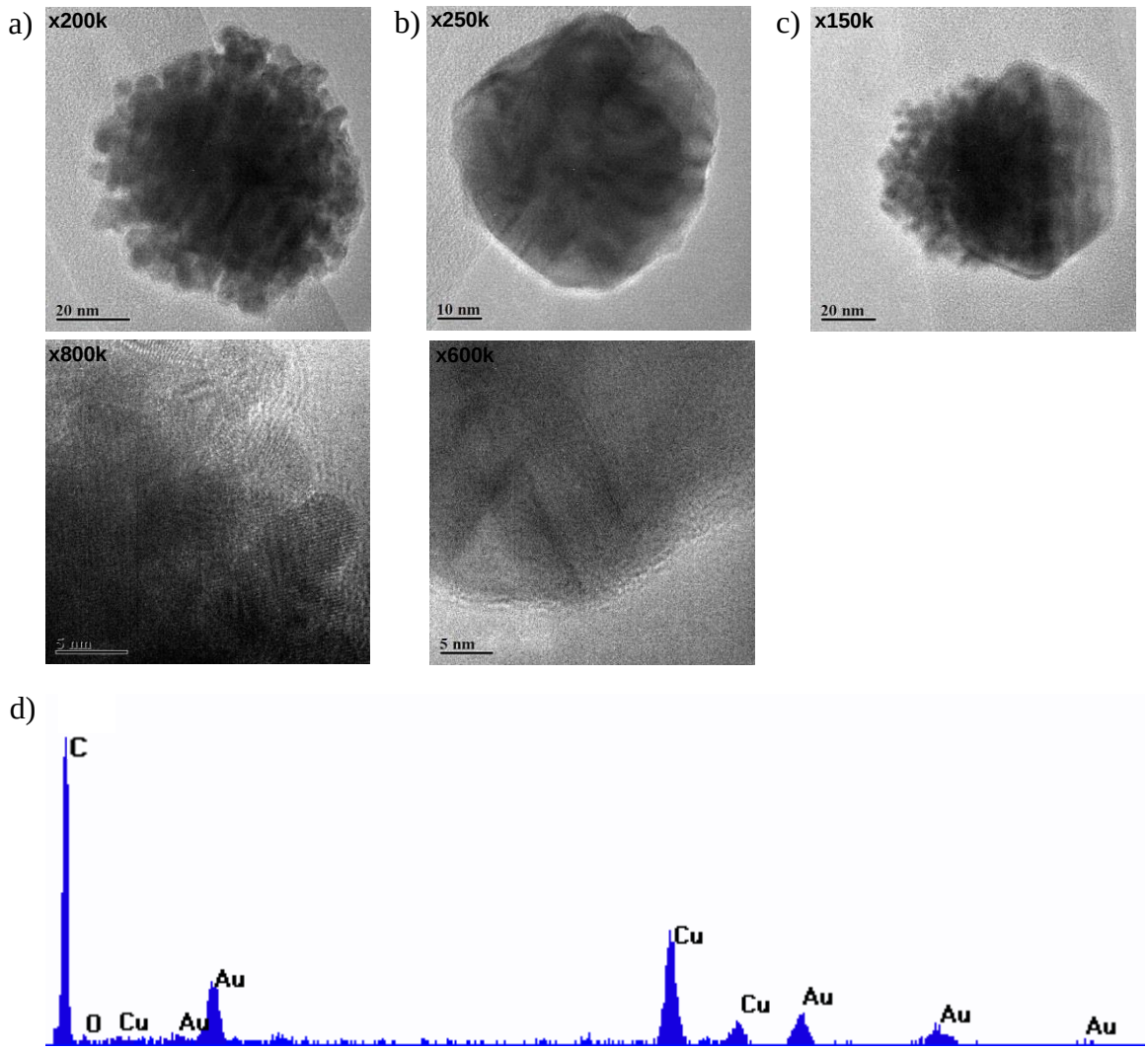

Figure S49. TEM images recorded after 90 min of reaction between equimolar amounts of **A** and $Au(tmbn)_2SbF_6$ displayed a) clusters of approximately 5 nm nanoparticles (with magnification), b) nanocrystalline species (with magnification), and c) a combination of both features; d) EDS spectrum obtained from (a).

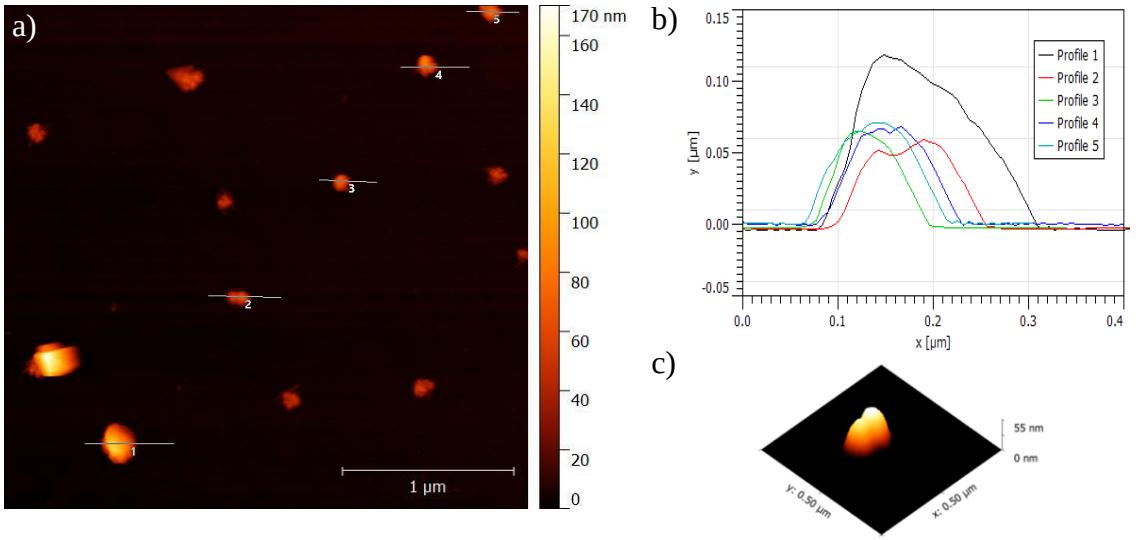

Figure S50. a) AFM image recorded after 90 min of reaction between equimolar amounts of **A** and $Au(tmbn)_2SbF_6$; the height profile is shown for five Au NPs (b), and magnified for Profile 2 (c).

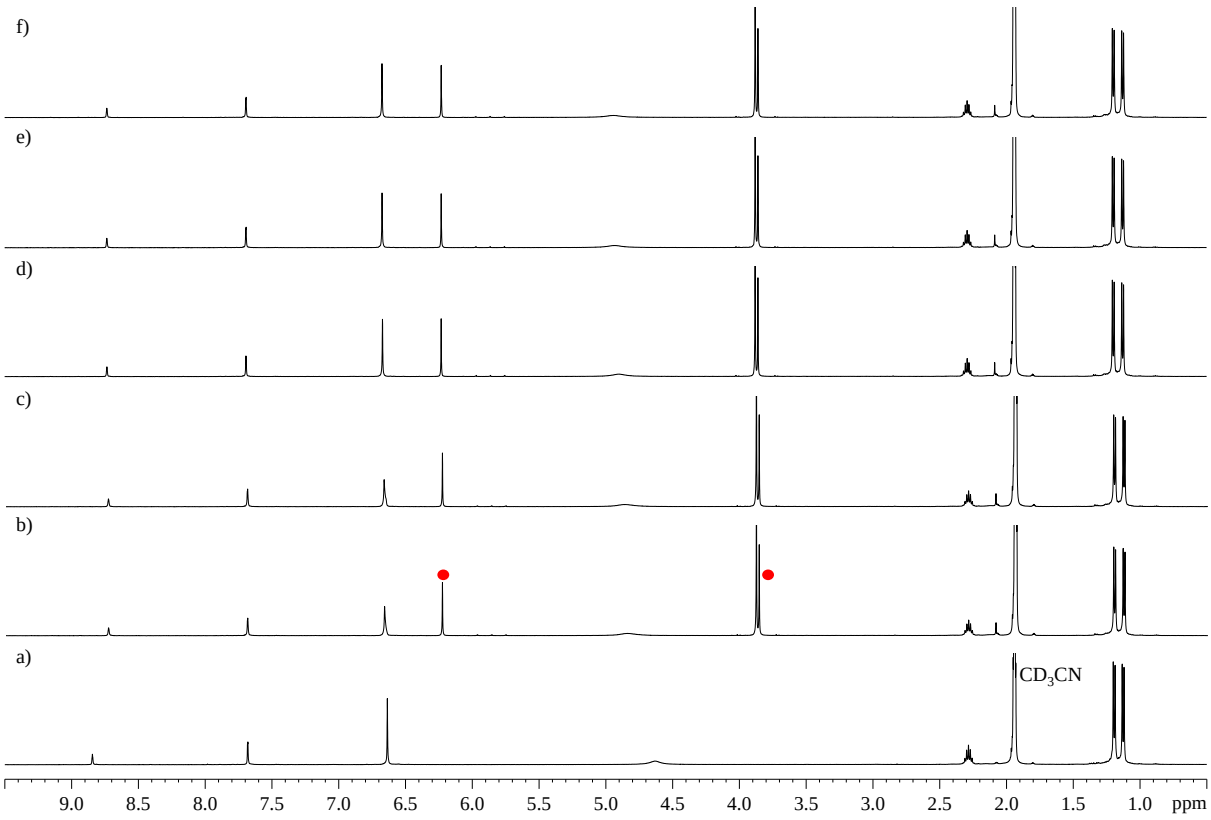

Figure S51. When 1.0 equiv. of $Au(tmbn)_2SbF_6$ was added to a solution of **A** (a) in dry CD_3CN at 25 °C, the ^1H NMR spectra were collected at: b) 2 min, c) 7 min, d) 13 min, e) 25 min and f) 55 min; peaks for tmbn are labelled with red dots.

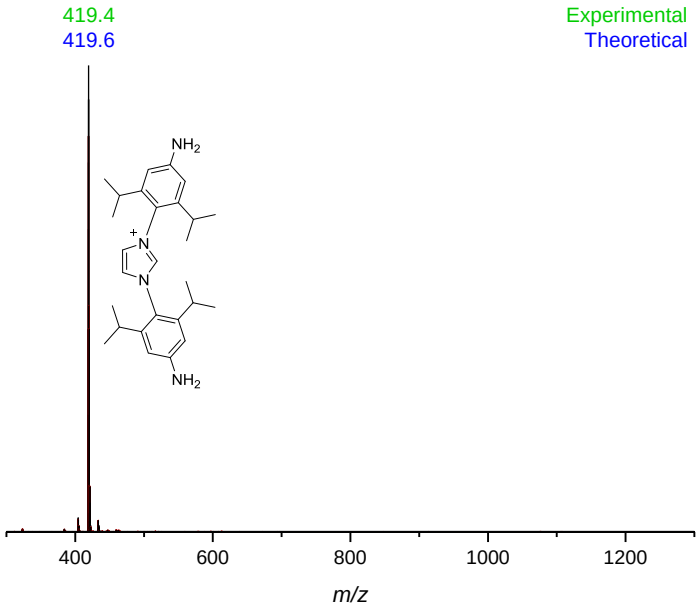

Figure S52. ESI-MS from a solution of Au NPs produced from **A** and 1.0 equiv. of $Au(tmbn)_2SbF_6$ (time of reaction: 90 min).

3.4 Production of Au NPs from D

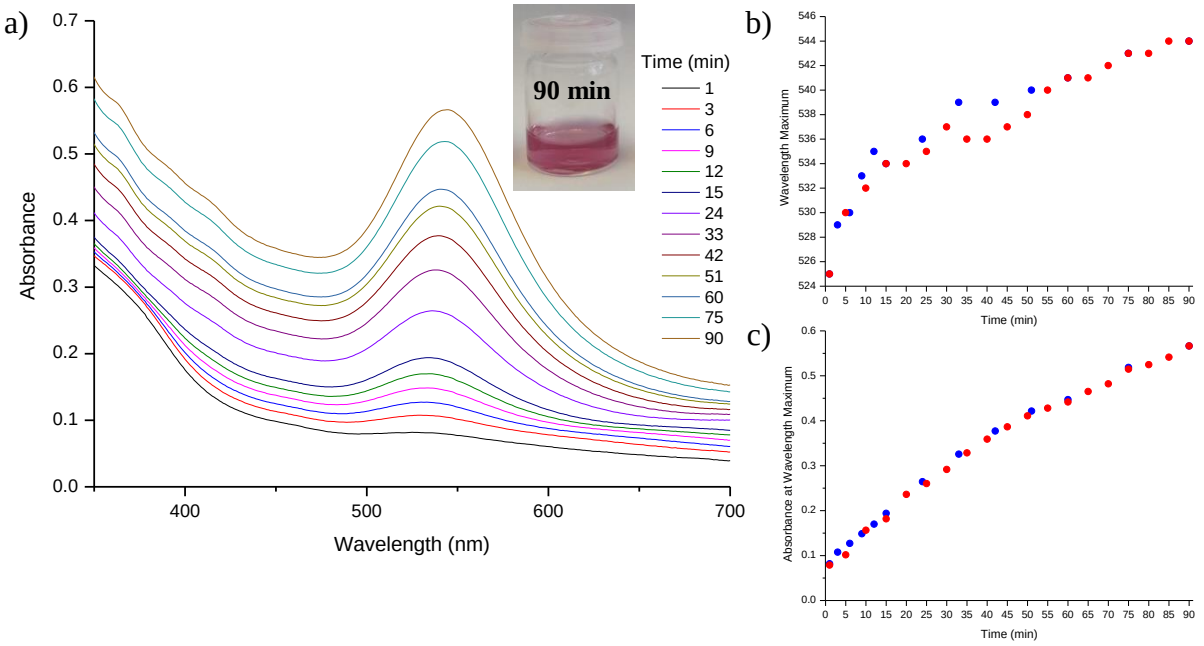

Figure S53. a) UV-Vis spectra of a 2.9×10^{-4} M solution of **D** and 1.0 equiv. of $Au(tmbn)_2SbF_6$ followed over a 90 minute period (inset: Au NP solution obtained after 90 min); b) the λ_{max} vs. time and c) absorbance at λ_{max} vs. time is plotted in blue from the UV-vis spectra presented in (a); the red points are the data collected in a repeated experiment.

The reaction of **A** with Au^I gave a maximum absorbance from synthesized Au NPs (Figure S48) of half the value observed when **D** reacted with Au^I (Figure S53) after 90 min of growth, which suggested that Au^I derived from **D** was incorporated into the synthesized Au NPs.

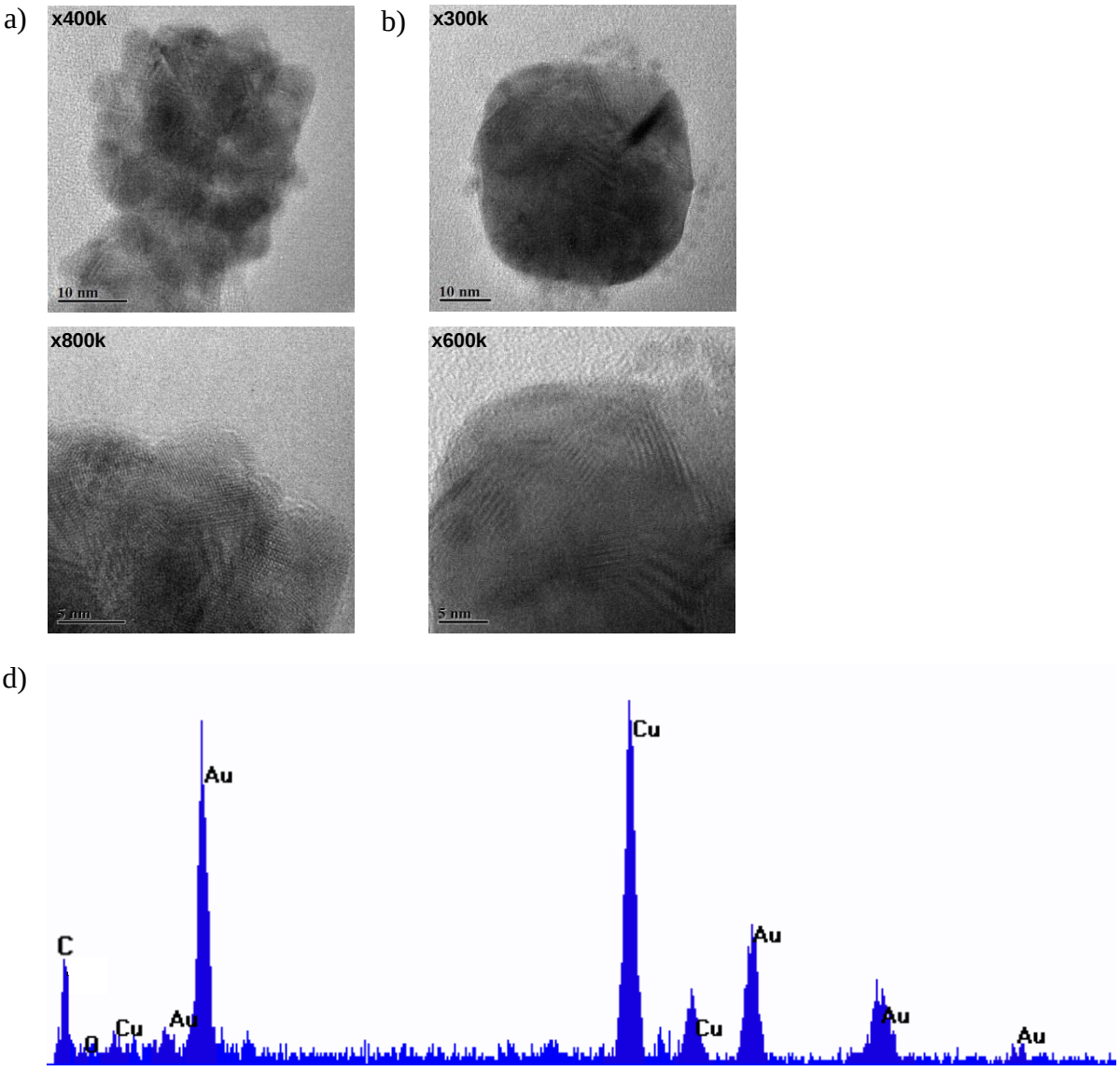

Figure S54. TEM images recorded after 90 min of reaction between equimolar amounts of **D** and $Au(tmbn)_2SbF_6$ displayed a) clusters of approximately 5 nm nanoparticles (with magnification) and b) nanocrystalline species (with magnification); d) EDS spectrum obtained from (b).

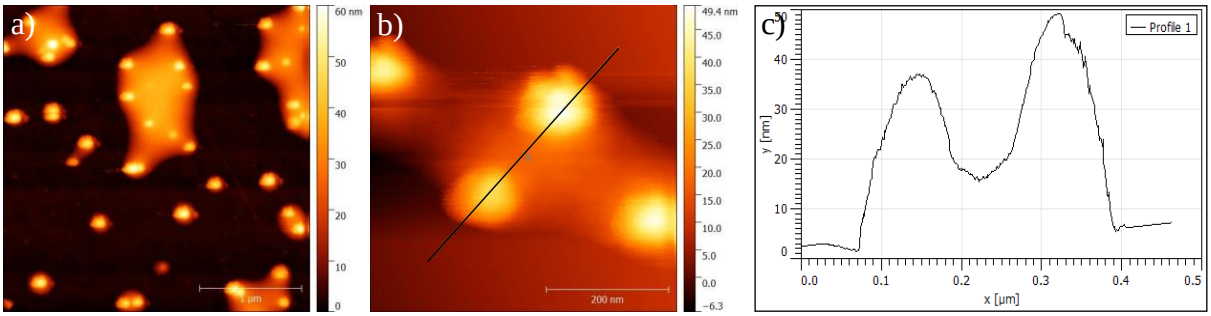

Figure S55. a) AFM image recorded after 90 min of reaction between equimolar amounts of **D** and $Au(tmbn)_2SbF_6$, with magnification (b); c) height profile of imaged Au NPs.

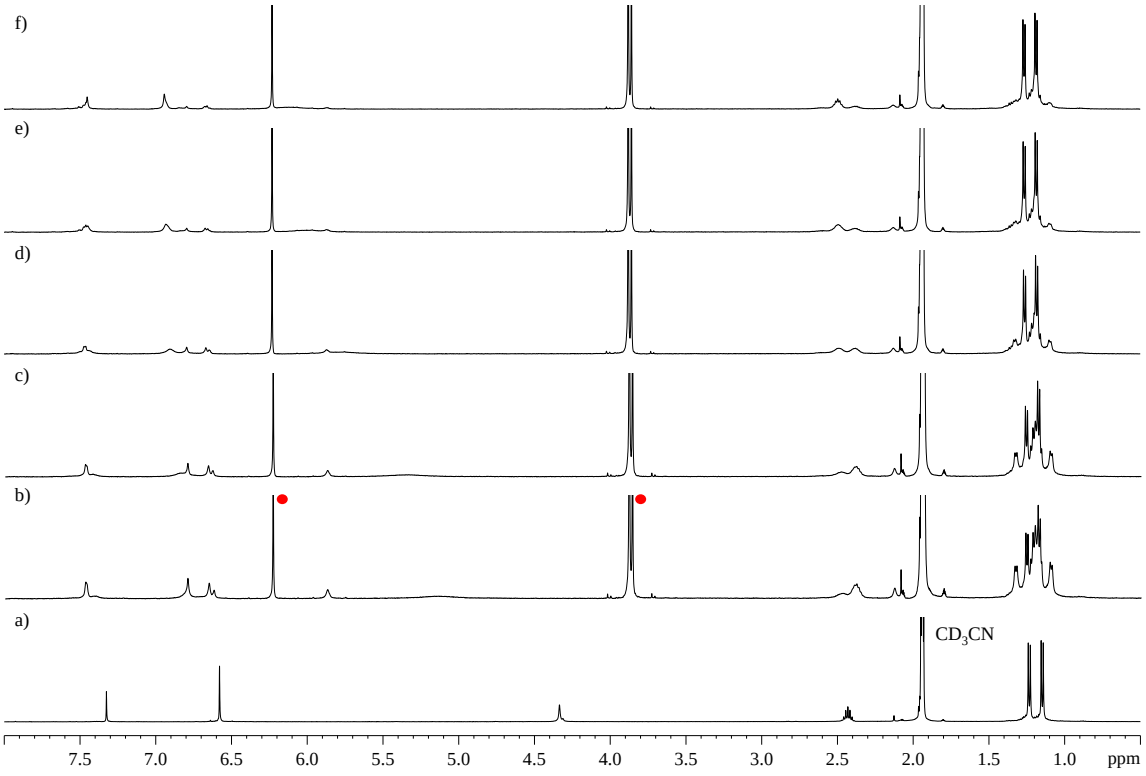

Figure S56. When 1.0 equiv. of $Au(tmbn)_2SbF_6$ was added to a solution of **D** (a) in dry CD_3CN at 25 °C, the ^1H NMR spectra were collected at: b) 2 min, c) 7 min, d) 13 min, e) 30 min and f) 56 min; peaks for tmbn are labelled with red dots.

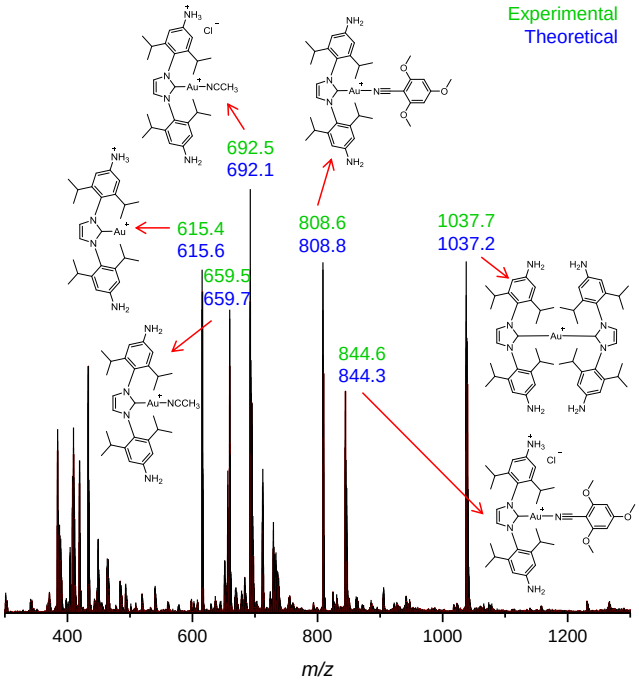

Figure S57. ESI-MS from a solution of Au NPs synthesized with **D** and 1.0 equiv. of $Au(tmbn)_2SbF_6$ (time of reaction: 90 min).

3.5 Effect of DIPEA on Au NP Production with 2

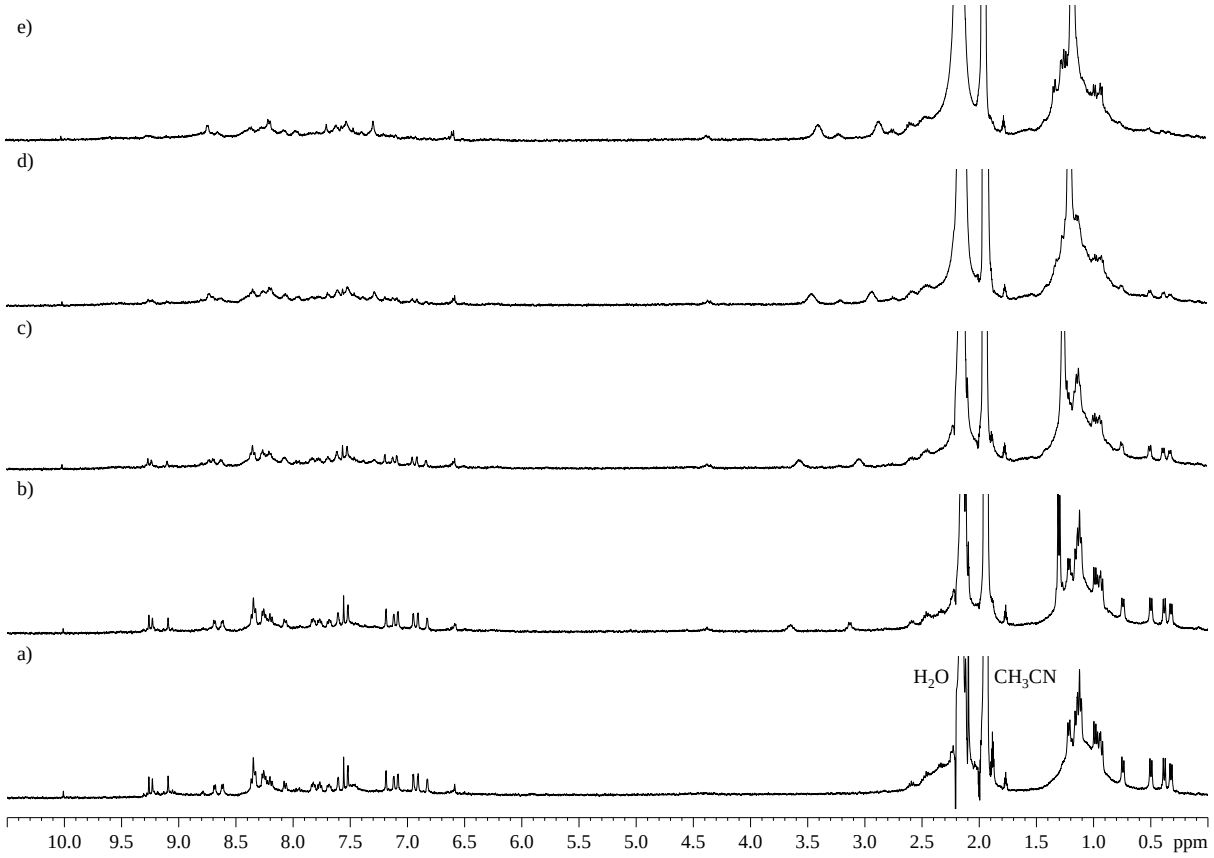

Figure S58. ^{1}H NMR titration of DIPEA into a solution of **2** in CD_3CN at 25 °C: a) 0.0 equiv., b) 1.0 equiv., c) 2.0 equiv., d) 3.0 equiv., and e) 4.0 equiv.

In the following experiments, a 2.0 mL solution (5.2×10^{-5} M) of **2** was prepared in acetonitrile, to which 100 μL (6.0 equiv.) of $Au(tmbn)_2SbF_6$ was added from a solution prepared in acetonitrile (time of reaction = 0 min); the UV-Vis spectrum was taken immediately. At t = 2 min, 0.5 – 4.0 equiv. of diisopropylethylamine (DIPEA; 5 μL) was added from a solution prepared in acetonitrile, and the UV-Vis collected every 2 min, with agitation of the solution for 30 seconds between spectra acquisition. The results of the experiments are summarized in Figure S59.

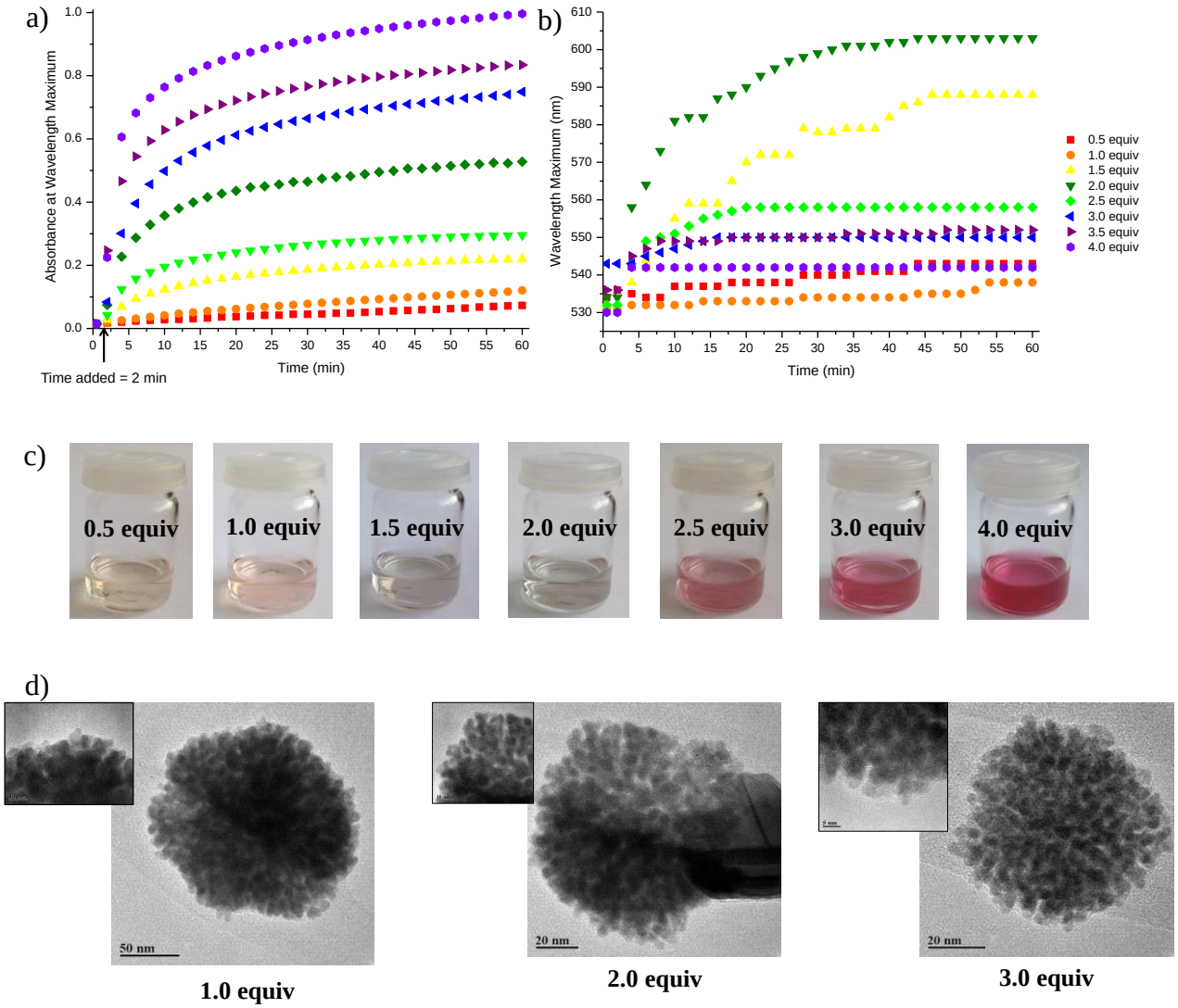

Figure S59. The results from the UV-Vis experiments following the synthesis of Au NP with **2** over time with varying equivalents of DIPEA added at *t* = 2min is shown: a) absorbance at λ_{max} vs. time and b) λ_{max} vs. time; c) the colors of the Au NP solutions at *t* = 90 min; d) TEM images of the Au NPs at *t* = 90 min, with magnified views.

3.6 Analysis of Kinetic Data

The absorbance (A) of the surface plasmon resonance (SPR) band observed in the UV-Vis spectrum can be related to the volume fraction of the nanoparticles grown in solution as a function of the reaction time (t), according to equation 1:[16]

$$A = C(1 - e^{-k_{app}t^n}) \quad (1)$$

Where k_{app} is the apparent rate constant, n is the critical growth exponent, and C is the proportionality constant. Fractional values of n arise from factors such as volume changes on crystallization, incomplete crystallization, annealing or different mechanisms involved during the process.[17]

Equation 1 was fitted to the UV-Vis data obtained from the production of Au NPs with various reductants and conditions; the results are summarized below, and the reference to each spectrum is provided.

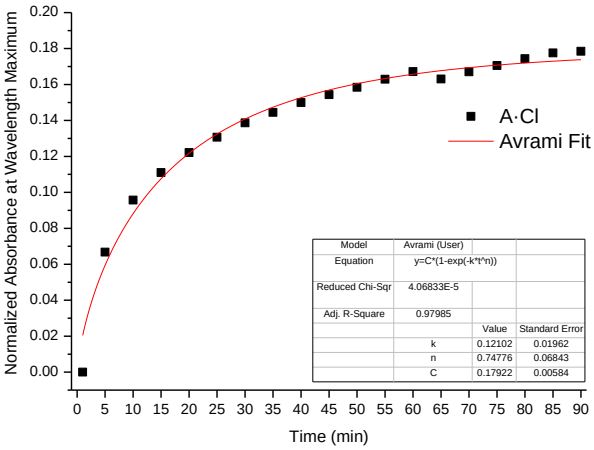

See Figure S48

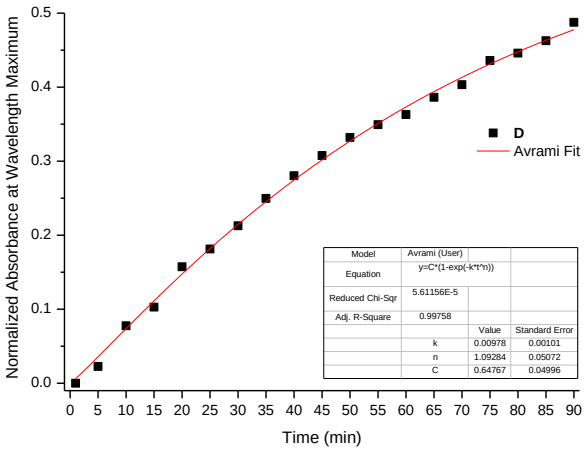

See Figure S53

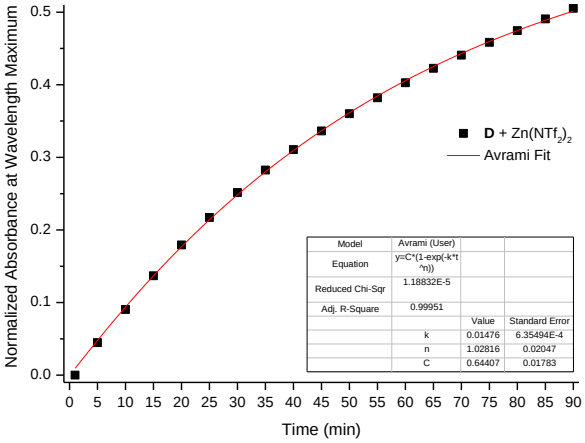

See Figure S31

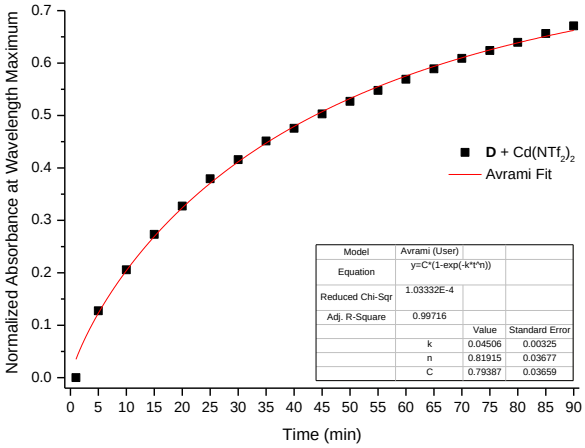

See Figure S43

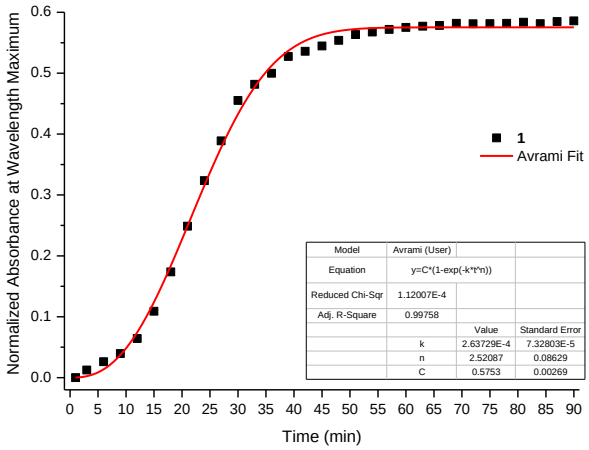

See Figure S26

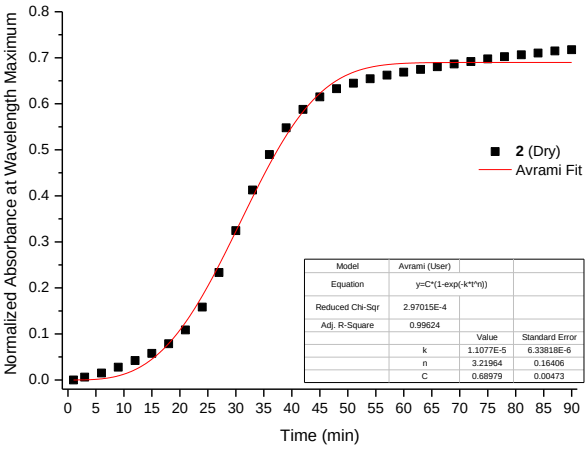

See Figure S36

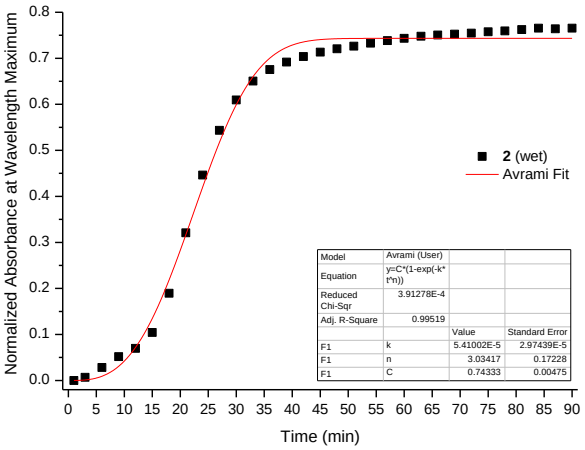

See Figure S42

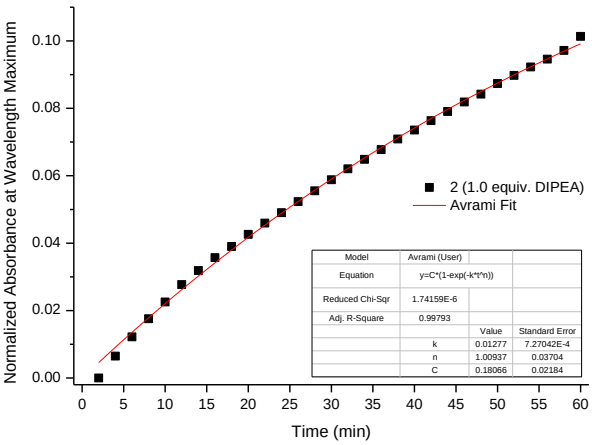

See Figure S59

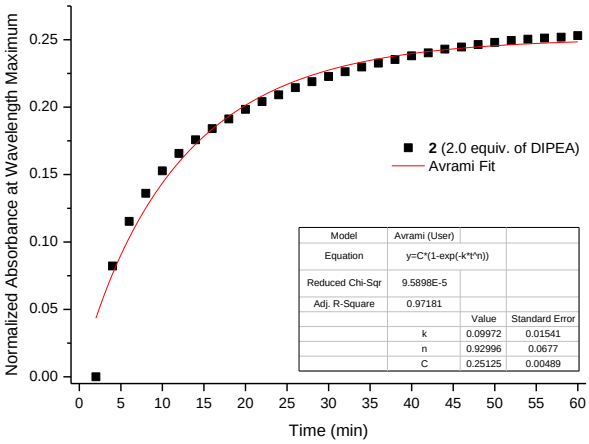

See Figure S59

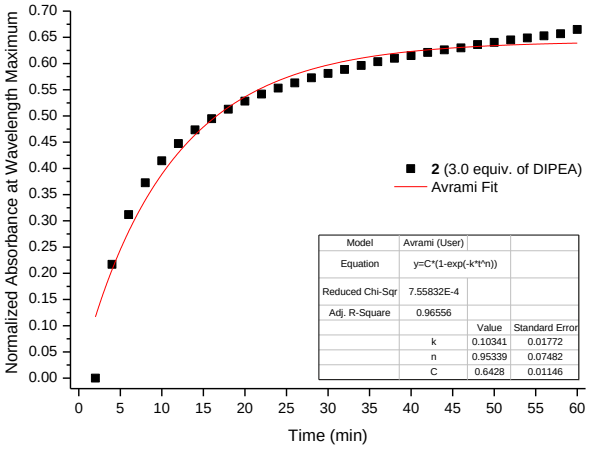

See Figure S59

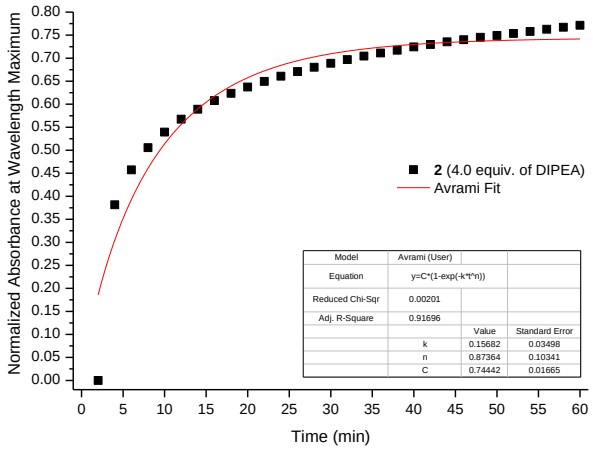

See Figure S59

The apparent rate constant (k_{app}) and critical growth exponent (n) from the experiments listed above are summarized in Table S1, and were calculated as a weighted average of two runs for each experiment.

Table S1. Apparent Rate Constants (k_{app}) and Critical Growth Exponents (n) Derived from the Fitting Results of the SPR Absorbance Data

Reductant	k_{app} (min^{-n})	n
A	$1.3 \pm 0.2 \times 10^{-1}$	0.72 ± 0.05
D	$1.01 \pm 0.06 \times 10^{-2}$	1.09 ± 0.03
D + Zn(NTf$_2$)$_2$	$1.70 \pm 0.06 \times 10^{-2}$	0.97 ± 0.02
D + Cd(NTf$_2$)$_2$	$3.8 \pm 0.2 \times 10^{-2}$	0.90 ± 0.03
1	$1.8 \pm 0.4 \times 10^{-4}$	2.59 ± 0.07
2 (Dry)	$1.5 \pm 0.9 \times 10^{-6}$	3.4 ± 0.1
2 (Wet)	$4.7 \pm 0.2 \times 10^{-5}$	3.1 ± 0.1
2 (4.0 equiv. DIPEA)	$1.6 \pm 0.4 \times 10^{-1}$	0.9 ± 0.1
2 (3.0 equiv. DIPEA)	$1.0 \pm 0.1 \times 10^{-1}$	0.95 ± 0.07
2 (2.0 equiv. DIPEA)	$1.0 \pm 0.2 \times 10^{-2}$	0.93 ± 0.07
2 (1.0 equiv. DIPEA)	$1.28 \pm 0.07 \times 10^{-2}$	1.01 ± 0.04

We attribute the difference in apparent rate constants of Au NP synthesis between **1** and **2** to the differences in thermodynamic stabilities between these two structures. A slower rate constant and larger value for the Avrami exponent n in the case of **2** (n = 3.4) than **1** (n = 2.59) is indicative of a longer nucleation stage,[14c] which is reflected in the anisotropic, triangular morphologies observed in the TEM for **2**-generated nanoparticles.

4. References

[1] R. Uson, A. Laguna, M. Laguna, D. A. Briggs, H. H. Murray, J. P. Fackler, in *Inorg. Synth.*, John Wiley & Sons, Inc., **2007**, pp. 85-91.

[2] W. Meng, T. K. Ronson, J. K. Clegg, J. R. Nitschke, *Angew. Chem. Int. Ed.* **2013**, *52*, 1017-1021.

[3] M. Raducan, C. Rodriguez-Escrich, X. C. Cambeiro, E. C. Escudero-Adan, M. A. Pericas, A. M. Echavarren, *Chem. Commun.* **2011**, *47*, 4893-4895.

[4] A. Hospital, C. Gibard, C. Gaulier, L. Nauton, V. Thery, M. El-Ghozzi, D. Avignant, F. Cisnetti, A. Gautier, *Dalton Trans.* **2012**, *41*, 6803-6812.

[5] O. Santoro, A. Collado, A. M. Z. Slawin, S. P. Nolan, C. S. J. Cazin, *Chem. Commun.* **2013**, *49*, 10483-10485.

[6] R. Visbal, A. Laguna, M. C. Gimeno, *Chem. Commun.* **2013**, *49*, 5642-5644.

[7] X.-F. Jiang, F. K.-W. Hau, Q.-F. Sun, S.-Y. Yu, V. W.-W. Yam, *J. Am. Chem. Soc.* **2014**, *136*, 10921-10929.

[8] W. Meng, T. K. Ronson, J. R. Nitschke, *Proc. Natl. Acad. Sci. USA* **2013**, *110*, 10531-10535.

[9] CAChe Workspace, WorkSystem Pro Version 7.5.0.85

[10] Bruker-Nonius, *APEX, SAINT and XPREP*, Bruker AXS Inc., Madison, Wisconsin, USA, **2013**.

[11] L. J. Farrugia, *J. Appl. Crystallogr.* **1999**, *32*, 837-838.

[12] L. Palatinus, G. Chapuis, *J. Appl. Crystallogr.* **2007**, *40*, 786-790.

[13] G. Sheldrick, *Acta Cryst.* **2008**, *A64*, 112-122.

[14] a) M. L. Personick, C. A. Mirkin, *J. Am. Chem. Soc.* **2013**, *135*, 18238-18247; b) K. Xu, Z. r. Guo, N. Gu, *Chin. Chem. Lett.* **2009**, *20*, 241-244; c) Y. Zhou, W. Lin, F. Yang, W. Fang, J. Huang, Q. Li, *Chem. Phys.* **2014**, *441*, 23-29.

[15] C. A. Schneider, W. S. Rasband, K. W. Eliceiri, *Nat Meth* **2012**, *9*, 671-675.

[16] P. N. Njoki, J. Luo, M. M. Kamundi, S. Lim, C.-J. Zhong, *Langmuir* **2010**, *26*, 13622-13629.

[17] M. L. Di Lorenzo, C. Silvestre, *Prog. Polym. Sci.* **1999**, *24*, 917-950.